PEOPLES DEMOCRATIC REPUBLIC OF ALGERIA

MINISTRY OF HIGHER EDUCATION AND SCIENTIFIC RESEARCH

UNIVERSITY OF MOHAMED BOUDIAF - M'SILA

FACULTY OF SCIENCES

DEPARTMENT OF PHYSICS

***N° :* PH/MAT/24/2025**

FIELD: SCIENCES OF MATIER

FIELD: PHYSICS

OPTION: MATERIAL PHYSICS

Memory presented for obtaining
academic Master diploma

Submitted by: MOHAMMED SAAD Samra

ENTITLED:

Quaternary Heusler alloys MnCrTiZ(Z=Al , As) investigates their structural stability

opto-electronic features and magnetic.

Defended on 18/06/2025 in front of a jury composed of:

Djelel Kherifi	University M. BOUDIAF-M'SILA.	Chairperson
Karim Bouferrache	University M. BOUDIAF-M'SILA.	Supervisor
Saber Saadessaoud	University M. BOUDIAF-M'SILA.	Examinator

Academic Year: 2024/2025

*I thank **ALLAH** the Almighty, who has granted me health, courage, patience, and determination, enabling me to complete this present work.*

*I sincerely thank my supervisor, **Prof.Dr. Karim BOUFERRACHE**, for proposing and guiding this work, and above all, for taking the time to provide me with all the necessary resources.*

*We extend our sincere gratitude and deepest appreciation to the distinguished professors, **Dr. Djelel Kherifi** and **Dr. Saber Saadessaoud**, for honoring us with their presence as members of the defense committee. We thank them for devoting their time and effort to review and evaluate this modest work with such objectivity and academic rigor.*

Mother Appreciation

To my beloved mother, the source of kindness and strength, thank you for every moment of love, every sacrifice, and every prayer you offered for me. Words are not enough to express my gratitude; you are the greatest blessing in my life.

Dear mother, I deeply appreciate all the care, love, and attention you have given. You are my true support and the heart that gives without limits. May God protect you and grant you a long life.

My dearest mother, you are the light of my life. Thank you for every moment you stood by my side, for every smile you planted in my heart, and for every kind word that lifted my spirits. I love you endlessly.

Brother Appreciation

To my dear brother, you are my support and companion. Thank you for your constant encouragement, for being by my side in every moment, and for your invaluable kindness. May you always remain my brother and friend for life.

My dear brother, your presence in my life is a great blessing. Thank you for every help, every support, and every moment you stood beside me. Nothing compares to having a wonderful brother like you.

To my beloved brother, I may not always say it, but I am truly grateful to you from the bottom of my heart. With you around, I feel safe and happy. Thank you for always being there.

Teacher Appreciation

I extend my sincerest thanks and appreciation to you for your great efforts in spreading knowledge and wisdom. You have always been a role model in dedication and sincerity. May God reward you abundantly.

My respected teacher, through you, we learned not only lessons but also the values of hard work and perseverance. Thank you for your endless giving and your constant care for our future.

Our deepest appreciation and respect to you. You were more than just a teacher; you were a guide and a light that illuminated our path to success.

Dedication

I dedicate this modest work:

To my mother: Touirat Ghania

To my brothers: Mohammed Saad Halim.

To my entire family, to all my friends.

To everyone who supported me in this work, whether directly or indirectly.

Nomenclature:

Most Commonly Used Abbreviations:	Most Commonly Used Abbreviations:
PP: Pseudo potentiel. **US:** Ultra-Soft. **PAW:** Projector Augmented Wave. **VASP:** Vienna Ab Initio Simulation Package. **DOS:** Density of States. **STT:** Spin-Transfer Torque. **STTNO:** Spin-Transfer Torque Nano-Oscillator. **NM:** Non-Magnetic **FIM:** Ferrimagnetic. **AGFM:** Alternating gradient force magnetometer **AMR:** Anisotropic magnetoresistance **CIP**: Current-in-plane **CMOS:** Complementary metal-oxide-semiconductor **CPP:** Current-perpendicular-to-plane **DCD:** DC demagnetised **EDX:** Electron dispersive X-ray spectroscopy. **FCC:** Face centred cubic **SG:** Space Group. **PWM:** Plane Wave Method. **FP-LAPW:** Full-Potential Linearized Augmented **LDA:** Local Density Approximation. **GGA:** Generalized Gradient Approximation. **APW:** Augmented Plane Wave. **MT:** Muffin-Tin.	**FFT** Fast Fourier transform **FWHM** Full width half maximum **HiTUS** High target utilisation sputtering **STEM** Scanning transmission electron microscopy (High resolution) **TEM** Transmission electron microscopy **IR** Isothermal remanence **MOSFET** Metal-oxide-semiconductor field effect transistor **RKKY** Ruderman Kittel Kasuya Yoshida **SFET** Spin field effect transistor **STT** Spin transfer torque **TM** Tunnelling magnetoresistance **VSM** Vibrating sample magnetometer **XRD** Weak-beam dark-field X-ray diffraction **PW91**: Perdew-Wang 91. **Wad**: Work of Adhesion. **HMF**: Half-Metallic Ferromagnets (High resolution). **GMR**: Giant Magnetoresistance. **TMR**: Tunnel Magnetoresistance. **MTJ**: Magnetic Tunnel Junction. **MRAM**: Magnetic Random Access Memory. **DRAM**: Dynamic Random Access Memory. **DFT**: Density Functional Theory.

Mathematical Scientific Symbols	Physical coefficients
E_{xc}: Exchange-Correlation Energy. **B_Z**: Brillouin Zone. **B_0:** Bulk Modulus (in GPa). **B_i**: Pressure Derivative of the Bulk Modulus. **E_F**: Fermi Energy. **Eg:** Energy Band Gap. **θ_D:** Debye Temperature (in K). **ρ:** Density (in g/cm³). **v_m:** Average Sound Velocity (in m/s).	**B**: Bulk Modulus. **G**: Shear Modulus. **E**: Young's Modulus. **ζ**: Poisson's Ration **AHform**: Formation Enthalpy. **Cijkl**: Elastic Constants Tensor. **Sijkl**: Compliance Constants Tensor. **Az** : Zener Anisotropy Factor. **Ag**: Every Anisotropy Factor. **E_f** : Fermi Level.

List of tables:

List of Figure:

Summary:

Introduction

Introduction

Humans have always sought to develop new materials to enhance well-being and drive industrial progress. Materials science is key in this pursuit by studying atomic and molecular systems' physical and chemical properties. This field focuses on understanding the relationship between a material's structure (metals, polymers, semiconductors) and its mechanical, electrical, thermal, optical and other properties.

Scientists can engineer materials with tailored properties by controlling microscopic phenomena (such as diffusion, atomic arrangement, and phase transitions). Researchers analyze electron behavior and atomic organization within materials to understand these properties, an area closely linked to condensed matter physics.

Calculating the electronic structure and total energy relies on solving the Schrödinger equation in quantum mechanics. However, the complexity of many-particle interactions makes an exact solution impractical. Thus, advanced approximation methods (as Dirac noted in 1929) are essential for accurately simulating quantum material properties.

Recent research has identified Heusler alloys as a significant class of materials, with over 1,000 known compounds. These alloys, best described as intermetallic compounds (rather than simple alloys), exhibit ordered atomic structures and follow the general formula XX'YZ, where X and Y are typically transition metals. Z is an element from groups III–V (sometimes replaced by rare or alkaline earth metals).

Given the complexity of material design, numerical modeling and simulation have become essential tools for studying metallic, semiconducting, and insulating materials. These "virtual experiments" enable cost-effective prediction of material properties, guiding industrial applications where real experiments are impractical.

Key computational methods include ab initio techniques, which rely on fundamental atomic constants to solve the Schrödinger equation. While limited by system size, they provide high-precision predictions of structural, electronic, and magnetic properties. This work applies the FP-LAPW method (via the WIEN2k code under Density Functional Theory) to analyze MnCrTiZ (Z = Al, As) Heusler alloys for spintronics applications, comparing results with experiments and other theoretical models.

Chapter I presents generalities about Heusler alloys and their properties.

The first part of this manuscript is devoted to some theoretical reminders about Heusler alloys: description of the structure, construction basis, physical properties, and dominant applications.

Chapter II focuses on computational methodologies, primarily examining Density Functional Theory (DFT)-based approaches for electronic structure calculations, particularly emphasizing the Local Density Approximation (LDA) method. The chapter begins by reviewing fundamental quantum mechanical concepts, including the Schrödinger equation and the system Hamiltonian. It then traces the evolutionary path of computational approximations that enabled DFT's development, drawing upon established quantum chemistry literature. The discussion systematically progresses through DFT's theoretical foundations and developmental milestones, culminating in examining the LDA method - the core computational tool employed in this work for determining material properties.

Chapter III provides a detailed description of the computational codes used in the present work: the WIEN2k code for simulating the structural, electronic, mechanical, and magnetic properties of the systems considered and the GIBBS program for calculating the Debye temperature.

This presents the results obtained using the methods described in the first part. It is devoted to delivering the results concerning the structural, electronic, mechanical, and magnetic properties of the Heusler alloys.

Finally, a conclusion summarizes the key points and lists the most significant results.

Chapter I:

Generalities on Heusler alloys:

Chapter I: Generalities on Heusler alloys

I.1. Introduction

Recently, a novel family of materials has gained significant attention due to their applications in spintronics, known as half-metallic ferromagnets (HMF). This concept originates from their electrical structure, which exhibits generally metallic behavior for one spin density while the other is semiconducting. The 100% spin polarization at the Fermi energy (EF) is one of the most unique features of these materials. It is predicted to maximize the efficiency of magnetoelectronic devices such as tunnel magnetoresistance (TMR) and giant magnetoresistance (GMR). In 1983, Groot et al. predicted the existence of HMF in the half-Heusler alloy NiMnSb. Following this discovery, theoretical studies were begun to anticipate new HMF in different Heusler alloy systems. Several Heusler alloys have been successfully synthesized. Ab initio calculations and experimental observations show that producing HMF in these alloys is doable. Heusler alloys are commonly split into two categories: ternary Heusler alloys and quaternary Heusler alloys. The former is given by the formula X_2YZ. When one of the two X atoms is substituted by another transition metal X′, a quaternary Heusler alloy with the formula XX′YZ is produced. A new line of research on quaternary Heusler alloys demonstrates that they exhibit HMF. Our computations were performed using the DFT formalism with the FP-LAPW method in the WIEN2k code, within the GGA approximation.

MnCrTiZ (where Z = Al, As) constitutes an essential class of quaternary Heusler alloys that exhibit remarkable electrical and magnetic properties, making them promising candidates for spintronics and magnetoelectronic applications. These compounds belong to the broader family of XX'YZ-type Heusler alloys, where Mn, Cr, and Ti are transition metals, while Al and As are main-group elements. Structural Properties is Crystal Structure: MnCrTiZ compounds form in the LiMgPdSn-type structure (F-43m space group), characteristic of quaternary Heusler alloys. Atomic Arrangement: The Mn, Cr, Ti, and Z (Al/As) atoms occupy certain Wyckoff locations (4a, 4b, 4c, and 4d), impacting their magnetic and electrical characteristics. Lattice Dimensions: Expected to be 5.8–6.2 Å, depending on the Z (Al or As) option. MnCrTiZ (Z = Al, As) are promising quaternary Heusler alloys with potential half-metallic ferromagnetism, making them suitable for next-generation spintronic and magnetic memory systems. Further theoretical and experimental studies are needed to explore their powers thoroughly.

I.2. Nomenclature of Heusler Alloys

The history of one of the most fascinating materials may be traced back to 1903, when Fritz Heusler found that an alloy with a formula like Cu_2MnAl functions as a ferromagnetic material, even if its constituent elements are not magnetic. [1] Today's unique class of materials encompasses a massive collection of over 1,000 compounds, known as Heusler compounds or Heusler alloys. They are ternary materials that can be semiconducting or metallic with stoichiometries of 0:1:1 (commonly known as "Half-Heusler") or 0:2:1:1. [2].

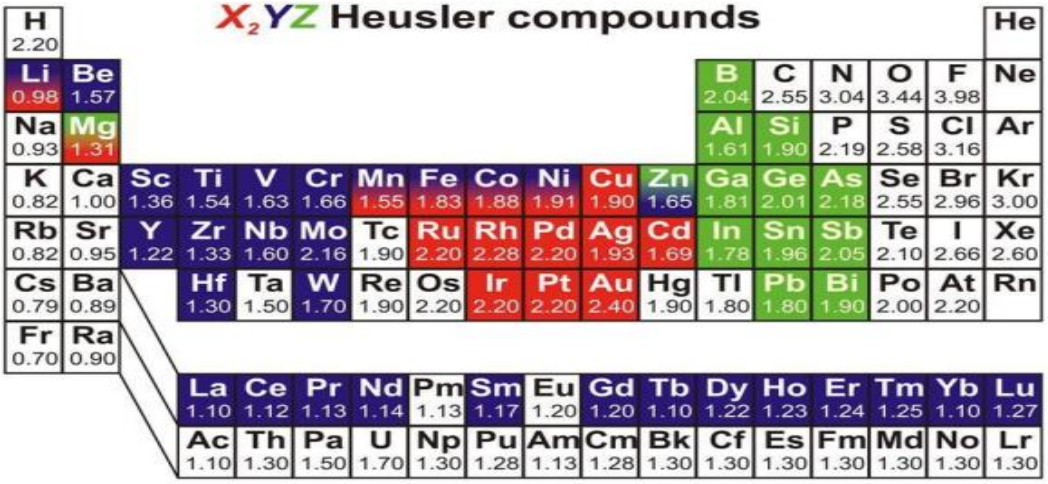

Table I.1. Periodic table of the elements. A combination of the different elements can form a huge number of Heusler materials according to the color scheme (reprinted with permission from [3].

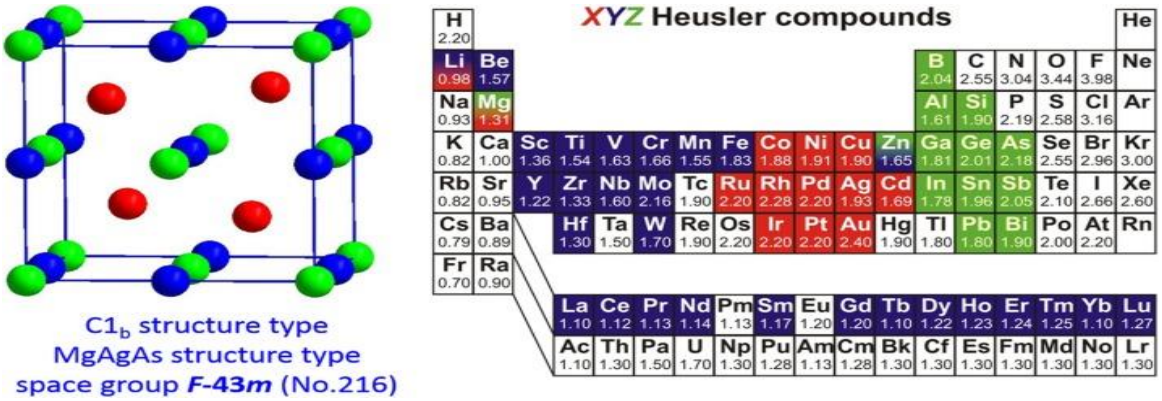

Figure I. 1. A. Crystal structure of a HH compound (left). Periodic table of the elements. The huge number of HH materials can be formed by the combination of the different elements according to the color scheme (right).[4] Thermoelectric: From history, a window to the future.

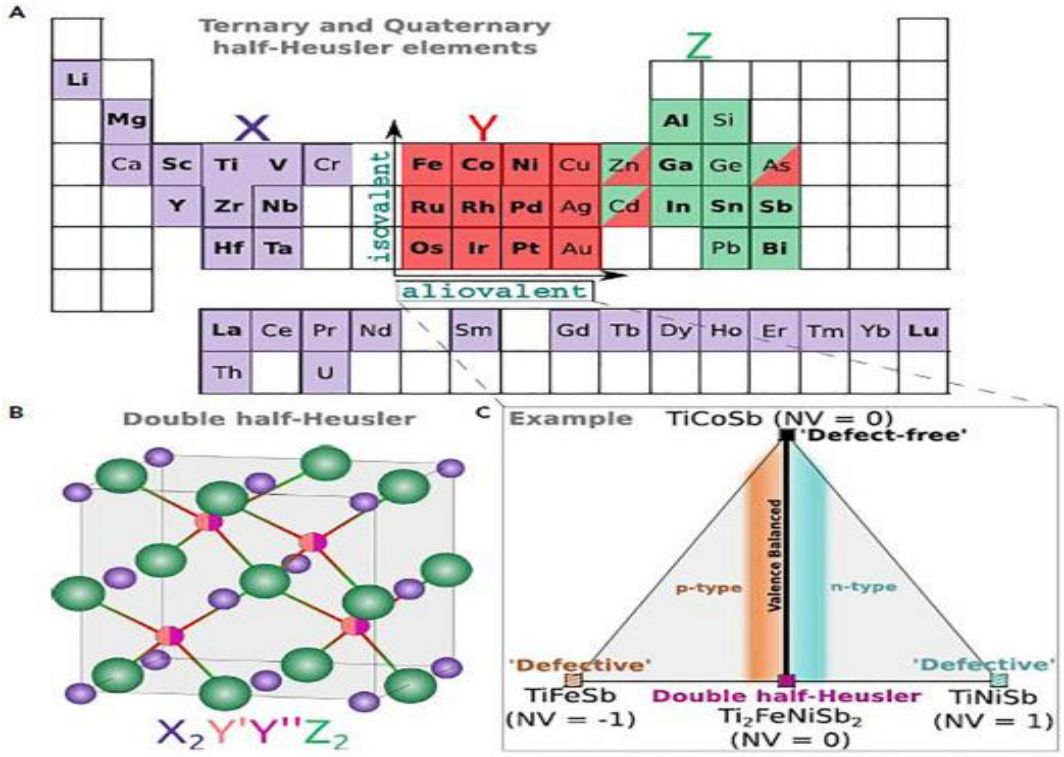

Figure I.1.B. Visualization of new double half-Heusler alloys.

The selection of constituent atoms X, Y, and Z is represented by violet, red, and green colors (medium, dark, and light gray in printed versions), correspondingly [5]. (B) Unit cell with general formula $X_2Y'Y''Z_2$ with equal occupancy on Y-site (in half-orange and half-magenta colors; light and dark gray in print versions) to have 18-electron configuration or net valence, NV = 0

I.3. Heusler Alloys

Full-Heusler, half-Heusler, and inverse-Heusler alloys are the three classifications for ternary Heusler alloys. Furthermore, binary and quaternary compounds are produced from Heusler alloys due to structural alterations and chemical substitutions. The usual formula for full-Heusler alloys is X2YZ (2:1:1), where Z atoms are members of the leading group (III or IV) of the periodic table, and X and Y atoms are transition metals or lanthanides [6].

I .3.1. Symmetric Heusler Alloys

I .3.1.1. Conventional Heusler Alloys

Conventional Heusler alloys are created by transition metals (d-metals) and the main group (p-group), which is represented by Z atoms (D sites). These alloys often have the X2YZ composition, where X and Y are transition metals, and Z is a main-group element and usually crystallizes in the face-centered cubic (FCC) structure. Moreover, the p-d

hybridization prevalent in ordinary Heusler alloys greatly impacts the parent phase's stability, atomic ordering and magnetic response [7]. However, the d-d hybridization affects the martensite transition, as Roy et al [8] reported. Per IUPAC standards, the most electropositive element is the initial component in the formula. As aforementioned, full-Heusler alloys have an L21 cubic structure and belong to the Fm-3m space group. However, full-Heusler alloys may display A2 (X-Y-Z disorder) and B2 (Y-Z disorder) structures, depending on the site-disordered state. Otto Heusler [9] initially identified the basic structure for Cu2MnAl, and Meyers et al. for Cu2MnSn [10]. In the full-Heusler alloys system, four interpenetrating FCC sublattices create the cubic unit cell, where atoms follow Wyckoff positions. X atoms are positioned at the 8c (1/4, 1/4, 1/4) location of the unit cell, while four Y and Z atoms are placed at the 4a (0, 0, 0) and 4b (1/2, 1/2, 1/2) positions, respectively, as proved by Otto Heusler. According to Graf et al. [11], this structure produced by a single X and Z atom is called a zinc blende sublattice. Furthermore, a Y atom is positioned in the octahedral sites, and the second X atom is in the tetrahedral sites.

I.3.1.2. All D-Metal Heusler Alloys

Conversely, all-metal Heusler alloys consist exclusively of transition metals, indicating that the Z atoms are likewise transition metals (D sites) [12]. All-metal Heusler alloys are distinguished by the absence of main-group metals in their composition. Their composition comprises transition metals (X, Y, and Z). These alloys are differentiated by having all-d-electron configurations in their constituents. The compositional difference may result in differing crystal structures for the two types of alloys. Accordingly, the crystal structure of all-d-metal Heusler alloys can differ and relies on the specific elements present. They may favor diverse topologies, such as non-FCC architectures. Otherwise, they may not adhere to the cubic symmetry characteristic of classic Heusler alloys [13]. The changes in hybridization and chemical elements between normal and all-d-metal Heusler alloys are depicted in Figure I.2.[14].

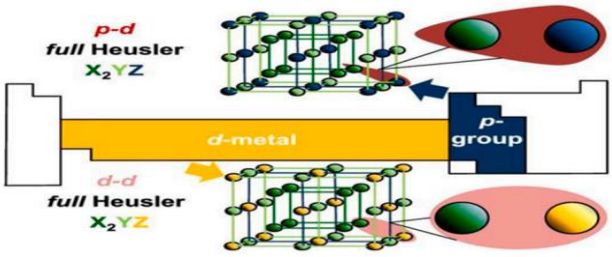

Figure I.2. Difference in hybridization and chemical elements between conventional and all-d-metal Heusler alloys (reprinted with permission from Ref. [14]).

I.3.1.3. Half - Heusler Alloys

Half-Heusler alloys are presented by the following chemical formula: XYZ (1:1:1). These compounds exhibit covalent and ionic characteristics, with elements X and Y demonstrating cationic properties and element Z exhibiting anionic properties. The X element is the most electropositive, producing a rock-salt (NaCl) sublattice with the main-group atom Z. This interaction reflects a heightened ionic nature in their connection. The Y and Z atoms constitute a zinc-blende (ZnS) sublattice, signifying covalent bonding [15]. Accordingly, the sum of zinc-blend and rock-salt lattice produces the structure of half-Heusler alloys.

I.3.2. Less Symmetric Heusler Alloys

I.3.2.1. Inverse Heusler Alloys

Inverse-Heusler alloys are produced from full-Heusler alloys through a rearranging of the atomic locations. Compared to the X2YZ formula of full-Heusler alloys, the' locations of X and Y in inverse-Heusler alloys are interchanged, leading to a different crystal structure. This inversion of the X and Y positions affects the electrical and magnetic characteristics of the material. Commonly, the site choice of the metal transition atoms depends on the number of valence electrons (ZV). In other words, if ZV(Y) > ZV(X), where X and Y are transition metal elements belonging to the same period of the periodic table, two X atoms occupy two sites, namely (½, ½, ½) and (¾, ¾, ¾). Conversely, Y and Z atoms occupy the other places, (¼, ¼, ¼) and (0, 0, 0), respectively, yielding the XA type structure with the F43m space group [16]. Referring to Graf et al., to better comprehend the XA crystal structure, X and Z atoms create a NaCl structure to attain an octahedral arrangement for X. Nonetheless, elements X and Y occupy the tetrahedral interstitial positions [17]. The distinction between the crystal structures of full-Heusler and inverse-Heusler alloys.

I 3.2.2. Binary Heusler Alloys

Binary Heusler alloys can display the X3Z (3:1) chemical formula, with X being the main group's transition metals and Z elements [18]. These alloys present a face-centered cubic structure D03-type and the same space group Fm-3m as full Heusler alloys. When the X and Y constituents of full-Heusler compounds contain identical chemical elements, a D03-type structure is established. Therefore, three X1, X2 and X3 atoms are positioned in the (¼, ¼, ¼), (½, ½, ½) and (¾, ¾, ¾) sites, whereas Z atoms fill up the (0, 0, 0) places. This

configuration results in a ferromagnetic contact among the X1, X3, and X2 atoms, as the locations of X1 and X3 are comparable [19].

I. 3.2.3. Quaternary Heusler Alloys

Quaternary Heusler alloys are a variety of Heusler alloy exemplified by a LiMgPdSn-type crystal structure (known as Y-type structure), whose primitive cell contains four atoms. Similarly, these alloys display the precise symmetry as half and inverse Heusler, characterized by an F43m space group [20]. Three nonequivalent structures are formed for the Y-type arrangement depending on the atom placements. Table 2 delineates three unique atomic configurations: type 1, type 2, and type 3, over various Wyckoff sites. The chemical formula XX′YZ is seen in quaternary Heusler compounds owing to the stability along the diagonal of the FCC cube. Rather than being synthesized by a single element, X and X′ are formed by independent chemical components. The valence of the constituents in these alloys is another characteristic; X atoms possess a higher valence than X′, whereas Y atoms exhibit a lower valence than X and X′ elements. Three-unit cell layouts with the possible arrangement sites of the quaternary Heusler are illustrated in Figure I.3.

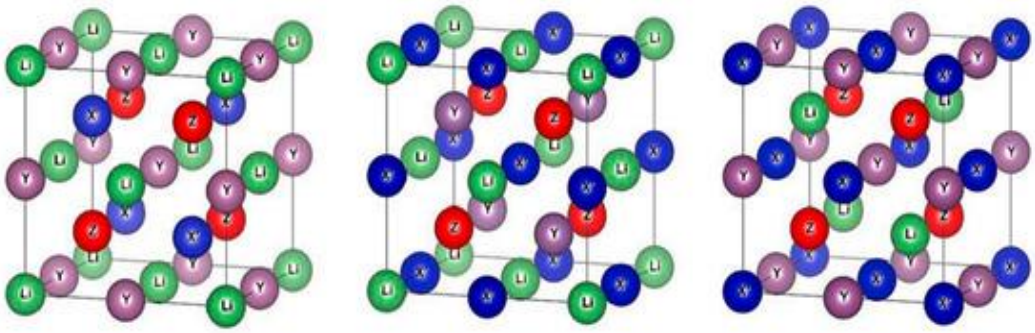

Figure I.3. Unit cells representation of quaternary Heusler Li (X)X′YZ; type Y_1, type Y_2 and type Y_3 (reprinted with the permission from Ref. [20]).

I.3.3. Non-Stoichiometric Heusler Alloys

Heusler alloys are categorized according to stoichiometry as previously stated. Conversely, numerous Heusler compounds possess non-stoichiometric compositions. Non-stoichiometry can occur due to several variables, including faults in the crystal lattice, replacements, vacancies or compositional changes within the material. These variations from stoichiometry can dramatically alter the alloy's physical, chemical and electrical properties. Under these conditions, the crystal's chemical arrangement may move from the ordered $L2_1$ structure to a partially ordered B_2 due to atomic exchanges at the Y and Z site positions, or to a completely disordered A_2 structure, wherein all elements, X, Y, and Z, are randomly

distributed [21,22]. As a result, the distance between the magnetic atoms may also alter, impacting the exchange contact between chemical components [23].

I.4. Half-Heusler Alloys

In general, semi-Heusler XYZ alloys can be seen as compounds comprised of two parts: a covalent component and an ionic part. The X and Y atoms exhibit unique cationic features, whereas Z might be viewed as the anionic counterpart. The nomenclature in the literature varies widely, ranging from ordering the elements alphabetically, by their electronegativity, or arbitrarily. Consequently, all three alternative permutations can be recognized. This thesis will follow an order that parallels electronegativity. The most electropositive element is positioned at the commencement of the formula. It may be a main-group, transition metal, or rare-earth element. The most electronegative element is situated at the end and is typically a main-group element from the latter section of the periodic table, including LiAlSi, ZrNiSn, and LuAuSn [24]. It should be stressed that the choice of atomic locations for the X, Y, and Z elements cannot be directly determined from this nomenclature, and care must be used in this selection because wrong placements utilized in theoretical models often lead to bad results [25].

I.5.Quaternary Heusler

I.5.1. Half-Metallic Heusler Alloys

The designation "half-metal" emerged in the early 1980s. De Groot claims that in a half-metal, only electrons with a unique spin orientation ("up" or "down") display metallic capabilities, whilst electrons with the opposing spin orientation behave as semiconductors. Half-metals display complete spin polarization, as the electron contributions at the Fermi level are constrained to a single spin orientation (either up or down).

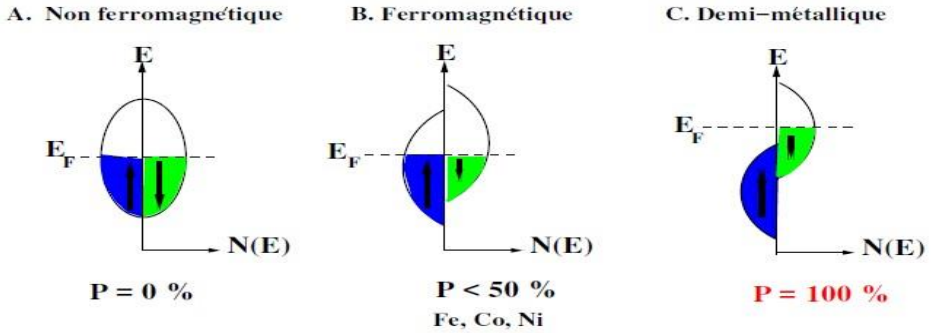

Figure I.4. Schematic representation of the density of states and spin polarization for: (A) a non-magnetic compound, (B) a ferromagnetic material, and (C) a half-metallic material [26].

A half-metallic material features the Fermi level intersecting an energy gap for one spin orientation and an energy band for the opposite orientation. Half-metals should not be confused with strong ferromagnets like cobalt or nickel. The 3d bands of Co or Ni display complete spin polarization, whereas their 4s bands at the Fermi level remain unpolarized. As a result, spin-up (↑) and spin-down (↓) electrons exist at the Fermi level. To achieve half-metallicity, hybridization between the 3d and 4s bands must occur so that the Fermi level no longer lies within the 4s band. This explains why no nanoelemental material exhibits half-metallicity. Half-metals must also be separated from semimetals (e.g., bismuth), which possess equal holes and electrons due to a bit of overlap between the valence and conduction bands.

I.5.2. Semiconducting Heusler Alloys

Ternary semiconductors with a stoichiometry of 0:1:1 are intricately associated with silicon semiconductors and binary compounds like GaAs. Starting from a lattice built from binary compounds, ternary materials can be derived by adding atoms in the vacant lattice sites. Thus, these compounds are referred to as "filled tetrahedral structures." In this class of materials, several subgroups must be distinguished: the Nowotny–Juza phases AIBII–CV with AI = Li, Cu, Ag; BII = Be, Mg, Zn, Cd; and CV = N, P, As, Sb, Bi, which are well known as wide-gap semiconductors. Juza and Hund initially documented them in the 1940s, and they became the focus of a comprehensive theoretical analysis in the 1980s.

I.5.3. Magnetocaloric Heusler Alloys

They are a class of materials that exhibit the magnetocaloric effect (MCE), making them promising candidates for magnetic refrigeration and energy-efficient cooling technologies. When exposed to a varying magnetic field, these alloys undergo a temperature change, which is the core principle behind their application in near-room-temperature cooling systems.

I.5.4. Shape Memory Heusler Alloys

(SMHAs) They are a unique class of intermetallic compounds exhibiting shape memory effect (SME) and superelasticity, making them valuable for actuators, sensors, and biomedical devices. When subjected to temperature variations or mechanical stress, these alloys undergo a reversible martensitic transformation (a diffusionless structural phase change).

I.6. Structure of Heusler alloys

Two families of Heusler alloys exist: one with a 0:1:1 stoichiometry and the other with a 0:2:1:1 stoichiometry. The alloys of the first family have the general formula XYZ and crystallize in a non-centrosymmetric cubic structure (space group number 216, F-3m, C1b) that can be derived from the tetrahedral ZnS-type structure by filling the octahedral sites of the lattice (Figure I.2). This type of semi-Heusler structure can be characterized by the interpenetration of three face-centered cubic (fcc) sublattices, each occupied by the X, Y, and Z atoms [27]. The occupied positions are 4a (0, 0, 0), 4b (½, ½, ½), and 4c (¼, ¼, ¼). In principle, three non-equivalent atomic arrangements are possible in this type of structure, as summarized in **Table I.2.**

	4A	4B	4C
I	X	Y	Z
II	Z	X	Y
III	Y	Z	X

Table I.2: Different non-equivalent site occupations in the C1_b-type structure.

Generally, the semi-Heusler structure can be considered a ZnS sublattice (Wyckoff positions 4a and 4c) in which the octahedral sites (4b) are occupied. This description emphasizes the covalent bonding interaction between two constituent elements, which plays a major role in the material's electronic properties. On the other hand, it is interesting to note that the atoms at sites 4a and 4b form a rock-salt type sublattice, meaning their interaction has a strong ionic character. The specific atomic ordering depends greatly on the chemical nature of the elements. Generally, the atomic order according to two types (I and II, see Table I.2) is frequently observed. In MgAgAs, the Ag and As atoms form a covalent ZnS-type sublattice, while Mg and Ag build a rock-salt lattice. Although MgAgAs is the prototype of all semi-Heusler compounds, it should be noted that this material crystallizes with an atomic order different from most other semi-Heusler compounds.

Table I.3. Site occupation and general formulas for different atomic orderings in semi-Heusler compounds.

Site Occupation	General Formula	ICSD Structure Type	SB	Pearson	Space Group
4a, 4b, 4c	XYZ	LiAlSi (MgAgAs)	$C1_\beta$	cF16	F-43m (No. 216)
4a=4b, 4c	XZ_2	CaF_2	C1	cF12	Fm-3m (No. 225)
4a, 4b, 4c=4d	X_2YZ	Cu_2MnAl	$L2_1$	cF16	Fm-3m (No. 225)
4a=4b, 4c=4d	XZ	CsCl	B2	cP2	Pm-3m (No. 221)
4a=4c, 4b=4d	YZ	NaTl	B32	cF16	Fd-3m (No. 227)
4a=4b=4c=4d	X	W	A2	cI2	Im-3m (No. 229)

Mixing of atoms in Wyckoff 4a and 4b positions results in a CaF_2-type structure (C1, space group Fm-3m, No. 225). Conversely, vacant sites may become partially occupied while vacancies are simultaneously introduced in other sublattices. Partial occupation of 4d sites accompanied by vacancies at 4c sites yields a Cu_2MnAl-type structure ($L2_1$, space group Fm-3m, No. 225). Further mixing of atoms in 4a and 4b positions leads to CsCl-type disorder (B2, Pm-3 m, No. 221).

Alternatively, partial occupation of vacant lattice sites by atoms from 4b positions combined with mixing of 4a and 4c positions produces a NaTl-type structure (B32, Fd-3m, No. 227). Complete random distribution of all three atoms across the four possible positions results in tungsten-type disorder (W, Im-3m, No. 229). Table I.2 summarizes these structural variants using different crystallographic database notations.

"Inorganic Crystal Structure Database" (ICSD), "Strukturberichte" reports (SB), Pearson's database, and space group designations.

Types of crystal structure. In 1903, German chemist Fritz Heusler discovered the Heusler alloys, in particular, Cu_2MnAl, which exhibits strong ferromagnetic properties with a high Curie point (although each of its constituent elements, Cu, Mn and Al is not a ferromagnet). Since then, about 1500 different Heusler alloys with diverse functional properties have been found (Figure I.5). Among them, there are compounds with the shape memory effect and the giant magnetocaloric effect, thermoelectrics, alloys with unusual thermal and semiconducting properties, superconductors, and many others.

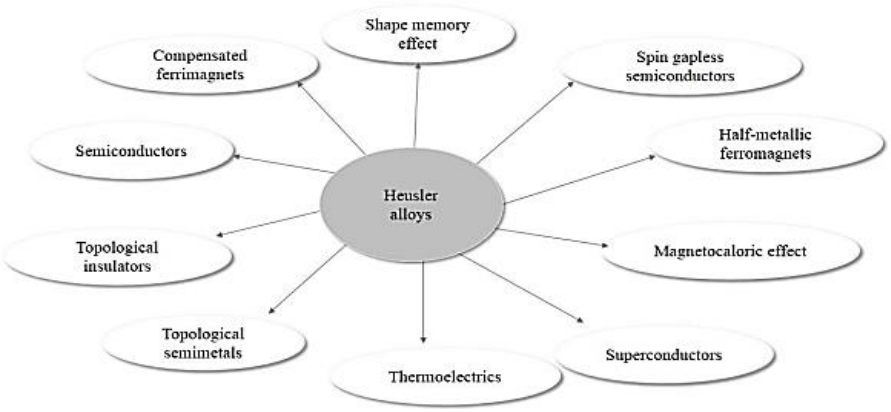

Figure I.5. Various types of Heusler alloys and their functional properties.

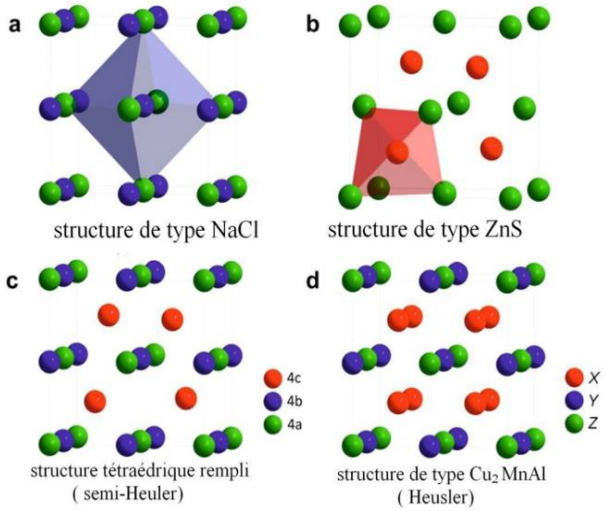

Figure I.6: (a) Rock salt structure, (b) Zinc blende structure and their relationships with the semi-Heusler structure (c) and the Heusler structure (d) [28].

In this case, a particular situation arises where the assigned prototype is an exception! MgCuSb is an example representing the atomic arrangement in most semi-Heusler alloys [29]. Cu and anionic Sb form the ZnS sublattice, while electropositive Mg and electronegative Sb occupy the NaCl-type ionic sublattice. Thus, as a perfect cube, Cu is surrounded by four Mg atoms and four Sb atoms. These two preferred atomic arrangements depend on the size difference between the involved atoms and the type of interatomic interactions.

The combination of two X-site FCC lattices results in a simple cubic lattice. Y and Z atoms occupy the centers of this simple cubic lattice, forming the CsCl-type superstructure. Such disorder between Y and Z sites is frequently observed in semi metallic Heusler systems but fortunately doesn't significantly affect their properties. The shifted Heusler cell and CsCl structure are presented in Figure I.7. This description provides an intuitive design rule: The

combination of two binary alloys crystallizing in CsCl-type structures leads to the formation of Heusler compounds [30].

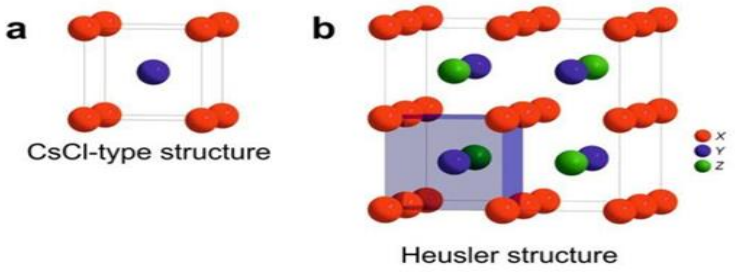

Figure I.7. (a) CsCl-type structure, (b) a Heusler structure shifted by (1/4, 1/4, 1/4) relative to the standard unit cell to make the CsCl superstructure visible.

In addition to the structure described above, an inverse Heusler structure is observed if the atomic number of Y is higher than that of X in the same period (Z(Y) > Z(X)), but it can also appear in transition metal compounds from different periods.

In all cases, element X is more electropositive than Y. Consequently, X and Z form a rock salt structure to achieve octahedral coordination for X. The remaining X and Y atoms occupy tetrahedral sites with 4-fold symmetry. Four interpenetrating FCC sublattices still describe the structure, but the X atoms do not form a simple cubic lattice. Instead, they are placed at the 4a (0, 0, 0) and 4d (3/4, 3/4, 3/4) positions, while the Y and Z atoms are located at 4b (1/2, 1/2, 1/2) and 4c (1/4, 1/4, 1/4), respectively.

These inverse Heusler alloys can also be distinguished from regular Heusler alloys by the formula (XY)X'Z. This inverse Heusler structure is often observed in Mn_2-based materials where Z(Y) > Z(Mn). A well-studied example is (MnCo) MnSn.

In the quaternary Heusler compounds, there are two elements, X and X'. They occupy the 4a and 4d positions, respectively, while Y is placed at 4b and Z at positions 4c. This structure follows the LiMgPdSn prototype. An illustration of the inverse Heusler structure and the quaternary Heusler alloy is provided in Figure I.8**.**

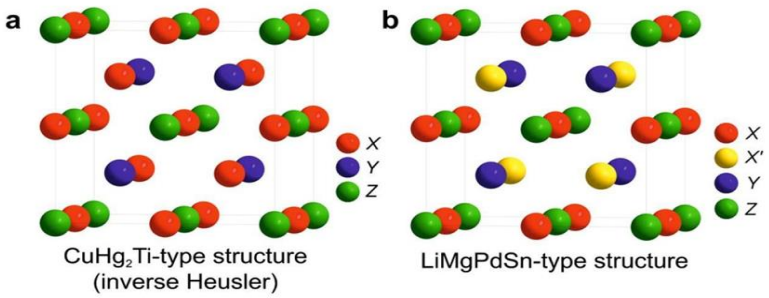

Figure I.8. Inverse Heusler structure $CuHg_2Ti$ (a), quaternary structure LiMgPdSn (b)[31].

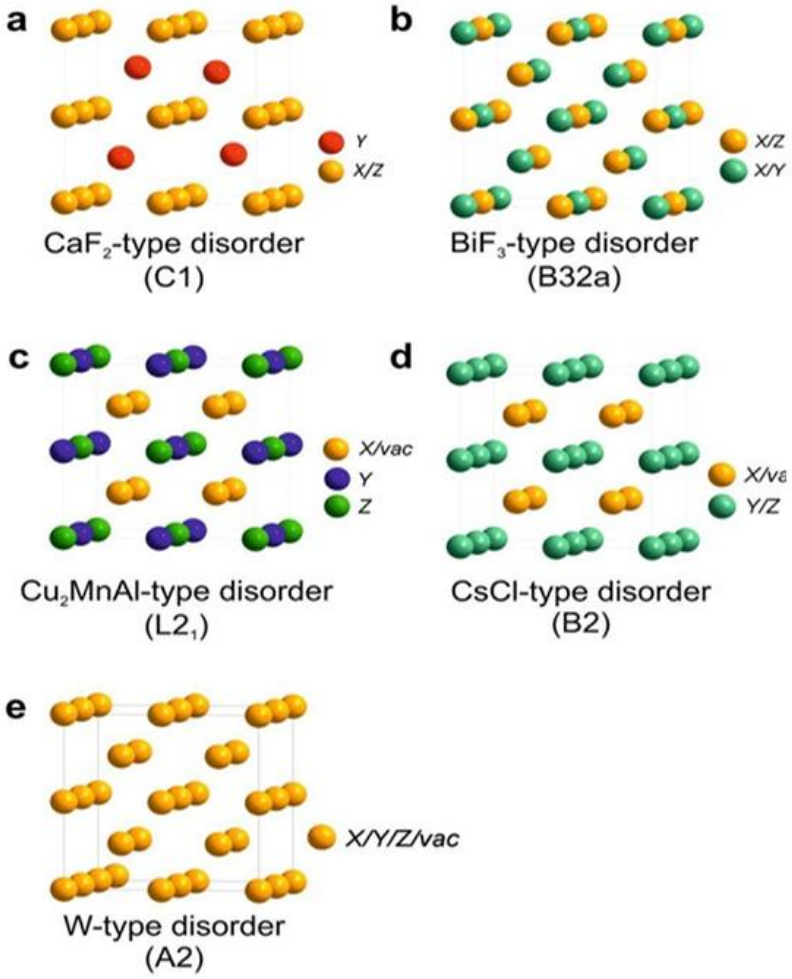

Figure I.9. Overview of the most important types of disorder that can occur in the semi-Heusler structure: (a) CaF2-type disorder, (b) NaTl-type disorder, (c) Cu_2MnAl-type disorder, (d) CsCl-type disorder, and (e) tungsten-type disorder [32].

I.7. Semiconductors

Juza and Hund first reported these phases in the 1940s [32, 33] and were the subject of extensive theoretical study in the 1980s [34]. We also have AIBIIICIV (e.g., LiAlSi and LiGaSi [35]), which also belong to the group of filled tetrahedral structures. If transition metals are present in the materials, they are considered semi-Heusler compounds.

A comparison of the various filled tetrahedral structures reveals differences in charge density distribution. As the parent material, Silicon is a covalent material with bonds oriented along connecting lines.

In the following sections, we will discuss bonding models for Nowotny-Juza phases, semi-Heusler, and Heusler compounds in greater detail and examine the exceptional properties of these semiconductor materials.

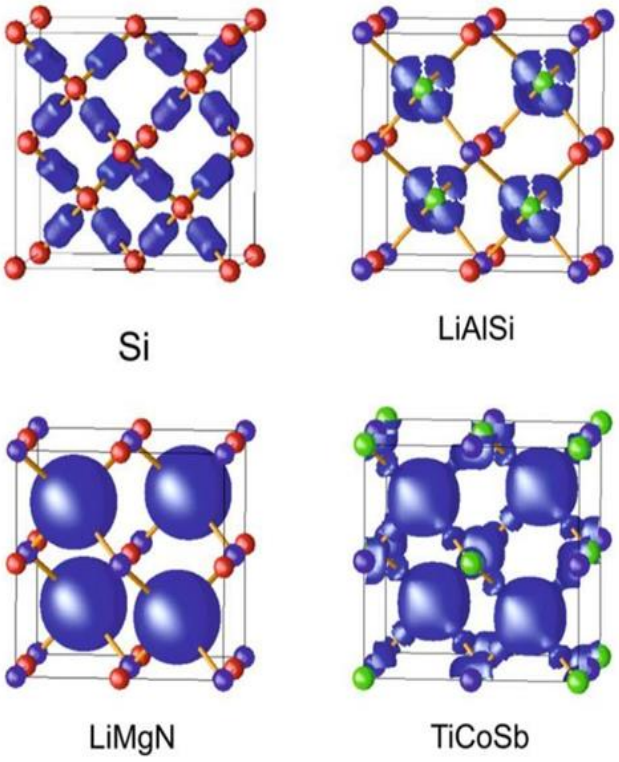

Figure I.10. Charge density distribution in Si and filled tetrahedral structures.

Semiconductor compounds of ternary and quaternary alloys, derived from tetrahedral

Here's a precise summary maintaining the original paragraph order and technical content:

The text discusses advanced semiconductor materials for optoelectronic applications, focusing on ternary and quaternary compounds. II-VI, III-V (sphalerite/wurtzite), I-III-VI_2, and II-IV-V_2 (chalcopyrite) families show growing potential in nonlinear optics and solar cells, with additional applications in nanotechnology, hybrid materials, and spintronics.

For I_x-III_{1-x}-VI_2 alloys (I=Cu, Ag; III=Al, Ga, In; VI=S, Se, Te), physical properties exhibit strong composition dependence, requiring precise control of stoichiometry through improved growth techniques and electronic structure analysis.

The quaternary $Ag_{1-x}Cu_xInSe_2$ system bridges ternary chalcopyrite's $CuInSe_2$ (CIS, Eg≈1.00eV, p/n-type) and $AgInSe_2$ (AIS, Eg≈1.22eV, n-type). While CIS maintains a near-ideal chalcopyrite structure, AIS shows a slight tetragonal distortion.

Regarding quaternary nanostructures, ZnCdSSe nanowires/nanobelts represented a breakthrough when first synthesized in 2009. By controlling ZnS/CdSe ratios, they enabled bandgap tuning across 350-710nm. However, this initial achievement required separate samples for different wavelengths rather than continuous tunability in single devices. Earlier work (Zapien et al., 2007) had suggested such quaternary combinations could span the visible spectrum.

I.8. Magnetism in Heusler Alloys

First, different forms of magnetism are presented. Then, examples of applications using magnetic materials are shown. Finally, the key features of Heusler alloys are discussed. Ferromagnetic materials are materials that exhibit magnetic properties similar to those of iron. They can become permanently magnetized. Examples of ferromagnetic materials are nickel, cobalt, and alnico, an aluminum-nickel-cobalt alloy .

Currents produce magnetic fields.

Permanent magnets come from "magnetization currents" flowing inside the material. The magnetization currents in materials come from the electrons' orbital motion and spin. Electrons have an intrinsic feature called spin. Because they contain spin, they have a magnetic moment, akin to a tiny current loop. Electrons by themselves function like little magnets. If you pick an axis, an electron's magnetic moment can be parallel or antiparallel to this axis. In an atom, the electrons are grouped in orbitals. A circling electron can have an extra magnetic moment similar to the magnetic moment of a small current loop.

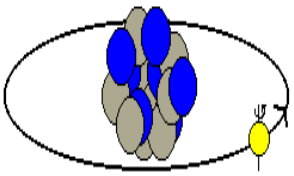

Figure I.11. The magnetic moments of the electrons in an atom do not completely cancel out, so the atom will act like a tiny magnet. Typically, an iron core magnifies the field by a factor of 100 to 1000. When the current in the coil is reduced to zero, the soft iron core loses its magnetization.

I.8.1. Full-Heusler Alloys (X_2YZ)

The magnetic behavior differs fundamentally due to two X atoms occupying tetrahedral sites.

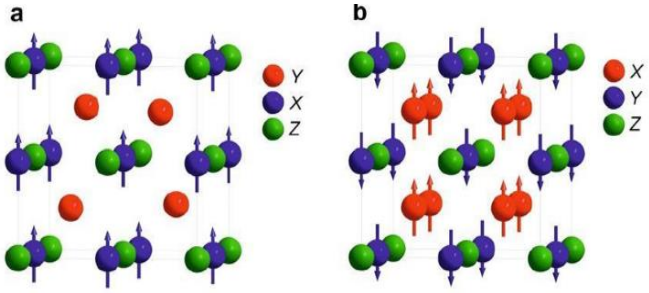

Figure I.12: (a) XYZ-type Half-Heusler alloys - only one magnetic sublattice exists since solely atoms in octahedral sites carry localized magnetic moments. (b) X_2YZ Heusler alloys

exhibit two magnetic sublattices capable of either ferromagnetic or antiferromagnetic coupling.

I.8.2. Half-Metallic Ferromagnetism

In the 1980s, the remarkable magneto-optical properties of numerous Heusler compounds stimulated the examination of their electronic structure, leading to an unexpected finding. Depending on the spin orientation, some Heusler materials exhibit metallic behavior while simultaneously displaying insulating qualities in the opposite spin orientation, a phenomenon referred to as half-metallic ferromagnetism [36]. De Groot et al. created a categorization system defining three unique forms of half-metallic ferromagnetism [37].

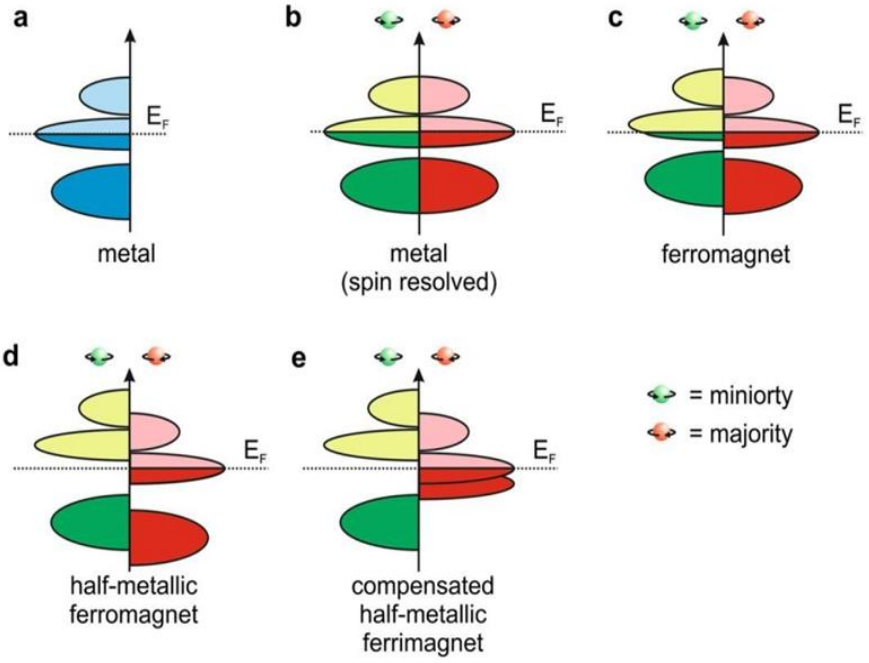

Figure I.13: Schematically illustrates the density of states (DOS) for four distinct cases: (a) A conventional metal showing finite DOS at the Fermi level with identical spin-up and spin-down states, (b) A spin-polarized metal demonstrating asymmetric spin distribution. (c) A ferromagnetic material with shifting majority/minority spin states causing net magnetization (d) A half-metallic ferromagnet (HMF) displaying metallic behavior for one spin channel and insulating for the other.

Theoretically, complete spin polarization in HMFs needs zero temperature and negligible spin-orbit coupling. Heusler compounds, mainly composed of 3d transition elements, characterized by inherently weak spin-orbit coupling, are ideal candidates for exhibiting half-metallic ferromagnetic characteristics.

I.8.4. Compensated Ferrimagnets

Half-metallic ferrimagnetic materials are prime candidates for magnetoelectronic applications. Their key advantage lies in their reduced net magnetic moment, which results from the compensation of moments carried by different sublattices.

- ✓ **Spin-Transfer Torque (STT) Technology:**

STT offers Ultra-low-power switching (writing) capability, scalable binary cells below 10 nm, and a critical development pathway for practical spintronic devices.

For RF applications, a novel integrated Spin-Transfer Torque Nano-Oscillator (STTNO) has been proposed for telecommunications. In such devices, STT drives: Magnetization precession in free magnetic layers. Microwave generation at GHz frequencies.

- ✓ **Tunnel Magnetoresistance (TMR) Discovery:**

The TMR effect was first observed at room temperature in magnetic tunnel junctions using disordered CsCl-type (B_2) electrodes. To clarify the relationship between atomic disorder and spin polarization, Miura et al. theoretically investigated the electronic structure of $Co_2Cr_xFe_{1-x}Al$ using first-principles calculations.

- ✓ **GMR in Modern Technology:**

Today, GMR-based spin valves are ubiquitous in daily life, particularly in hard disk drives. A typical spin valve consists of two ferromagnetic layers sandwiched around an ultra-thin non-magnetic metallic spacer.

I.8.5. Half-Heusler Alloys

Semi-Heusler compounds possess only one magnetic sublattice, as magnetic moments are exclusively carried by atoms occupying octahedral sites (see Figure I.15). While numerous ferrimagnetic or antiferromagnetic compounds in literature are casually classified as semi-Heusler materials, most—including CrMnSb and FeMnSb—crystallize in different structural types rather than the genuine semi-Heusler structure [43].

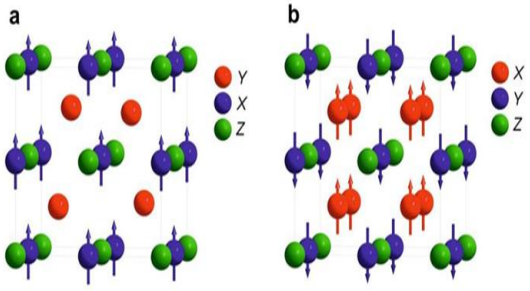

Figure I.14: (a) Half-Heusler XYZ Alloys exhibiting a single magnetic sublattice, where only octahedral-site atoms carry localized magnetic moments.

(b) Heusler X_2YZ compounds possessing two magnetic sublattices capable of ferromagnetic or antiferromagnetic coupling.

I.8.6. Heusler Compounds

In Heusler alloys, two magnetic sublattices enable antiferromagnetic coupling of atomic magnetic moments, yielding ferrimagnetic, ferromagnetic, or even fully compensated ferrimagnetic materials.

I.9. Different Forms of Magnetism

The objective of this chapter is to introduce the context of this thesis. First, different forms of magnetism are presented. Then, examples of applications using magnetic materials are provided. Finally, the main characteristics of Heusler alloys are detailed.

Magnetism represents a set of physical phenomena in which objects exert attractive or repulsive forces on other materials through the quantum spin state of electrons, their orbital motion around the nucleus, and the quantum spin state of the nucleus. In a magnetic atom, the predominant contribution to its total moment comes from the spin and orbital moment of the electrons.

All materials are influenced by the presence of a magnetic moment in more or less complex ways. The magnetic behavior of a material depends on its temperature (and other variables such as pressure and external magnetic field), meaning a material can exhibit different forms of magnetism depending on its temperature.

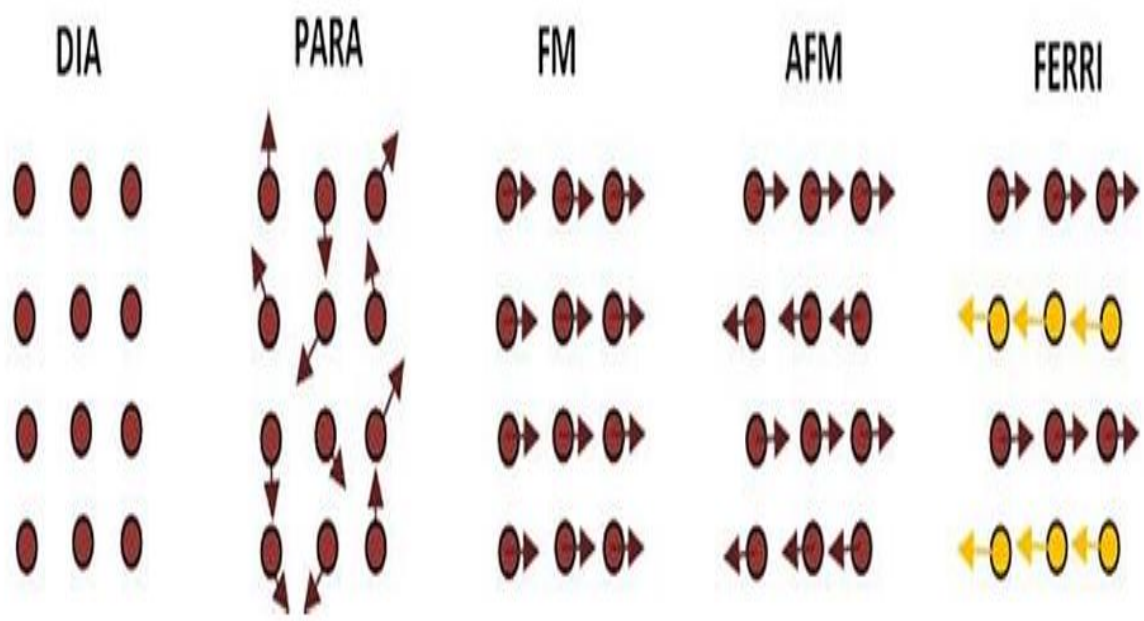

Figure I.16: Different Forms of Magnetism.

I.9.1. Diamagnetism

Diamagnetic materials are materials that possess no intrinsic magnetic moments in the absence of an applied magnetic field. When a field is applied, they develop a magnetic polarization opposite to the field direction. This phenomenon originates from the distortion of atomic orbitals and can be explained by Lenz's law. A negative magnetic susceptibility thus characterizes an isotropic diamagnetic material. In reality, all matter exhibits some diamagnetic response, though it is typically negligible compared to other forms of magnetism. Bismuth, mercury, and silver are examples of diamagnetic materials.

I.9. 2. Paramagnetism

Paramagnetic materials exhibit no net magnetic moment without an external field due to random alignment of magnetic moments at room temperature. When exposed to a magnetic field, their moments align with the field, showing positive magnetic susceptibility. Examples include aluminum, manganese, and tungsten.

Paramagnetism arises from unpaired electrons in atomic orbitals, giving atoms magnetic dipole moments that align with external fields. Materials like aluminum, oxygen, titanium, and FeO demonstrate this property. A key chemical rule states: particles with all paired electrons are diamagnetic, while those with unpaired electrons are paramagnetic.

I.9. 3. Ferromagnetism

In ferromagnetic materials, magnetic moments interact and tend to align parallel to one another. This inter-moment interaction is called exchange coupling. Without an applied field, the moments organize into complex geometries called magnetic domains. This arrangement minimizes the system's total energy. Numerous moments are aligned within a domain, with abrupt directional changes at domain boundaries.

I.9.4. ferrimagnetism

Ferrimagnetic materials contain atomic populations with opposing but unequal magnetic moments, resulting in net spontaneous magnetization. This occurs when different atoms/ions (e.g., Fe^{2+} and Fe^{3+}) contribute unequal moments. Similar to ferromagnets, ferrimagnets are magnetically responsive and can form permanent magnets.

Magnetite (Fe_3O_4), historically misclassified as ferromagnetic, was recognized as the first ferrimagnetic material after Néel's 1948 discovery. Modern applications include data storage (hard drives) and biomedical technologies.

I.9.5. antiferromagnetism

Antiferromagnetic materials feature an ordered alignment of atomic magnetic moments where neighboring spins (on different sublattices) orient in opposite directions. First theorized by Lev Landau (1933), this phenomenon persists below the Néel temperature, above which materials become paramagnetic.

I.9.6. Pauli paramagnetic

For some alkali metals and noble metals, conduction electrons are weakly interacting and delocalized in space forming a Fermi gas. For these materials one contribution to the magnetic response comes from the interaction between the electron spins and the magnetic field known as Pauli paramagnetic.

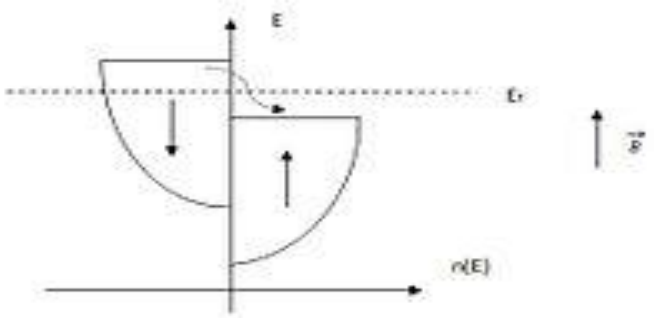

Figure I.16. the additional energy per electron from the interaction between an electron spin and the magnetic field

I.10. Magnetic Resonance Imaging and Cell Tracking

Molecular and cellular imaging are typically used to study disease or transgene expression. SPIONs are excellent contenders for MRI-based molecular and cellular imaging because they have a biodegradable iron core, can be magnetically controlled, and can reduce signal intensity. A successful MRI application of SPIONs is in specific cell tracking. In vivo, cell tracking will allow monitoring of cell migration across and within tissues and provide molecular data illustrating cell survival and function there. Another application is in pancreatic islet cell transplantation and novel stem-cell-based therapies that can be followed using MRI cell tracking. NPs should have colloidal stability and be less hazardous in a biological context for magnetic resonance imaging (MRI) with MNPs. MNPs have been engaged as non-invasive and non-radioactive nano tracers.

I.10.1. Toxic Effects of Magnetic Nanoparticles

Safety considerations are crucial when thinking about both in vivo and extracorporeal MNP usage. Initially, it was thought that nanoparticles had little to no impact on living things

because of their small size. Adverse consequences were not found until later when scientists began more thorough investigations into the potential hazards of nanoparticles. Although the same procedures used to evaluate chemical compounds in solution are used to assess the toxicity of nanoparticles in vitro, the problem with this is that nanoparticles may behave differently and do not have the same properties as chemical molecules in solution. As a result, it is crucial to create methodologies that are specific to the risk evaluation of nanoparticles and any potential negative effects that MNPs may have.

I.10. 2. Future of Magnetic Nanoparticles in Medicine

Although magnetic nanoparticles have been reported for great clinical application, some challenges still exist. The major challenges associated with the use of nanoparticles are safety, toxicity, and characterization. Future experiments should be directed toward the improved characterization of magnetic nanoparticles as well as drug loading efficiency. There is a need to minimize dose dumping and reduction in immune response. The toxicity of magnetic nanoparticles depends on many factors; therefore, future research must be focused on better ways of assessing the toxicity of magnetic nanoparticles, not only in in vitro experiments but also in in vivo applications.

In conclusion, all compounds obey the Slater-Pauling rule, the origin of which can be explained in orbitals hybridization. Among the considered compounds, we have identified 41 half-metals, 8 spin gapless semiconductors which have either 21 or 26 valence electrons per unit cell, 2 magnetic semiconductors (CrVTiAl is an antiferromagnetic and CoVTiAl a ferromagnetic semiconductor), and 9 semiconductors. All magnetic compounds are expected to have high Curie temperatures making them suitable for spintronics/magneto electronics applications. The effect of deformations and defects on these alloys' properties remains an open issue to be addressed in future studies 51 quaternary Heusler compounds. Firstly:5 Heusler compounds spin-gapless semiconductors $M_T = Z_T$-18. Secondly: 36 Heusler compounds Similar for the compounds obeying the $M_T = Z_T$-18 slater-Pauling rule. Thirdly: for the compounds obeying magnetic semiconductors or spin-gaples semiconductor 4 Heusler compounds ($M_T = Z_T$-18) and 10 HA ($M_T = Z_T$-24)

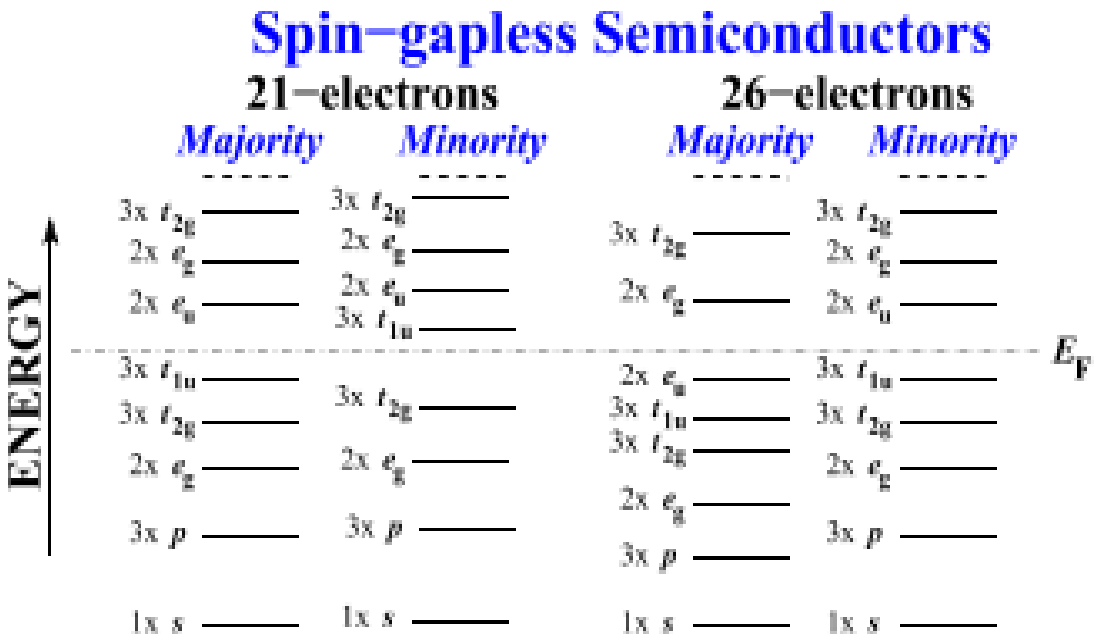

Figure I.17. Schematic representation of the majority-and minority-Spin electronic band

Chapter II

The theory of density functional DFT

Chapter II: The theory of density functional DFT

II.1. Introduction

In the 1920s, the mathematical formalization of the motion of a collection of electrons and atoms was introduced by Erwin Schrödinger in the form of a wave equation. This equation is the cornerstone of quantum physics. Unfortunately, however, it has an exact solution only for atomic or molecular systems containing a single electron. For this reason, in most cases, the equation is too complex to admit an analytical solution, so its resolution is approximated. The goal of quantum physics is to obtain a solution to the Schrödinger equation that is as close as possible to that of the real physical system.

One of the challenges in solid-state physics, which remains a current topic of research for condensed matter physicists, is understanding and mastering the intricate organization of the particles that make up crystals.

In this chapiter II will introduce the various approximation methods used to calculate electronic properties in solids. After discussing the limitations of approaches based directly on the N-body wave function, I will present Density Functional Theory (DFT), which is based on the Hohenberg-Kohn theorem and will serve as the general theoretical framework for this thesis. The principles discussed here are very general, and only developments in the field of condensed matter are addressed. Subsequently, I will explain the formalism used, particularly the Kohn-Sham equations and the importance of the exchange-correlation functional, as well as the different types of functionals (GGA, mBJ…. etc.).

II.2. The Schrödinger equation of a crystalline solid

A crystal can be considered as a system consisting of a large number of interacting particles (electrons and nuclei), where electrons are light particles and nuclei are much heavier.

In the case of a stationary state, the Schrödinger equation is expressed as follows:

$$\mathrm{H}\Psi = \mathrm{E}\Psi \qquad \text{(II. 1)}$$

H : The Hamiltonian operator includes the kinetic energy and potential energy of the particles.

Ψ : The wave function of the system.

E : The total energy of the crystal.

$$H = T_e + T_n + V_{e-e} + V_{n-n} + V_{e-n} \qquad \text{(II. 2)}$$

The kinetic energy of the *N* electrons, each with mass m_e :

$$T_e = \sum_{i=1}^{N} \frac{P_i^2}{2m_e} = \sum_{i=1}^{N} \frac{-\hbar^2}{2m_e} \Delta_i \qquad \text{(II. 3)}$$

The kinetic energy of the *N* nuclei, each with mass M_n :

$$T_n = \sum_{i=1}^{n} \frac{P_i^2}{2M_n} = \sum_{i=1}^{n} \frac{-\hbar^2}{2M_n} \Delta_i \qquad \text{(II. 4)}$$

The repulsive Coulomb electron-electron interaction is given by:

$$V_{e-e} = \frac{1}{2} . \frac{1}{4\pi\varepsilon_0} \sum_{i \neq j} \frac{e^2}{\left| \vec{r_i} - \vec{r_j} \right|} \qquad \text{(II. 5)}$$

The repulsive Coulomb nucleus-nucleus interaction is described by:

$$V_{n-n} = \frac{1}{2} . \frac{1}{4\pi\varepsilon_0} \sum_{\alpha \neq \beta} \frac{Z_\alpha \, Z_\beta \, e^2}{\left| \overrightarrow{R_\alpha} - \overrightarrow{R_\beta} \right|} \qquad \text{(II. 6)}$$

The attractive Coulomb electron-nucleus interaction is given by:

$$V_{e-n} = -\frac{1}{4\pi\varepsilon_0} \sum_{i,\alpha} \frac{Z_\alpha \, e^2}{\left| \vec{r_i} - \overrightarrow{R_\alpha} \right|} \qquad \text{(II. 7)}$$

$Z_\alpha \, Z_\beta$ are the atomic numbers of the α and β nuclei.

$\vec{r_i}$ $i = 1 \ldots N$ represents the coordinates of the electrons.

$\overrightarrow{R_\alpha}\ \alpha = 1 \ldots\ldots n$ are the coordinates of the nuclei.

The Schrödinger equation can therefore be represented in the form:

$$(T_e + T_n + V_{e-e} + V_{n-n} + V_{e-n})\Psi\left(\overrightarrow{r_1}, \overrightarrow{r_2}, \ldots \overrightarrow{R_1}, \overrightarrow{R_2} \ldots\right) = \mathrm{E}\Psi(\overrightarrow{r_1}, \overrightarrow{r_2}, \ldots . \overrightarrow{R_1}, \overrightarrow{R_2} \ldots) \quad \text{(II.8)}$$

For a system with n atoms and N electrons, the problem to be addressed is a problem with (n + N) particles in electronic interaction. The exact resolution of the equation is impossible except for the hydrogen atom and hydrocenid systems. For polyelectronic systems the equation contains $3(z+1)n$ variables. Since we find in a $1cm3$ of a crystalline solid nearly 10^{22} atoms, it is necessary to use approximation methods to solve the Schrödinger equation approximately. The three main levels of simplification generally used are:

1- The Born-Oppenheimer approximation or adiabatic.

2- The Hartree-Fock approximation or the formalism of Density Functional Theory.

3- The approximations inherent in solving equations.

II.3. The Born-Oppenheimer approximation

This approximation consists of assuming that nuclei much heavier than an electron move relatively slowly and can be considered as stationary. We can therefore admit that the nuclei are considered immobile [45]. The resolution of the Schrödinger equation only concerns the wave function of the electrons, since the kinetic energy of the nuclei becomes zero.$(T_n = 0)$ et energy interaction noyau-noyau (v_{n-n})becomes constant, but which can be made zero by a suitable choice [46] of the origin. Therefore, the new Hamiltonian is written in the form as follows:

$$H_e = T_e + V_{e-e} + V_{e-n} \quad \text{(II. 9)}$$

$$H_e = \sum_{i=1}^{N} \frac{-\hbar^2}{2m_e}\Delta_i + \frac{1}{2}.\frac{1}{4\pi\varepsilon_0}\sum_{i\neq j}\frac{e^2}{\left|\ \vec{r_i} - \vec{r_j}\ \right|} - \frac{1}{4\pi\varepsilon_0}\sum_{i,\alpha}^{n}\frac{Z_\alpha\, e^2}{\left|\ \vec{r_i} - \overrightarrow{R_\alpha}\ \right|} \quad \text{(II. 10)}$$

The electronic Schrödinger equation can then be written as follows:

$$\mathrm{H_e}\Psi = \mathrm{E_e}\Psi \quad \text{(II. 11)}$$

E_e: represents the energy of electrons moving in the field created by fixed nuclei.

L'approximation adiabatique réduit le degré de complexités mais reste difficile à résoudre l'équation, pour cela d'autres approximations sont introduites comme la méthode de Hartree et Hartree-Fock.

II.4. The Hartree approximation and Hartree-Fock approximation

II.4.1. The Hartree approximation

which considers that the electrons move independently of each other, in which each electron moves in a mean field created by the nuclei and the other electrons. There fore the Hamiltonien of the system as written:

$$H = \sum_{i=1}^{N} h(i) \qquad \text{(II. 12)}$$

And the electronic wave function that allows this Hamiltonian to be solved is made up of a mono-electronic product [47]:

$$\Psi(\vec{r}\,) = \prod_{i=1}^{N} \Psi_i(\vec{r}_i) \qquad \text{(II. 13)}$$

The Schrödinger equation for N electrons reduces to N Schrödinger equations for 1 electron:

$$\left[-\frac{\hbar^2}{2m_e}\nabla^2 + V_{ext}(\vec{r}) + V_H(\vec{r})\right]\psi_i(\vec{r}) = E\,\psi_i(\vec{r}) \qquad \text{(II. 14)}$$

$V_{ext}(\vec{r})$ Represents the attractive interaction between the electron and the nuclei.

$V_H(\vec{r})$ is the potential of Hartree:

$$V_H(\vec{r}) = \sum_j \int \left|\psi_j(r')\right|^2 \frac{e^2}{|r-r'|} dr' \qquad \text{(II. 15)}$$

II.4.2. Hartree-Fock approximation

However, the obtained wave function called Hartree product (Eq. 5) is not antisymmetric and does not respect the Pauli exclusion principle [48]. Taking into account the indistinguishability and the spin of the electrons, Fock [49] and Slater proposed to express the total wave function Ψ in the form of a Slater determinant [50]:

$$\psi(\vec{r}_1,\vec{r}_2,.....\vec{r}_N) = \frac{1}{\sqrt{N!}}\begin{vmatrix} \psi_1(\vec{r}_1) & \psi_2(\vec{r}_1).....\psi_N(\vec{r}_1) \\ \psi_1(\vec{r}_2) & \psi_2(\vec{r}_2).....\psi_N(\vec{r}_2) \\ . & . & . \\ \psi_1(\vec{r}_N) & \psi_2(\vec{r}_N).....\psi_N(\vec{r}_N) \end{vmatrix} \qquad \text{(II. 16)}$$

$\frac{1}{\sqrt{N!}}$ is a normalizing factor. [51] :

The variational principle then makes it possible to calculate this function by minimizing the total energy with respect to the monoelectronic wave functions ψ_i. This reduces us to a monoelectronic wave equation which is a generalization of the Hartree equation:

$$\left[-\frac{\hbar^2}{2m_e}\nabla^2 + V_{ext}(\vec{r}) + V_H(\vec{r}) + V_X(\vec{r})\right]\psi_i(\vec{r}) = E\,\psi_i(\vec{r}) \qquad \text{(II. 17)}$$

$V_x(\vec{r})$ is the Fock term [52] defined by its action on a wave function$\psi_i(\vec{r})$:

$$V_x(\vec{r})\psi_i(\vec{r}) = -\sum \delta_{\sigma_i\,\sigma_j}\,\psi_j(\vec{r}) \int \frac{\psi_j^*(\vec{r})\,\psi_i(\vec{r})}{|\vec{r}-\vec{r}'|}\,d^3\,\overrightarrow{r'} \qquad \text{(II. 18)}$$

The spin term $\delta_{\sigma_i\,\sigma_j}$ take into account here.

This potential is zero for electrons with antiparallel spins whereas $V_{ext} et\, V_H$ are the same as those in the Hartree equation. The Fock exchange term arises because electrons are fermions and therefore obey the Pauli principle. Let's consider a system with only two electrons. We will find that the exchange term is responsible for the separation of energy between the two electrons: we then see that the exchange is an effective magnetic interaction between spins, which emerges from a purely electrostatic interaction. The energy obtained from the Hartree-Fock approximation is not exact due to the absence of correlation energy; it will be parametrized in the density functional theory.

II.4.3. Modern Ab Initio Methods

To be able to perform ab initio calculations of large molecules in a reasonable amount of time, more approximations must be accepted in wave or Hamilton functions and waveforms expressed as linear summation of a properly selected function base. The rule of functions is chosen based on physical considerations or the efficiency of calculations.

For optimized single electron functions, this method is called the Hartry method. Hartree-Foock proposed using the product of space functions and spinning functions as single electron functions and writing the total wave function as the slitter determinant. These total wave functions are called the self-harmonized field Hartry-Fock SCF-HF. Even in these advanced models of a single electron, the instantaneous effect of electrons is not included in the calculations. The error in the total energy due to this effect is called correlation energy, which may lead to completely wrong results in some calculations.

II.5. Density Functional Theory (DFT)

II.5.1. Origin of DFT

Using density as a variable instead of the wave function is the idea that Thomas and Fermi suggested in 1927 [53]. They proposed modeling the kinetic term of the Schrödinger equation using a particular explicit density functional. The weak point of this approach lies in the expression of the kinetic energy, which does not consider the atomic orbitals (it does not allow for the explanation of the covalent bond, for example). And also, the precision

obtained was lower than that of Hartree-Fock because of the absence of the exchange term. Dirac improved this theory by adding an exchange energy functional of the electron density to the latter, but the electron correlation term was still absent in this new approach. Nevertheless, using the density leads to simpler resolutions than in the case of the wave function. The approach of Hohenberg and Kohn made it possible to establish a rigorous working framework to free oneself from any approximation.

II.5.2. Formalism of Density Functional Theory (DFT)

The Density Functional Theory (DFT) is a theoretical framework for studying systems with numerous interacting electrons. Unlike traditional methods that rely on analyzing the wave functions of individual electrons, DFT characterizes the system's total energy primarily in terms of its electronic density.

II.5.3. Hohenberg and Kohn's theorem

The main objective of DFT is to replace the multi-electron wavefunction with the electron density as the basic quantity for calculations. While the multi-electron wavefunction depends on 3N variables (where N is the total number of particles in the system), the density is a function of three variables, making it an easier quantity to treat mathematically and conceptually.

II.5.4. Definition of Electron Density

Electron density $\rho(\vec{r})$ is the probability of finding one of the N electrons in the volume element $d^3\vec{r}$. $\rho(\vec{r})$. Is a positive function depending only on the 3 coordinates (x, y, z) of space (3 variables) which tends to zero when r tends to infinity and whose integral over all space gives the number N of electrons [54,55,56,57] :

$$\int \rho(\vec{r}) d_{\vec{r}} = N \qquad \text{(II. 19)}$$

$$\rho(\vec{r} \longrightarrow \infty) = 0$$

II.5.5. First theorem of Hohenberg and Kohn

If we consider an electron gas, the external potential acting on these particles determines the ground state of this system and the corresponding charge density. Thus, all physical quantities concerning this state (such as the system's total energy) are functionals of the external potential. As was initially demonstrated by Hohenberg and Kohn, due to the one-to-one correspondence between the external potential V_{ext}et the ground state electron density

$\rho(\vec{r})$: $\rho(\vec{r}) \leftrightarrow V_{ext}$, allowing the first to be expressed as a functional of the second, the total energy of the system in the ground state is also a unique universal functional of the electronic density, i.e.: $E = E[E(\rho)]$

II.5.6. Second theorem

The second theorem of Hohenberg and Kohn [58] is a variational principle analogous to that initially proposed in the Hartree-Fock approach for a functional of the wave function:

$$\frac{\partial E(\psi)}{\partial(\psi)} = 0 \qquad \text{(II. 20)}$$

but this time applied to an electron density functional:

$$\left(\frac{\partial E[\rho(\vec{r})]}{\partial\, \rho(\vec{r})}\right)_{\rho_0(\vec{r})} = 0 \qquad \text{(II. 21)}$$

$\rho_0(\vec{r})$s the ground state electron density. This second theorem states that for any multi-electronic system with electron number N and an external potential V_{ext}.t.tthe total energyf the system $E[\rho(\vec{r})]$ reaches its minimum value when the density ρrcorresponds to the exact density of the ground state Rho$\rho_0(\vec{r})$:

$$E(\rho_0) = minE(\rho) \qquad \text{(II. 22)}$$

The demonstration that the total energy of a system in the ground state is a functional of the electron density, Hohenberg and Khon express this functional $E[\rho(\vec{r})]$ according to the following expression:

$$E[\rho(\vec{r})] = F_{HK}[\rho(\vec{r})] + \int V_{ext}(\vec{r})\rho(\vec{r})d^3\vec{r} \qquad \text{(II. 23)}$$

In which $V_{ext}(\vec{r})\rho(\vec{r})$ represents the external potential acting on these particles and $F_{HK}[\rho(\vec{r})]$ rrepresents the universal Hohenberg-Kohn functional. Unfortunately, the Hohenberg-Kohn theorem gdoes not indicate the form of, cap F end subscript sub cap H cap K , open bracket rho open paren r $\vec{}$, close paren close bracket. Here is no exact formulation to express kinetic energy as a functional of electron density. The Khon and Sham equations [59,60,61] present the only solution to this problem, which is established to provide the necessary foundations to effectively exploit the Hohenberg and Khon theorems.

II.6. The Kohn and Sham equations

The solution of Kohn and Sham equations is the basis of DFT calculations, as we have already mentioned the exact form of exchange-correlation potential VXC is unknown. In 1967 Kohn-Sham [59,60,61] proposed that there exists a so-called auxiliary or fictitious system of non-interacting electrons subjected to an external potential $V_{ext}(\vec{r})$ such that it has the same electron density as the real system. By application of the Hohenberg-Kohn theorem, this auxiliary potential is defined uniquely. The electron density can then be exactly identified with the Sum over occupied states:

$$\rho(\vec{r}) = \sum_{i=1}^{N_{occ}} |\emptyset_i|^2 \qquad \text{(II. 24)}$$

This approach achieves an exact correspondence between the electron density, the ground state energy of a system consisting of non-interacting fermions placed in an effective potential and the real system with several interacting electrons subjected to the potential. Therefore, the electron density and energy of the real system are conserved in this fictitious system.

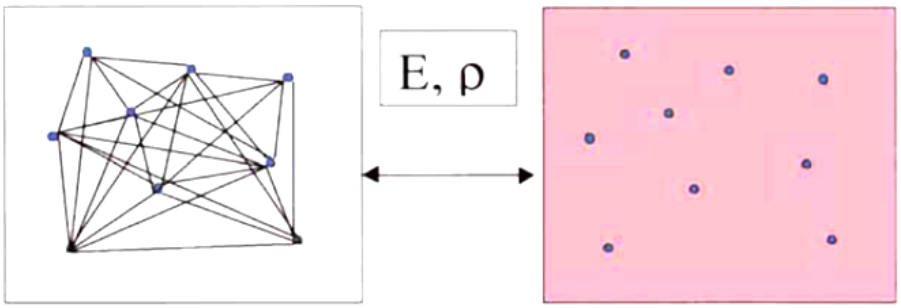

Figure II.1. (a) Real system consisting of several electrons in mutual interaction, (b) Fictitious system of independent fermions of the same energy and electronic density as the real system.

For this fictitious system of non-interacting fermion-like particles, the Hohenberg-Kohn theorem also applies. The density functional $F_{HK}[\rho(\vec{r})]$ Therefore, the interacting system can be expressed as the sum of the kinetic energy of the non-interacting electron gas characterized by the same density as that of the real system. The classical Coulomb interaction between electrons described through their charge density (i.e. the Hartree term) is an additional functional describing the inter-electronic interaction not provided from the

non-interacting system. The difference between the real kinetic energy and that of the non-interacting electrons as well as the difference between the real interaction energy and that of the Hartree are taken into account in the exchange and correlation energy $E_{xc}[\rho(\vec{r})]$:

$$E_{xc}[\rho(\vec{r})] = \left[T_r[\rho(\vec{r})] - T_0[\rho(\vec{r})] + V_{ee}[\rho(\vec{r})] - V_H[\rho(\vec{r})]\right] \quad \text{(II. 25)}$$

$T_r[\rho(\vec{r})]$: The kinetic energy of an interacting electron gas (real)

$T_0[\rho(\vec{r})]$: The kinetic energy of a non-interacting gas.

V_H : Hartree's term

The density functional $F_{HK}[\rho(\vec{r})]$ for the interactive system can be expressed by the following expression:

$$F_{HK}[\rho(\vec{r})] = T_0[\rho(\vec{r})] + V_H[\rho(\vec{r})] + E_{xc}[\rho(\vec{r})] \quad \text{(II. 26)}$$

The Schrödinger equation to be solved using the Kohn and Sham approach is of the following form:

$$H_{KS}\phi_i(\vec{r}) = \left[-\frac{\hbar^2}{2m_e}\nabla^2 + V_{eff}(\vec{r})\right]|\phi_i(\vec{r})\rangle = \epsilon_i|\phi_i(\vec{r})\rangle \quad \text{(II. 27)}$$

Where the effective potential is of the form:

$$V_{eff} = V_{ext} + V_H + V_{xc} \quad \text{(II. 28)}$$

$$V_{eff} = V_{ext} + \frac{1}{4\pi\varepsilon_0}\int \frac{\rho(\vec{r})}{|r - r'|}d^3\vec{r} + \frac{\partial E_{xc}[\rho(\vec{r})]}{\partial\rho(\vec{r})} \quad \text{(II. 29)}$$

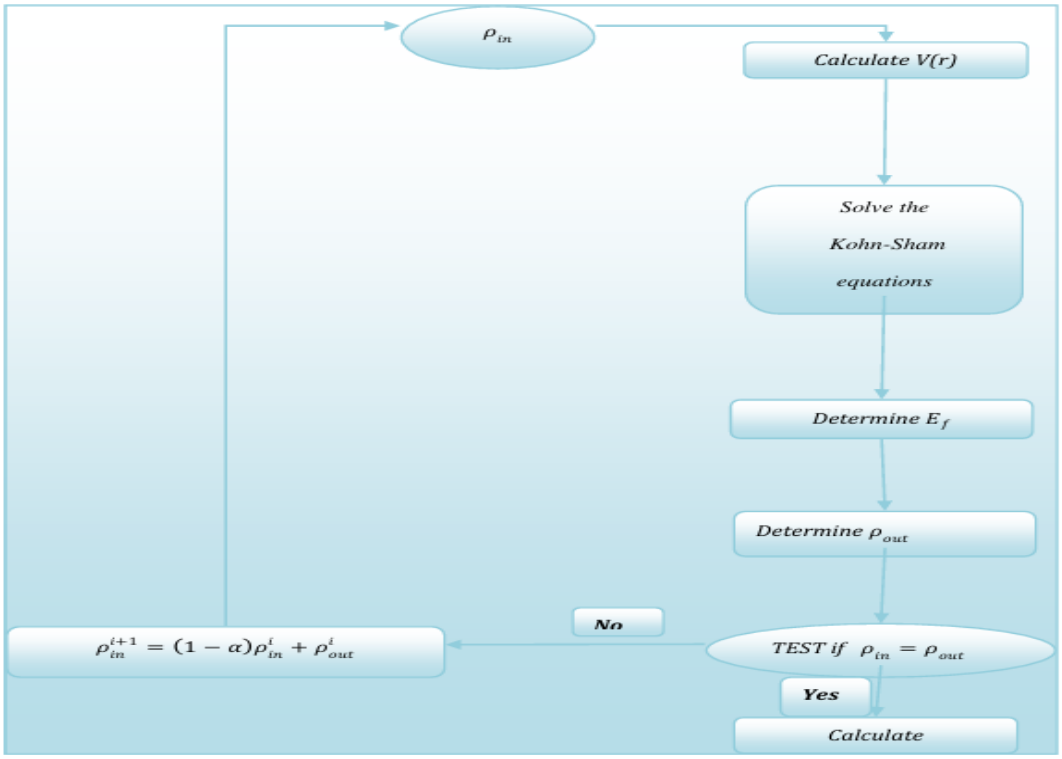

Figure II.2. Self-consistent calculation steps.

II.7. Different types of functionals

II.7.1. Local density approximation (LDA)

The LDA approximation [62] consists in considering that the electron density can be treated locally in the form of a uniform electron gas. The correlation exchange part of the total energy of the ground state of the electronic system is expressed according to the following equation:

$$E_{xc}^{LDA}[\rho(\vec{r})] = \int \rho(\vec{r})\varepsilon_{xc}^{hom}[\rho(\vec{r})]d^3\,\vec{r} \qquad (II.30)$$

$E_{xc}^{LDA}[\rho(\vec{r})]$ Represents the exchange–correlation energy of mutually interacting electrons of uniform density $\rho(\vec{r})$.

In the case of magnetic materials, the electron spin provides an additional degree of freedom and LDA must then be extended to the local spin density approximation (LSDA):

$$E_{xc}^{LSDA}[\rho(\vec{r})] = \int \rho(\vec{r})\varepsilon_{xc}^{hom}[\rho_{\uparrow}(\vec{r})\ \rho_{\downarrow}\ (\vec{r})]d^3\,\vec{r} \qquad (II.31)$$

II.7.2. The advantages and disadvantages of the LDA method

In general, LDA and LSDA approximations give good results for describing structural properties, also concerning the lattice parameter for the majority of solids. The treatment of the exchange-correlation energy from LDA works relatively well in the case of metals for which the density is highly uniform but this model remains insufficient in inhomogeneous systems or materials containing transition metals. Besides the problem of the band gap. LDA generally slightly underestimates bond distances and overestimates cohesion energies [62].

II.7.3. Generalized Gradient Approximation (GGA)

The generalized gradient approximation (GGA) [63] consists of making dependent not only on the electron density but also on its gradient, i.e. including a gradient correction, to take into account locally inhomogeneities of the densities in the treatment of the exchange-correlation energy. The expression E_{xc} is written as a function of the electron density and its gradient will be in the following form [64]:

$$E_{xc}^{GGA}[\rho(\vec{r})] = \int \rho(\vec{r})\varepsilon_{xc}[\rho(\vec{r})\ \nabla\rho\ (\vec{r})]d^3\,\vec{r} \qquad (II.32)$$

GGA gives a better description of the equilibrium volume although it leads to a significant increase in the lattice parameters of some materials containing heavy elements (transition metals), also provides good results for elastic moduli and magnetic properties of the compounds compared to calculations carried out in LDA.

$$E(\rho) = \sum_{ioccup} \varepsilon_i - \int \frac{\rho(r)\rho(r')}{|r-r'|} dr dr' + E_{XC}(\rho) - \int V_{XC}(r)\,\rho(r)\,dr \qquad \text{(II. 33)}$$

II.7.4. The mBJ approximation

The electronic structure of periodic solids can be calculated using the Kohn and Sham equations given by:

$$\left(-\frac{1}{2}\nabla^2 + \upsilon_{eff.\sigma}^{K-S}(r)\right)\psi_{i,\sigma}(r) = \varepsilon_{i,\sigma}\psi_{i,\sigma}(r) \qquad \text{(II. 34)}$$

Where $\psi_{i,\sigma}$: are the single-electron wave functions.

The Kohn and Sham effective potential is written as follows:

The Kohn and Sham effective potential is written as follows:

$$V_{eff.\sigma}^{KS} = V_{ext} + V_H + V_{xc,\sigma} \qquad \text{(II. 35)}$$

$V_{eff.\sigma}^{KS}$: is the sum of the external potential, the Hartree potential, and the exchange-correlation term. Here, the first two terms are calculated precisely, while the exchange-correlation term requires approximations.

The most commonly used approximate functionals for solids are the Local Density Approximation (LDA) and the Generalized Gradient Approximation (GGA). Although LDA and GGA are reliable approximations for calculating many ground-state energy-related properties of solids such as elastic constants, the stability of different structures, theoretical volume, and compressibility modulus they are not always sufficient for accurately describing other properties, such as the band structure of many semiconductors and insulators.

Recently, Tran and Blaha proposed an alternative approximation to improve the calculation of the energy gap by modifying the Becke-Johnson potential. The Tran and Blaha functional, denoted as (mBj), is a modified version of the Becke and Johnson functional. This functional has quickly demonstrated its effectiveness compared to the most commonly used computational methods, such as LDA or PBE (the GGA version for solids).

$$\upsilon_{x;\sigma}^{mBJ}(r) = c\upsilon_{x;\sigma}^{BR}(r) + (3c-2)\frac{1}{\pi}\sqrt{\frac{5}{12}}\sqrt{\frac{2t_\sigma(r)}{\rho_\sigma(r)}} \qquad \text{(II. 36)}$$

With: $\rho_\sigma(r) = \sum_{i=1}^{N_\sigma}\left|\psi_{i,\sigma}\right|^2$ The electron density.

$t_\sigma(r) = \frac{1}{2}\sum_{i=1}^{N_\sigma}\left|\psi_{i,\sigma}^{*}\nabla\psi_{i,\sigma}\right|^2$ The kinetic energy density.

$\nu_{x,\sigma}^{BR}(r) = -\frac{1}{b_\sigma(r)}\left[1 - e^{X_\sigma(r)} - \frac{1}{2}X_\sigma(r)e^{-X_\sigma(r)}\right]$: The Becke–Roussel potential.

The Becke-Roussel potential is introduced to minimize the Coulomb potential.

$X_\sigma(r)$ is determined by a nonlinear equation involving ρ_σ, $\nabla\rho_\sigma, \nabla^2\rho_\sigma$ and t_σ

The function b_σ is given by:

$$b_\sigma = \left[\frac{x_\sigma^3 e^{-x_\sigma}}{(8\pi\rho_\sigma)}\right]^{\frac{1}{3}} \qquad (II.37)$$

The Becke-Roussel potential proposed here is approximately equivalent to the Slater potential used in Becke and Johnson [66]. The main modification lies in the introduction of the parameter c in the functional formula. Note that if c=1 is taken, the original Becke and Johnson functional is recovered. This parameter was chosen to depend linearly on the square root of the spatial average of $\frac{|\vec{\nabla}\rho(r)|}{\rho(r)}$.

The proposed form for is as follows:

$$c = \alpha + \beta\left(\left(\frac{1}{V_{cell}}\int\frac{|\vec{\nabla}\rho(r')|}{\rho(r')}d^3r'\right)\right)^{\frac{1}{2}} \qquad (II.38)$$

α and β are two free parameters, and V_{cell} is the unit cell volume of the system.

$A = -0.012$ et $\beta = 1.023 bohr^{1/2}$

I.8. Self-consistency in calculations

Solving the Kohn-Sham equations for high-symmetry points in the first Brillouin zone simplifies the calculations. The solution of these equations is performed iteratively using a self-consistent iteration cycle, as illustrated in the flowchart in Figure II.3**.**

The process begins with an initial trial density ρ_{in} for the first iteration. Typically, a superposition of atomic densities is used. The Kohn-Sham (K-S), matrix is then computed, and the expansion coefficients are determined by solving the equations to obtain the (K-S), à cette étape, orbitals. At this stage, the new density ρ_{out}. is calculated. If the density or energy has changed significantly (convergence criterion), the procedure returns to the first step, mixing the two charge densities $\rho_{in}$and ρ_{out} as follows:

$$\rho_{in}^{i+1} = (1-\alpha)\rho_{in}^{i} + \alpha\rho_{out}^{i} \qquad (II.39)$$

Here:

i: Represents the i^{ieme} iteration.

α: A mixing parameter.

This iterative procedure continues until convergence is achieved [64]. The process can be summarized by the schematic below.

II.9. Simulation Code WIEN2K

The Institute of Materials Chemistry in Vienna has harnessed technological advancements, particularly in programming languages, to create the wien2k program package [65], a significant achievement in computational materials science. This esteemed program is renowned for its utility in investigating the properties of solid materials. It encompasses a plethora of subprograms coded in the Fortran language, with the latest iterations boasting sophisticated algorithms designed to adeptly translate crystal system equations rooted in density functional theory (DFT). These cutting-edge algorithms leverage the full potential linearized augmented plane wave (FP-LAPW) method to meticulously compute and analyze compound properties. Through the utilization of wien2k, researchers can delve deeper into the intricate nature of materials, unveiling valuable insights into their structural and electronic characteristics. [66]. The most important subprograms and its role in the Wien2k program are shown in the diagram shown in Figure I.3 which are organized as follows: [67]: NN: This program computes the distances between adjacent neighbors within a set limit, aiding in the calculation of the atomic sphere's radius.

✓ **SGROUP:** determines the space group of the compound.

✓ **SYMMETRY:** is a program that defines the symmetry number and space group symmetry operations of our structure.

✓ **LSTART:** calculates electron densities in free atoms and show how different orbitals will be treated in band structure calculations.

✓ **KGEN:** generates a mesh of K points in the irreducible part of the first Brillouin zone (B.Z). We specify the number of K points in the whole 1^{st}B.Z.

✓ **DSTART**: produces an initial density for the SCF cycle (self-consistent cycle) by a superposition of atomic densities produced in the LSTART subprogram. After the last subprogram; we enter a loop of SFC calculations and therefore we shall reach five steps:

✓ **LAPW0** (POTENTIAL): uses the total electron density to calculate the coulombien and exchange potential (Hartree-Fock potential). In addition to that, it divides the space into a MT (muffin-tin) sphere and an interstitial region.

✓ **LAPW1** (BANDS): calculate eigenvalues and wave functions for valence electrons from solving the equation (III.1).

✓ **LAPW2** (RHO): calculate the valence electron densities obtained in the step LAPW0.

✓ **LCORE**: calculates eigenvalues and wave functions to obtain core electron densities.

✓ **MIXER**: calculate the new density by mixing.

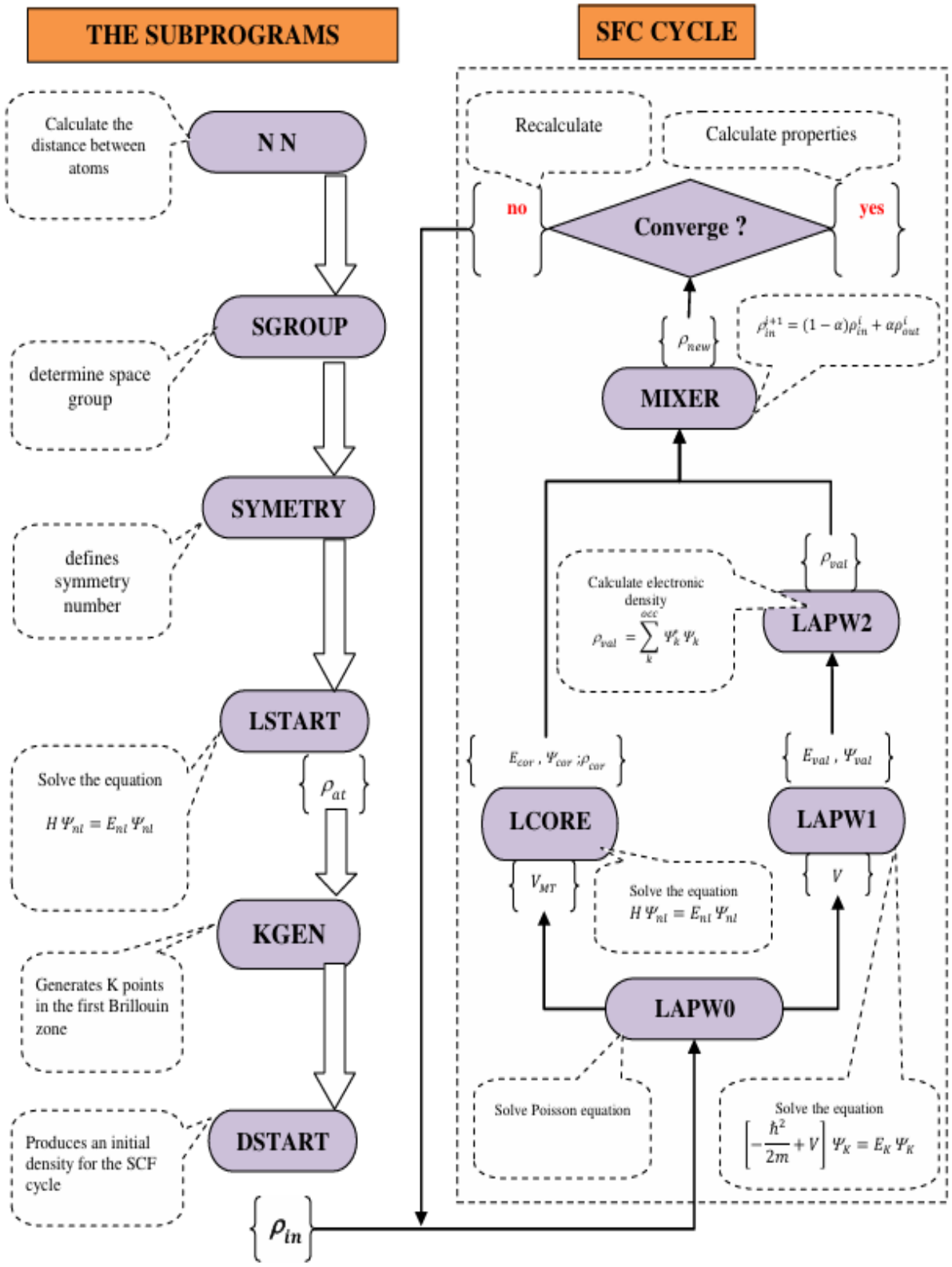

Figure II.3: The flowchart of the program code Wien2k.

Here are several study models to understand the different physical properties of matter at the microscopic scale, which can be classified into four categories:

Empirical models: These are based on experimental data to determine the physical properties of matter.

Semi-empirical models: Simplified quantum models that require experimental data to predict other properties of matter.

Ab initio models: Quantum models that describe all the physicochemical properties of systems. These models rely solely on fundamental physical parameters (such as fundamental constants like atomic number, atomic positions, etc.) and contain no empirical parameters.

Statistical predictions from DFT calculations:

Recently, the results of physical properties of materials calculated using ab initio methods have often been used as databases to predict the properties of new materials. Indeed, there is a growing number of databases that conveniently compile a large number of DFT calculations. Today, these databases are widely used to develop statistical models to reproduce known structure-property correlations of materials and to predict the chemistry of new crystals. Among these databases, we mention: Materials Project, AFLOW (Automatic Flow for Materials Discovery), MPDS Materials Platform, and OQMD (Open Quantum Materials Database).

Chapter III

Results and discussion

Chapter III: Results and discussion

III.1. Introduction

In this work, we conducted a theoretical study to calculate the structural, electronic, magnetic, and optical properties of two compounds, MnCrTiAl and MnCrTiAs, within the framework of Density Functional Theory (DFT) using the Wien2k program based on Ab-initio. We utilized both the Generalized Gradient Approximation (GGA) and the modified Becke-Johnson (mBJ) approximation to calculate the exchange-correlation potential. For the structural properties, we determined the values of the lattice constant, compressibility modulus, and cohesive energy. To understand the electronic behavior of each compound, we calculated and analyzed the electronic band structure and the total (TDOS) and partial (PDOS) electronic density of states. Additionally, we studied the total and partial magnetic moments of the atoms constituting the three compounds. Finally, we calculated the optical properties of both MnCrTiAl and MnCrTiAs by computing the real and imaginary parts of the dielectric function and subsequently deriving other optical parameters such as absorption, refractive index, extinction coefficient, and optical conductivity.

Today, scientific research is primarily based on two complementary approaches: theory and experimentation. However, there remained a major drawback: the analytical resolution of realistic physical models which are highly complex to accurately describe experimental behaviors.

On the other hand, recent advances (in recent years) in computers and algorithms, and more specifically in numerical experimentation, have partially helped overcome this difficulty, despite computation times that can remain long in some cases.

The objective of this chapter is to study the structural properties of the spinel compound MnCrTiZ (Z=Al, As) such as (the lattice parameter, bulk modulus, and its derivative…), the electronic properties, including (the band structure, total and partial density of states) for this compound, and finally the magnetic properties.

The electronic configuration of each element is:

[*Mn*]: $1s^2 2s^2 2p^6 3s^2 3p^6 3d^5 4s^2$.

[*Cr*]: $1s^2 2s^2 2p^6 3s^2 3p^6 3d^5 4s^1$.

[*Ti*]: $1s^2 2s^2 2p^6 3s^2 3p^6 3d^2 4s^2$.

[*Al*]: $1s^2 2s^2 2p^6 3s^2 3p^1$.

[*As*]: $1s^2 2s^2 2p^6 3s^2 3p^6 3d^{10} 4s^2 4p^3$.

III.2. Details of the calculations

We carried out our calculations using the augmented plane wave plus local orbitals method with a full-potential approach implemented in the *Wien2k* code [68]. The algorithm is based on density functional theory (DFT). For the exchange-correlation potential, two approximations were employed [69]:

The Generalized Gradient Approximation (GGA) as parameterized by Perdew, Burke, and Ernzerhof (PBE) [70] Approximation (mBj-GGA), Approximation (mBj).

In the framework of the augmented plane wave method plus local orbitals, space is divided into two regions: a region consisting of non-overlapping spheres surrounding the atomic sites (muffin-tin spheres), of radii R_{MT} and an interstitial region located between the spheres.

The Kohn and Sham wavefunctions are expanded in terms of spherical harmonics inside the muffin-tin spheres for a maximum value of l_{max}=10 and in Fourier series in the interstitial region whose wave functions are extended into plane waves with a cutoff ($R_{MT}\, X\, K_{max} = 9$) R_{MT} is the smallest radius of the muffin-tin spheres and K_{max} is the maximum value of the wave vector used in the plane-wave expansion of the eigenfunctions). Self-consistent calculations are considered to be converged when the total energy is stable. The process of iterative calculations is repeated until the charge convergence is stable within 1mRyd.

The number of special points used in our calculations was determined by convergence tests. These tests were carried out by calculating the variation of the total energy of the system as a function of the number of points *k*. The number of points k chosen for the rest of the calculations is the smallest number for which convergence is achieved. For the integration we use a mesh of 1000 *k*- points in the first Brillouin zone. The radii of the atoms used in the calculations are shown in table III.1.

Table III.1. The values of $R_{M.T} \times K_{max}$, K_{points}, $R_{MT}(X)$ of each constituent and k-point MnCrTiZ (Z=Al, As*)* using GGA.

	R_{MT} x K_{max}	R_{MT}(Mn)	R_{MT}(Cr)	R_{MT}(Ti)	RMT(Y)	k-point
MnCrTiAl	9	2.50	2.46	2.40	2.27	1000
MnCrTiAs	9	2.47	2.41	2.35	2.35	1000

(k-point =10000) for optical.

III.3. The Crystal Structure of Compounds MnCrTiZ (Z=Al, As)

The compounds MnCrTiZ crystallize under ambient conditions in the face-centered cubic structure with a space group $Fd\bar{3}m$ (227), and the following atomic positions: MnCrTiZ (Z=Al, As) Or each atom of Mn.

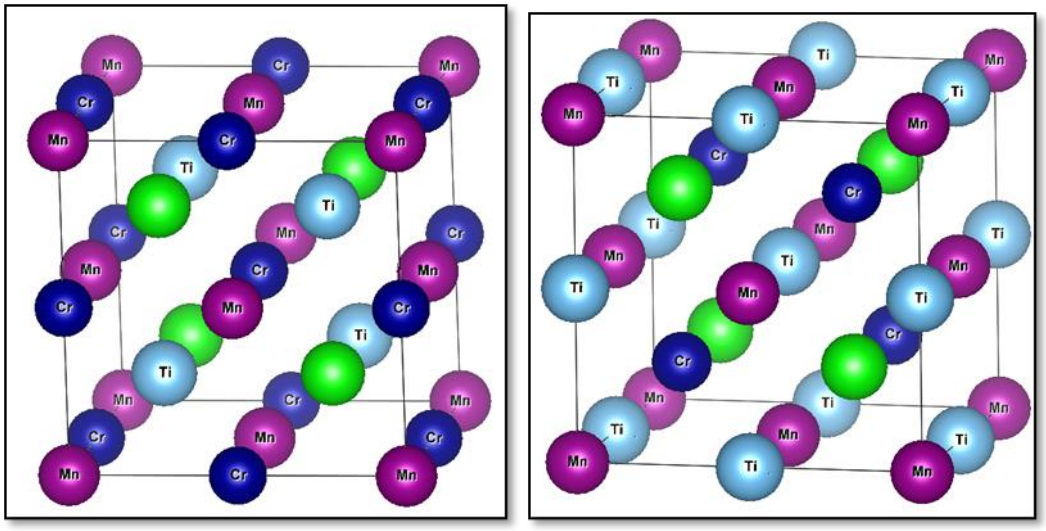

(a) (b)

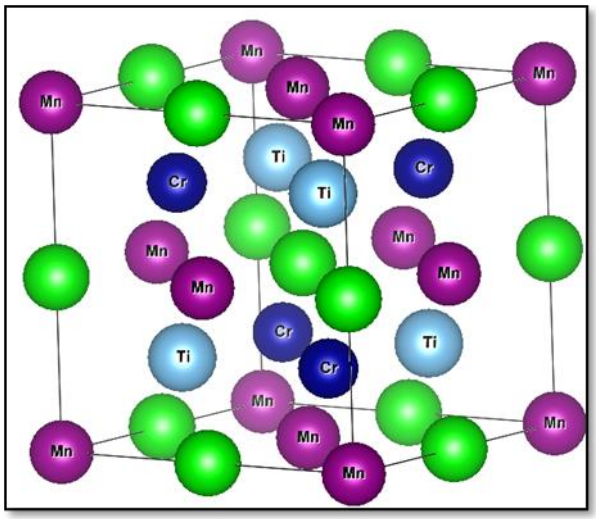

(c)

Figure III.1. Schematic representation of the primitive cell of quaternary Heusler MnCrTiZ (Z=Al, As) (a) type Y_1, (b) type Y_2,(c) type Y_3.

Here we focus our attention on the technologically important crystal structure of the spinel compound MnCrTiZ (Z=Al, As). In this study the face-centered cubic (FCC) phase is completely relaxed for all volumes using force optimization. The calculated atomic positions for our compound using LDA and GGA approximations in the FCC phase are presented in

Table III.2. Atomic positions for three distinct types of quaternary Heusler compounds Heusler MnCrTiZ (Z=Al, As) alloys [71].

	4a (0,0,0)	4c (1/4,1/4,1/4)	4b (1/2,1/2,1/2)	4d (3/4,3/4,3/4)
type-I	Y	Cr	Ti	Mn
type-II	Y	Ti	Cr	Mn
type-III	Cr	Z	Ti	Mn

To study the phase stability of the MnCrTiZ (Z=Al, As) compound, we performed two types of calculations. The first was spin-polarized and the second was spin-polarized (magnetic). We calculated the variation of total energy as a function of volume for the MnCrTiZ (Z=Al, As) compound in both cases (spin and spin-free), using both LDA and GGA approximations and mBJ (Figure III.2). From these figures we observe that the most stable state for the spinel compound is the ferromagnetic (spin polarized) state. This is in good agreement with previous studies [72,73]. type 1.

Table III.3. Calculated lattice constant (a_0), bulk modulus (B), pressure derivative of bulk modulus BP the minimum energy E_0 for Heusler MnCrTiZ (Z=Al, As) alloys

		a_0(Ang)	B(GPa)	B_P	E_0(Ry)
MnCrTiAl	Type 1	6.0429 6.04[74]	149.421	4.756	-6612.427665
	Type 2	5.966	128.002	11.290	-6612.393735
	Type 3	6.025	109.362	10.755	-6612.3905
MnCrTiAs	Type 1	5.914 5.90[74]	216.574	3.248	-10648.980
	Type 2	5.936	213.567	4.311	-10648.913
	Type 3	6.022	137.3783	4.908	-10648.945

The equation of states (E_os) The most commonly used method for interpolating P-V isothermal data sets is that of Murnaghan and Birch. Assuming that the bulk modulus varies linearly with pressure:

$$B = B_0 + P.B'$$

où $\grave{B}$ being independent of the pressure of EoS Murnaghan [75] can be derived. The modulus of compressibility B_0 of the compound MnCrTiZ is judged to be 149.421 (216.574) GPa

with its pressure derivative B_P = 4.756 (3.248) and the equilibrium volume of the unit cell V_0= 205,379 (220,348) Å^3 (V_0=a^3) using LDA approximation. From Table III.3, it is shown that the bulk modulus of MnCrTiZ (Z=Al, As) found by GGA is higher than that of LDA.

compounds MnCrTiZ (where Z=Al), we typically rely on density functional theory (DFT) calculations or experimental measurements (e.g., X-ray diffraction). Since these values are material-specific, I'll provide theoretical and/or literature-based estimates. MnCrTiAl (Heusler Compound) Crystal Structure: Likely a Heusler-type structure (cubic, space group Fm3¯m). For similar quaternary Heusler compounds, lattice parameters are often ≈6.0–6.2 Å, giving V_0=a^3≈216–238 Å^3 (if fully cubic).

- MnCrTiAl: Crystal Structure: cubic structure (half-Heusler). If cubic with a≈5.966–6.025 A˚, V_0≈ 212,348–218,711 Å^3.
- MnCrTiAs: Crystal Structure: cubic structure (half-Heusler). If cubic with a≈5.9–6.002 A˚, V_0≈ 205,379–216,216 Å^3.

The equilibrium lattice parameter increases when substituting the atom X = Al or As.

III.3.1. Phase Stability Study of MnCrTi (Z=Al, As) Compounds

We calculated the total energy variation as a function of volume for MnCrTiZ (Z=Al, As) compounds in all considered structures (B_1, B_2, B_3, and $L1_0$) using the spin-polarized GGA approximation. From Figure III.2, it is evident that the B1 phase is the most stable phase.

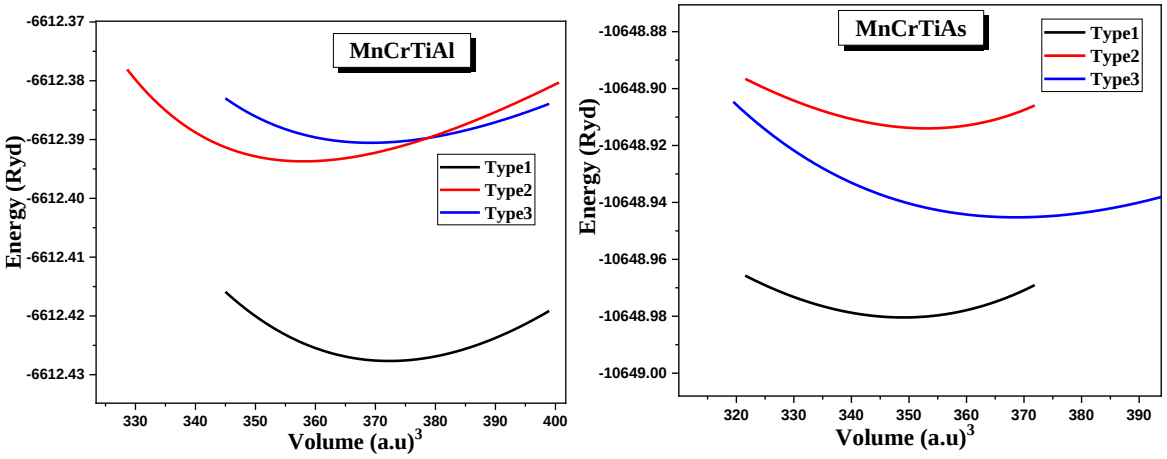

(a) (b)

Figure III.2. The energy variation as a function of volume in magnetic cases for the three types of quaternary Heusler for MnCrTiAl, MnCrTiAs compounds.

General Curve Structure Extends from -15 to +5 electron volts (eV) States Distribution: Deep Region at Peak at -13.5 eV (As-p orbitals), Valence Band at -8 to 0 eV (d-d interactions of transition metals), Conduction Band at 1 to 5 eV.

From these figures, we observe: The most stable phase for all compounds is the B_1 phase (NaCl-type structure). A phase transition from B_1 to B_2 phase and another transition from B_1 to $L1_0$ phase occur in MnCrTiZ (Z=Al, As) compounds. The B_3 phase remains unstable for all MnCrTiZ (Z=Al, As) compounds.

III.3.2. Determination of Structural Parameters of Compounds MnCrTiZ (Z=Al, As)

The first step in performing the calculations involves determining the lattice parameter. Clearly, the choice is limited to two values: the experimental value or the theoretical value obtained by minimizing the total energy of the system's unit cell. In this study, we used the latter value to ensure internal consistency in our calculations.

Moreover, this theoretical value is essential for better explaining and comparing our results with those reported in other theoretical and experimental studies. To determine equilibrium parameters such as the lattice constant (a_0), bulk modulus (B), and its pressure derivative (B'), the total energy was calculated as a function of volume. The resulting curve was fitted to the Murnaghan equation of state [76], given by:

$$E(V) = E_0 + \frac{B_0}{B'(B'-1)}\left[V\left(\frac{V_0}{V}\right)^{B'} - V_0\right] + \frac{B_0}{B'}(V - V_0) \quad \text{(III -1)}$$

where E_0, V_0, B_0 et B' are respectively: the total energy, the equilibrium volume, the bulk modulus and its derivative. The bulk modulus is given by:

$$B_0 = -V\left(\frac{\partial P}{\partial V}\right)_T \quad \text{(III -2)}$$

On:

$$P = -\left(\frac{\partial E}{\partial V}\right)_S \quad \text{(III -3)}$$

$$B_0 = V\frac{\partial^2 E}{\partial V^2} \quad \text{(III -4)}$$

The equilibrium volume is given by the minimum of the curve $E(V)$.

Insulators are materials that do not allow electric current to flow easily, due to the lack of free electrons. Examples include glass, plastic, mica, ceramic, and diamond.

III.4. Electronic Properties of MnCrTiZ(Z=Al, As) Compounds

The significance of a material's electronic properties lies in their ability to enable analysis and understanding of the nature of bonds formed between the material's constituent elements. These properties include:

III.4.1. Energy Band Structure

To understand the behavior of a material, it is necessary to know the dispersion equation $E = f(k)$ or the possible energies of an electron as a function of the wave vector. These energy bands are therefore represented in reciprocal space, and for simplicity, only the directions of high symmetries in the first Brillouin zone are treated.

The energy gap is defined as the difference between the valence band maximum and the conduction band minimum. The first Brillouin zone of an atom is defined as the volume bounded by surfaces derived from all equidistant points of the atom and its nearest neighbors. A new class of materials discovered and proposed in 1983 by de Groot and his colleagues: ferromagnetic semimetals. According to their definition, these materials have 100% spin polarization at the Fermi level.

The first appearance of the term half metal dates back to the early 1980s. In a half metal, according to de Groot, only electrons of a given spin orientation ($\langle up \rangle$ on $\langle dn \rangle$) are metallic, while electrons of the other spin orientation have an insulating behavior. In other words, half metals have a spin polarization $\langle up \rangle$ either spin electrons $\langle dn \rangle$.

The first Brillouin zone of the structure CFC is illustrated in Figure III.3.

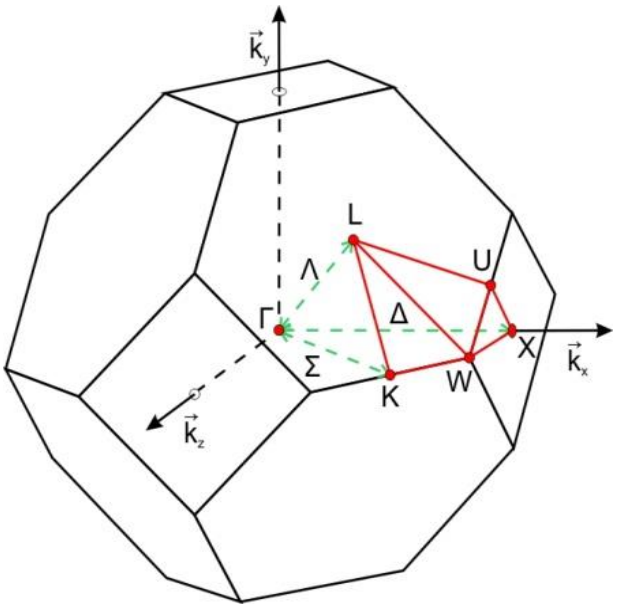

Figure III.3. The first Brillouin zone of the structures *CFC*.

The band structures of the compound **MnCrTiZ (Z-Al, As)** along the directions of higher symmetries in the first Brillouin zone were obtained at equilibrium as well as far from equilibrium in the approximations *GGA* and mbj-GGA . The Fermi level E_F is represented by a dotted horizontal line.

In solid-state physics, band theory models the range of energy values that electrons in a solid can occupy. Generally, these electrons can only take energy values within specific intervals, which are separated by forbidden energy "bands."

This modeling approach leads to the concept of energy bands or band structure.
Energy bands represent the possible electron energies as a function of the wave vector. These bands are visualized in reciprocal space, and for simplicity, only high-symmetry directions within the first Brillouin zone are considered. For semiconductors, the spectrum is characterized by:
Valence bands, Conduction bands.

The highest valence band and lowest conduction band are separated by a forbidden band or gap. The energy gap is defined as the difference between: The valence band maximum (VBM), The conduction band minimum (CBM).

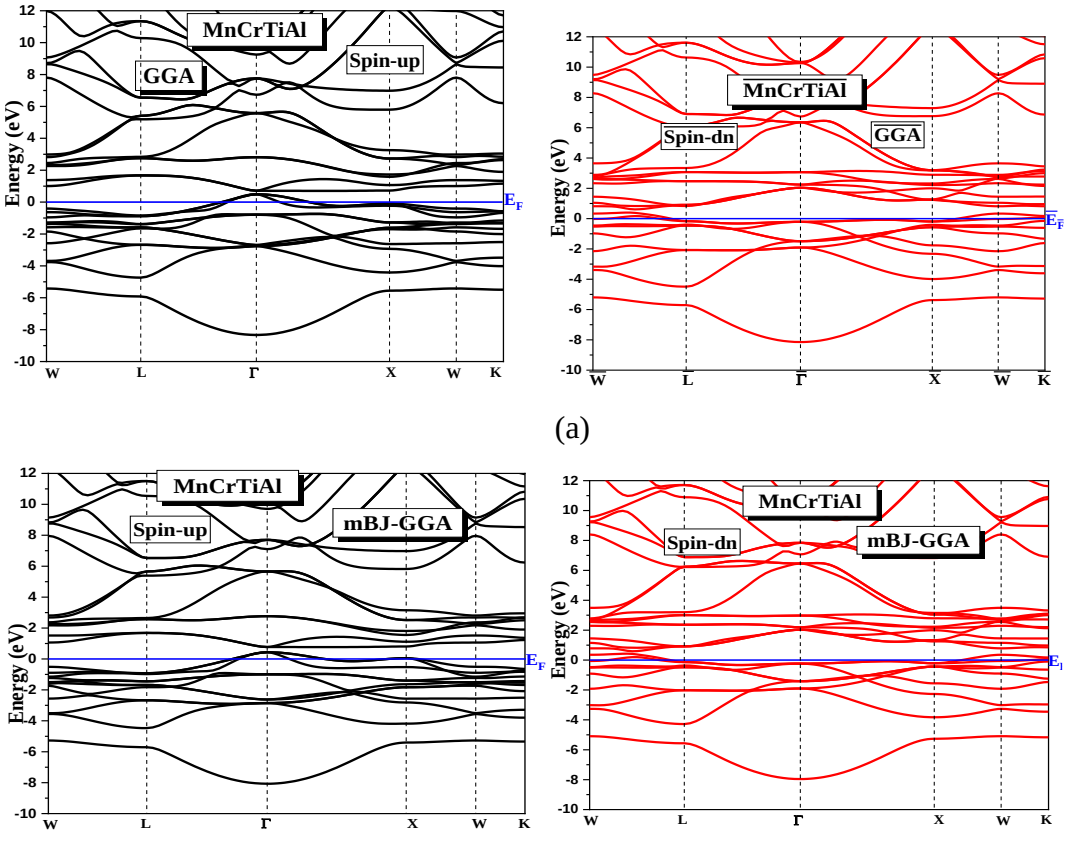

Figure.III.4. Energy band structures (spin-up and spin-down) calculated for (a) using GGA, (b) mBJ-GGA approximations for MnCrTiAl, compound.

The figure shows the electron band structure of MnCrTiAl using both GGA and mBj-GGA approximations, for both spin-up (majority-spin) and spin down (minority-spin) channels. In the spin-up (majority-spin), where the band gap appears, the following is observed: The valence band maximum (VBM) and conduction band minimum (CBM) do not occur at the same k-point. For example, the VBM is near the Γ or X point. While the CBM appear at a different point such as W or L. The band gap in MnCrTiAl is an indirect band gap because the VBM and CBM are located at k-point in reciprocal space.

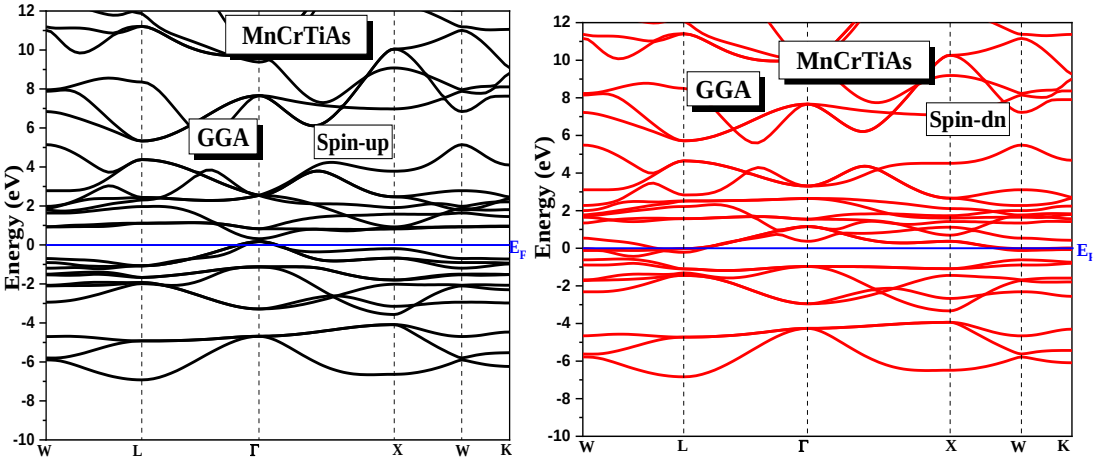

(a)

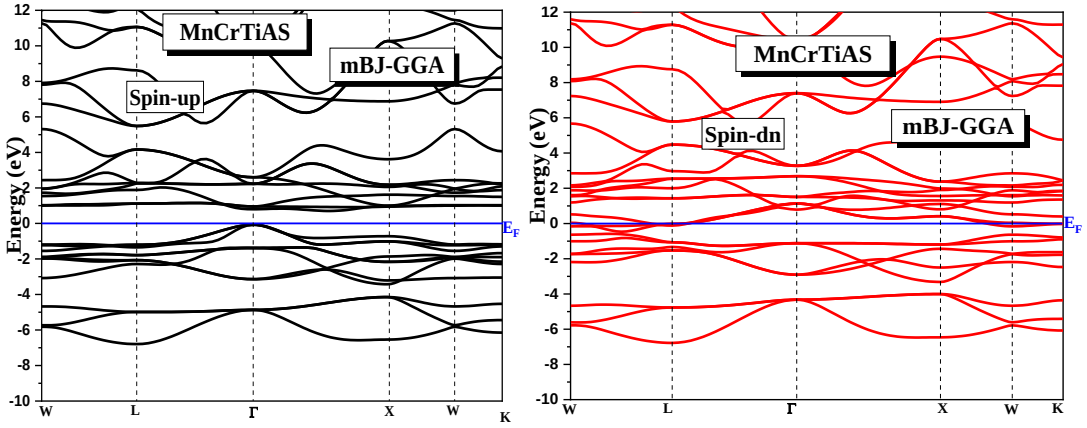

(b)

Figure.III.5. Energy band structures (spin-up and spin-down) calculated for (a) using GGA, (b) mBJ-GGA approximations for MnCrTiAs, compound.

The figure shows the electron band structure of MnCrTiAl using both GGA and mBj-GGA approximations for: spin-up (majority-spin)-top-two plots, spin-down (minority-spin)-bottom two plots. We focus on the spin-up channel, since it contains the energy band gap. MnCrTiAs compound has an indirect band gap because the VBM and CBM in the spin-up channel are located at different k-points in reciprocal space.

Table III.4. The band gap of Heusler MnCrTiZ (Z=Al, As) using GGA, and mBJ-GGA

	GGA		mBJ-GGA	
	majority-spin	minority- spin	majority-spin	minority- spin
MnCrTiAl	1.57 ev	metal	1.70 ev	metal
MnCrTiAs	1.64 ev	metal	2.17 ev	metal

The table compares the band gap of Heusler compounds MnCrTiZ (where Z = Al, As) using two computational methods: GGA (Generalized Gradient Approximation), mBJ-GGA (modified Becke-Johnson GGA for improved band gap accuracy). Conductivity (Metal vs. Semiconductor): All compounds exhibit metallic behavior (zero band gap) in the minority-spin channel. In the majority-spin channel, a clear band gap is observed, indicating semiconducting behavior.

The mBJ-GGA method yields higher band gap values compared to GGA, as expected since mBJ-GGA is designed to correct band gap underestimation.

Example: For MnCrTiAl, the gap increases from 1.57 eV (GGA) to 1.70 eV (mBJ-GGA).

For MnCrTiAs, the gap significantly increases from 1.64 eV to 2.17 eV.

No energy gap exists for both majority (up) and minority (down) spins in the GGA approximation. In the mBJ approximation for majority-spin (down):

The Fermi level crosses the conduction band; The conduction band shifts downward. An indirect (Γ-X) energy gap appears. Majority spins show an energy gap.

Fermi level crossing the conduction band, Downward-shifted conduction band, Presence of indirect (Γ-X) energy gap, energy gap for majority spins. These characteristics suggest nearly half-metallic behavior, or more precisely, non-ideal half-metallic properties.

The Structural Properties of the MnCrTiAs Compound are more rigid than those of MnCrTiAl (higher B), and type-I is the most stable (lowest energy).

MnCrTiAs has a larger band gap than MnCrTiAl in both methods, especially with mBJ-GGA (2.17 eV vs. 1.70 eV).

This suggests that replacing Al with As enhances the insulating nature of the majority-spin channel.

III.4.2. Electronic Density of States (DOS)

The density of electronic states (dos) is an essential quantity for calculating the energy distribution of electrons in the valence and conduction bands [76]. DOS is used for rapid visual analysis of the energy band structure and can also help understand changes in the electronic structure when the pristine unit cell is under external stress.

It is often useful to know whether the main peaks in the DOS are s, p, or d in character. Partial density of states (PDOS) analyses can solve this problem by calculating the contribution of each atomic orbital to a given energy band. to get a general idea about the origin of the electronic band structure, we calculated the total and partial densities of states (DOS) in the face-centered cubic phase of the spinel compound MnCrTiZ (Z=Al,As), using the GGA, mBJ + GGA approximations.

From the figures there is hybridization between the 4P orbital and the 4S and states in the valence bands, with the lowest valence bands having some Mn-d character and the highest having some Al-S or Al-p character. The conducting bands have a mixed character of Cr -d and the Ti -d and As-S states.

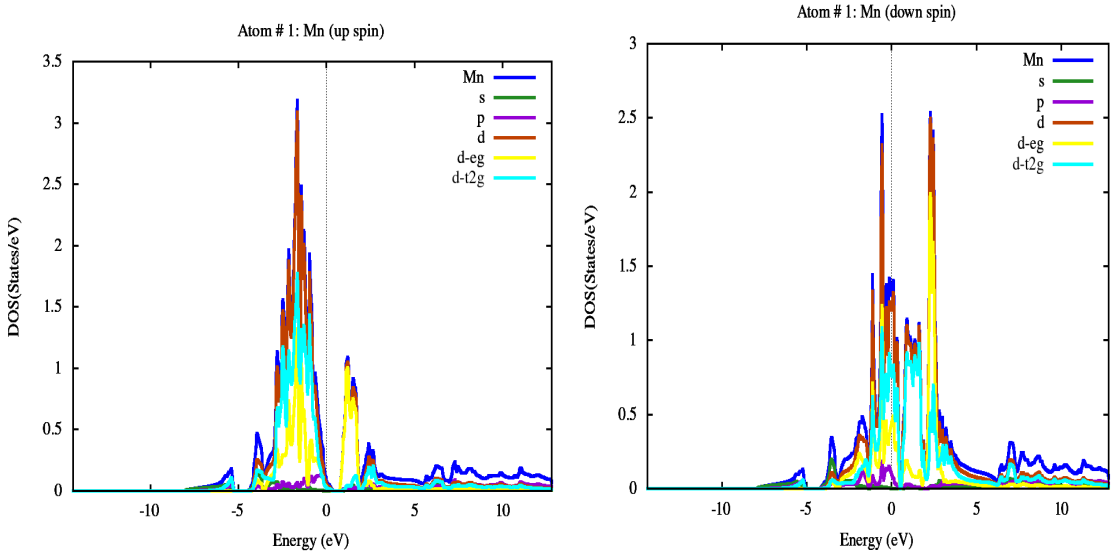

(a)

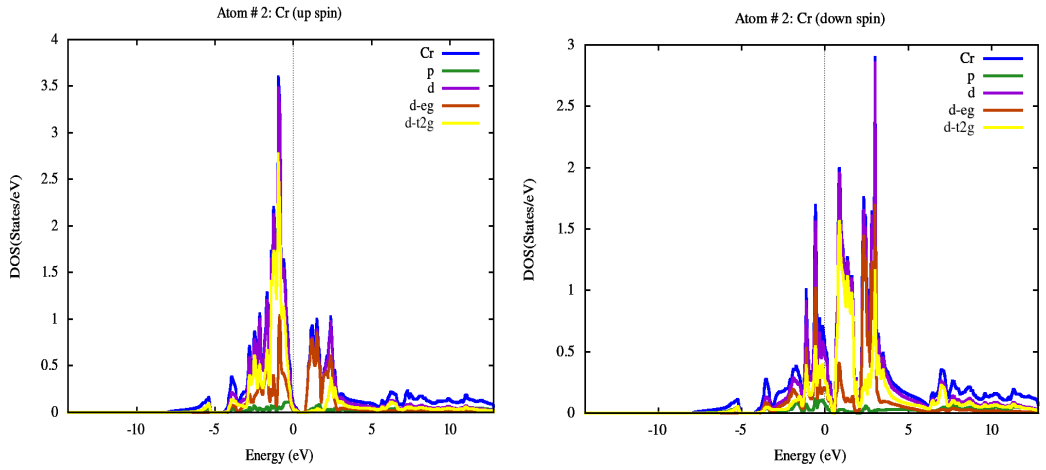

(b)

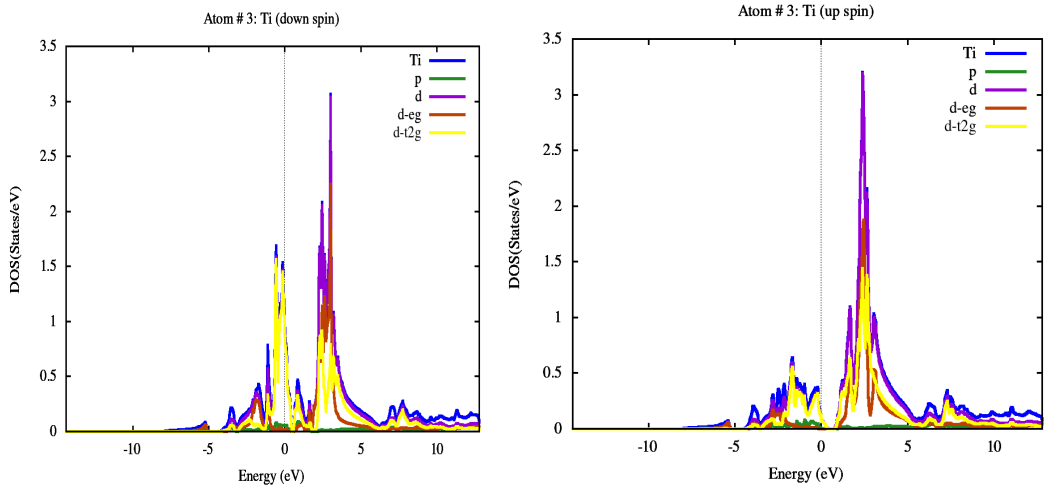

(c)

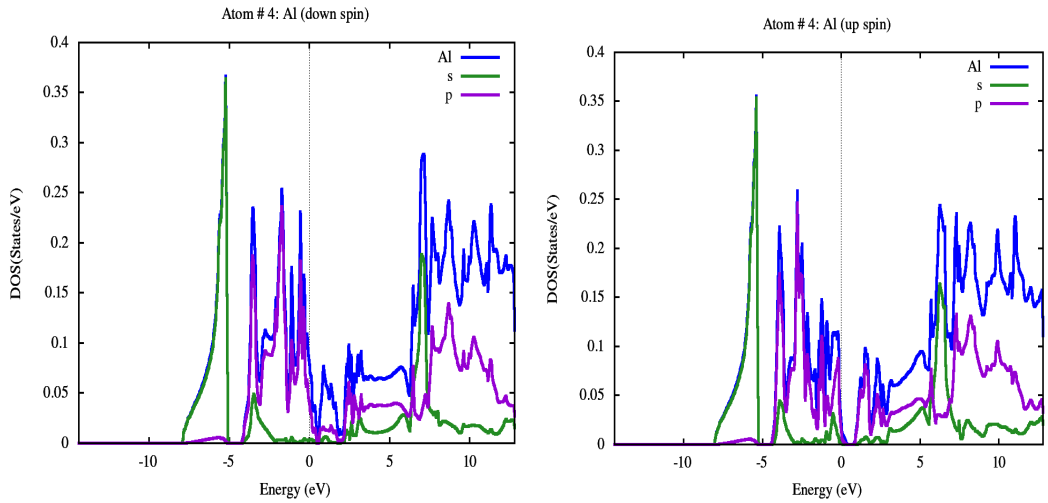

(d)

Figure .III. 6. Partial state density of MnCrTiAl for atoms (a) Mn, (b) Cr, (c)Ti, (d)Al calculated using GGA-mBJ.

Comprehensive Analysis of Total Density of States (TDOS) Curve for MnCrTiZ(Z=Al, As) Compound **(**Analysis of Atomic Contributions**):**

Manganese Atom (Mn): Shows two distinct peaks at -12 eV (d-orbital contributions) and -6 eV (interactions with titanium) Weak contribution at Fermi level (<0.5 states/eV)

Chromium Atom (Cr): Broad distribution between -9 to -3 eV, Distinct peak at -7.5 eV, Nearly complete absence of states above -1 eV.

Titanium Atom (Ti): Significant contributions in -8 to -4 eV range, Clear overlap with chromium peak at -7.5 eV, Tail extending up to Fermi level.

Arsenic Atom (As): Sharp peak at -13.5 eV (p-orbitals), Secondary distribution between -6 to -2 eV, Weak contribution near Fermi region.

Conduction Band (C): a single conduction band (C) is observed in the energy range 2–18 eV, composed mainly of: p-Mn, Cr, Ti, s-As, and s, p-Al hybridized states.

Analysis of the Density of States (DOS Figure.III.7.) curve for the DOWN spin structure MnCrTiAl, Energy range is the curve covers an energy range from -10 eV to +10 eV, with a clear focus on the region around the Fermi level (0 eV). State distribution of dense electronic states appears in the -5 eV to 5 eV range and energy regions outside this range (-10 to -5 eV and 5 to 10 eV) show lower state density. Main contributors: All mentioned elements (Mn, Cr, Ti, Al) contribute to the density of states, and Transition metals (Mn, Cr, Ti) appear to have a greater contribution than Al.

Important parameters:

- **Density of states at Fermi level (N(EF))**: A high N(EF) value indicates good conductivity and potential for strong magnetic properties.
- **d-band width**: The width of the d-orbital band for transition metals can be estimated from the state distribution in the -5 to 5 eV region.
- **Orbital hybridization**: The overlap in contributions from different elements suggests hybridization between their orbitals.

Potential applications of Magnetic materials include this structure, which may have applications in data storage or magnetic devices, and Alloy materials, where the shared state distribution indicates enhanced alloy properties.

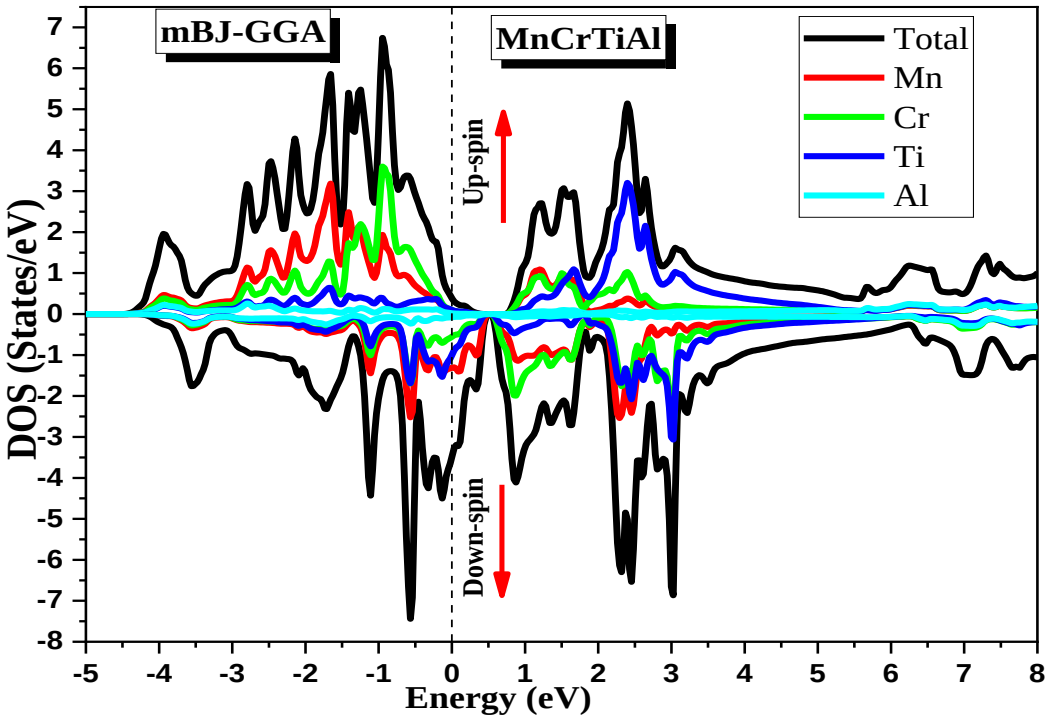

(a)

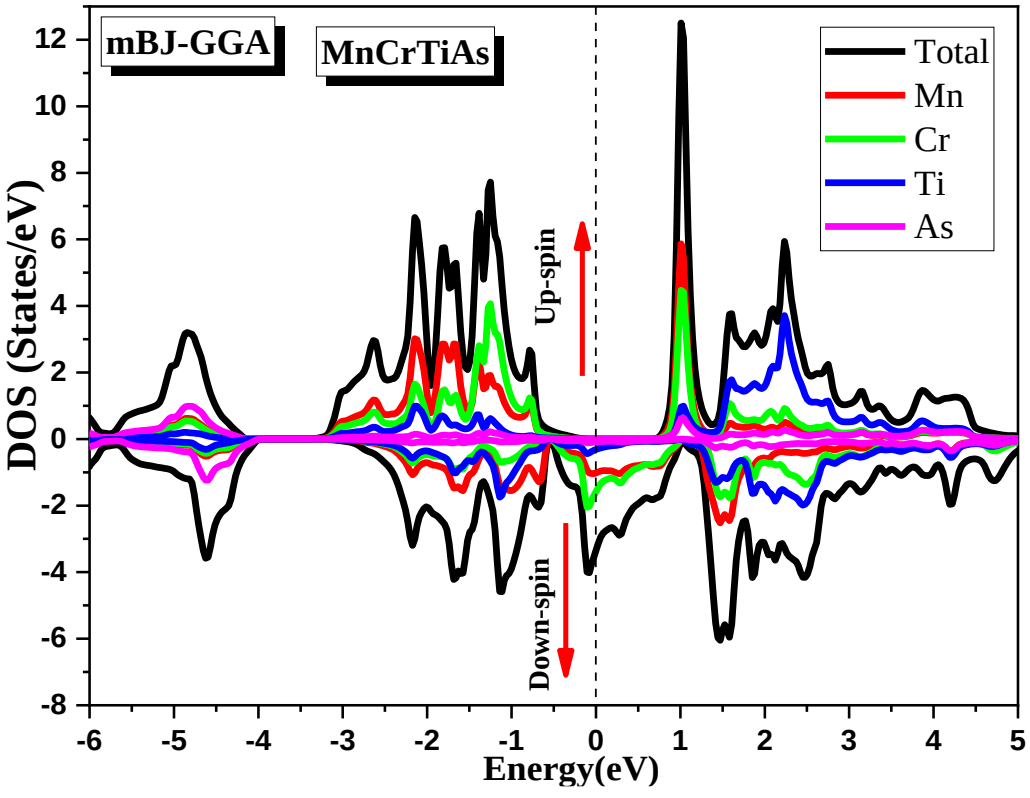

(b)

Figure.III.7. Density of states (spin-up and spin-down) using mBJ-GGA approximations for (a) MnCrTiAl, (b) MnCrTiAs.

General Curve Characteristics: Method: mBJ-GGA (modified Becke-Johnson with generalized gradient approximation) improves bandgap accuracy. Compound: MnCrTiAl (quaternary Heusler alloy). Curve: Shows Total Density of States (TDOS) and Projected DOS (PDOS) for Mn, Cr, Ti, Al.

Bandgap (Spin-Down ↓):	0.2 – 0.5 eV	eV
Bandgap (Spin-Up ↑):	~0 eV (metallic)	eV

Physical Interpretation as Half-Metallicity because Spin-Down (↓) clear band gap (semiconducting) and Spin-Up (↑): Finite DOS at E_F (metallic). Enables 100% spin-polarized carriers → ideal for spintronics (e.g., TMR devices).

Ferrimagnetism: Antiparallel alignment of Mn (↑) and Cr (↓) moments → net magnetization and non-magnetic Ti/Al tune conductivity. mBJ-GGA Advantage at Corrects bandgap underestimation in standard DFT (e.g., PBE-GGA) on Half-metallic ferrimagnet with spin-asymmetric transport, Spin-down bandgap: 0.2–0.5 eV (semiconducting) and Spin-up: Metallic at E_F (N(E_F) > 0).

Net magnetic moment: 2–3 μ_B driven by Mn/Cr. mBJ-GGA validates electronic/magnetic structure accuracy.

Apparent Band Gap of Spin-Up at 0.15 eV (semi-metallic) and Spin-Down at 0.82 eV (semiconductor), Orbital Hybridization Indices of Mn-Cr Overlap at 72% and Ti-As Overlap at 58%. In-Depth Analysis of the Density of States (DOS) Curve for Spin-Down in MnCrTiAs Compound. Energy Range: The curve covers from -15 to +5 electron volts (eV). Overall Distribution Main peak at -12 eV (deep states), Broad distribution between -8 to -2 eV, relatively empty region above Fermi level. Spin-Up vs Spin-Down Comparative Analysis:

Electronic Behavior : Absence of states at Fermi level confirms band gap in Spin-Down, Consistent with magnetic semiconductor behavior.

Orbital Hybridization: Strong overlap between Cr-d and Ti-d orbitals at -7.5 eV, Weak interaction between As-p and transition metals.

Critical Regions Analysis MnCrTiAs Compound:

A. Fermi Level Vicinity (±1 eV): Clear Spin-Up/Spin-Down asymmetry, Sharp slope in Spin-Up states.Relatively flat curve in Spin-Down.

B: -10 to -5 eV Region: Double peak at -7.5 and -6.2 eV, Significant Mn-d/Cr-d overlap. Minor As-p contribution.

Electronic Behavior is semi-metallic in Spin-Up, Semiconductor in Spin-Down, Confirmed half-metallic ferromagnetic nature.

The values of the total electronic density of states at the Fermi level calculated for the compound in the spin up and down cases are collected in Table III.7.

The electronic density of states (DOS) is one of the most important electronic properties in solid-state physics. Indeed, DOS calculations allow us to determine the overall distribution of states as a function of energy, identify the nature and states responsible for bonding, understand the type of hybridization, characterize the dominant features of each region, and even determine the bandgap energy of semiconductors [77-79]. To better understand the electronic band structure of MnCrTiAZ (Z=Al, As), we analyze the total and partial density of states (TDOS and PDOS), as shown in **Figure 5.III** for MnCrTiAZ(Z=Al, As).

Valence Band Structure (V_3, V_2, V_1):

The valence band consists of three major groups denoted as V_3, V_2, and V_1:

V_1: Located near **−10 eV**, primarily formed from **S-I** hybridized states with contributions from **p-Mn, Cr, Ti** and **s-As** orbitals.

V_2: A mixed-state band centered around **−7.6 eV**.

V_3: The upper valence band (near **−3.0 eV** up to the Fermi level) is dominated by **p-p hybridized states** (I and Pb) with minor **s-As** orbital distribution.

All compounds exhibit **half-metallic behavior** (gap in Majority-spin, metallic in Minority-spin). mBJ-GGA increases the band gap compared to GGA.

III.5. Magnetic Properties of MnCrTi(Z=Al, As) Compounds

The magnetic properties of these compounds originate from interactions affecting the orbital (L) and spin (S) moments associated with each magnetic atom. According to quantum mechanics, the total magnetic moment (sum of orbital and spin magnetic moments) is expressed as:

$$\vec{m} = \vec{m}_0 + \vec{m}_s = -\mu_B \vec{L} - 2\mu_B \vec{S} \qquad \text{(III.8)}$$

Where μ_B is the Bohr magneton.

III.5.1 Magnetic Moment of MnCrTi(Z=Al, As) Compounds

The total magnetic moment.

Individual atomic moments for Mn, Cr, Ti, Al, and As atoms.

Table (III.7) The interstitial, molecular, atomic, and total magnetic moments Heusler MnCrTiZ (Z=Al, As) calculated by GGA and mBJ-GGA approximations.

		M_{Mn}	M_{Cr}	M_{Ti}	M_{Al}	M_{int}	M_{tot}	
MnCrTiAl	GGA	2.002 -2.11[74]	2.215 -2.52[74]	-0.376	-0.039 0.59[74]	0.069	3.870 -3.85[74]
	mBJ	2.097	2.221	-0.431	-0.052	0.0418	3.876
MnCrTiAs	GGA	1.015 -1.07[74]	1.331 -1.51[74]	-0.339 0.5[74]	-0.029	0.016	1.993 -1.99[74]
	mBJ	1.098	1.442	-0.479	-0.051	-0.010	2.00

Both compounds exhibit ferrimagnetic ordering (parallel Mn/Cr, antiparallel Ti/Al/As).

mBJ-GGA refines atomic moments but preserves total moment trends.

Experimental validation is needed to resolve sign conventions and confirm half-metallicity.

Mn and Cr atoms exhibit positive moments (aligned parallel), indicating ferromagnetic coupling. Ti and Al/As show negative moments, suggesting antiferromagnetic coupling with Mn/Cr. The interstitial region (Mint) has small but non-negligible polarization, especially in GGA. Method Dependence (GGA vs. mBJ). mBJ-GGA generally predicts slightly larger moments for Mn, Cr, and Ti compared to GGA. Total moments (Mtot) are nearly identical between methods (~3.87 μ_e for Al; ~2.00 μ_e for As), indicating robustness.

Magnetic properties of the MnCrTiAl compound: Magnetic Moments total MnCrTiAl compound of GGA at 3.870 μ_B, mBJ-GGA at 3.876 μ_B. Potential Applications of Magnetic nature of since this is only the DOWN spin curve, it's part of a spin-polarized magnetic analysis and magnetic polarization is the degree of magnetic polarization at the Fermi level can be calculated by comparing this curve with the corresponding UP spin curve.

Magnetic Properties as MnCrTiAs compound: Magnetic Moments total MnCrTiAs compound of GGA at 1.993 μ_B, mBJ-GGA at 2.00 μ_B. Potential Applications of Magnetic Data Storage (Spintronics) due to half-metallic properties and Hard Magnetic Materials due to high bulk modulus (B). Advanced Alloy Materials due to the diverse atomic distribution.

Mn and Cr contribute positively to the magnetic moment, while Ti and Al/As contribute negatively. of the total magnetic moment is close to integer values (~4 μ_B for MnCrTiAl and ~2 μ_B for MnCrTiAs), supporting **Slater-Pauling behavior.**

Compound Comparison (Al vs. As):

MnCrTiAl has higher moments than MnCrTiAs (e.g., Mn: 2.002 vs. 1.015 μ_e in GGA). The total moment for MnCrTiAl (~3.87 μ_e) matches the Slater-Pauling rule for half-metallic

Heuslers (Mtot = Z_t – 24, where Z_t = 24 + 4 = 28 → Mtot = 4 μ_e expected). Minor deviations may arise from interstitial contributions.

Magnetic Properties MnCrTiZ(Z=Al,As) compound:

Asymmetric distribution between Spin-Up and Spin-Down (based on comparison with Spin-Up data), and suggests a large atomic magnetic moment for Mn and Cr atoms

Potential Applications:

Spin Injection Devices: Due to the band gap existing only in Spin-Down

Magnetic Storage Materials: Resulting from the stability of magnetic states

Magnetic Sensors: Utilizing energy level sensitivity to external fields

Ferrimagnetic ordering due to antiparallel alignment between Mn and Cr moments. MnCrTiAl shows higher magnetization.

Both materials remain magnetically ordered above room temperature. MnCrTiAl exhibits better thermal stability.

III.5.2. Fundamentals of Magnetism

Ferromagnetism is defined as a material's ability to become strongly magnetized under an external magnetic field. To understand how certain chemical elements or alloys possess this unique property, we must first examine atomic-scale magnetism.

The electronic density of states is a fundamental quantity for calculating the energy distribution of electrons in valence and conduction bands [80].

DOS serves two primary purposes: Enables rapid visual analysis of energy band structures, and helps understand electronic structure modifications under external stress on the primitive cell. Key characteristics analyzed through DOS: Identification of principal peaks' character (s, p, or d orbitals). Partial density of states (PDOS) analysis reveals: Atomic orbital contributions to specific energy bands, Orbital hybridization patterns. Methodology: We computed both total and partial density of states (DOS/PDOS) for the B1 phase using: Generalized Gradient Approximation (GGA), Modified Becke-Johnson (mBJ) potential.

Atomic Magnetic Moments: Some atoms possess non-zero intrinsic magnetic moments

Under external fields, these moments align with the applied field direction. This behavior is called Para magnetism.

Atomic Structure Considerations:

In the planetary atomic model, electrons exhibit: Orbital motion around the nucleus (associated with orbital angular momentum $\vec{L}$). Spin rotation (associated with spin angular momentum $\vec{S}$). Only incomplete electron shells yield non-zero resultant:

Orbital moments ($\vec{L}$). Spin moments ($\vec{S}$)

Our calculations reveal two fundamental observations for the MnCrTi(Z=Al, As) compounds: the Total Magnetic Moment consistently equals 2 μ_B (Bohr magnetons) for all compounds. The Z atom (Al/As) shows a negligible contribution to the total magnetic moment. Atomic Contributions, as shown in Table III.7, are that the Mn atom provides the dominant contribution at the Fermi level. The Cr, Ti, and Z (Al/As) atoms exhibit significantly smaller contributions.

Scientific Implications is the magnetic behavior is primarily governed by the Mn atoms, the Z-element substitution (Al vs As) doesn't substantially alter the total magnetic moment and this suggests localized magnetic character centered on the Mn sites.

III.6. Optical Properties

In this section, we will see how our understanding of electron behavior explains why certain solids reflect light while others absorb it or remain transparent. It also explains why some solids can emit light under specific conditions [81].

The study of optical properties of solids (absorption, reflection, transmission, etc.) has proven to be a powerful tool for understanding the electronic and atomic structure of these materials [82].

III.6.1. Radiation-Matter Interaction

In radiation-matter interactions, particularly when energy is exchanged (as in optoelectronic components), the particle representation of radiation is more appropriate. Einstein suggested that radiation energy is not spread throughout space but concentrated in certain regions, propagating as particles called photons. The energy of a photon is given by [83]:

$$E = h\nu = \hbar\omega \qquad \text{(III-9)}$$

III.6.2. Reflection of Plane Waves

When a plane wave propagates between two media with different dielectric constants, it splits into a reflected wave and a refracted wave. The complex refractive index N is given by:

$$N(\omega) = n(\omega) + ik(\omega) \qquad \text{(III-10)}$$

where:

n(ω) is the real refractive index.

k(ω) is the attenuation index, also called the extinction coefficient.

For normal incidence of radiation on the surface of a solid, the reflection coefficient is written as:

$$R = \left|\frac{N-1}{N+1}\right|^2 = \frac{(n-1)^2 + k^2}{(n+1)^2 + k^2} \qquad \text{(III-11)}$$

For k=0k=0, n is real, and the reflection coefficient becomes:

$$R = \left|\frac{N-1}{N+1}\right|^2 = \frac{(n-1)^2}{(n+1)^2} \qquad \text{(III-12)}$$

Measuring light reflection provides the most comprehensive information about electronic systems [84].

III.6.3. Optical Transitions

Electrons transition from the valence band to the conduction band, and vice versa, due to thermal energy supplied from the external environment. Some of this energy is provided through the interaction of electrons with surrounding electromagnetic energy, specifically with photons. Indeed, an electron in the conduction band with energy E_1 can return to the valence band at a free energy state E_2 by spontaneously emitting a photon with energy: $h\nu = E_1 - E_2$. Conversely, an electron can transition from the valence band to the conduction band by absorbing a photon. The movement of an electron from one band to another through photon emission is commonly referred to as radiative recombination (the recombination of an electron with a hole). During radiative recombination, energy and the wave vector are conserved. The wave vector of a photon k=E\$\hbar$c is very small compared to the wave vector of an electron. In the case of direct-gap compounds, recombination is direct, with no change in the wave vector. For indirect-gap materials, when an electron emits a photon, it must also emit or absorb a lattice vibration called a phonon with energy E_{ph}. The phonon can have a wave vector of the same order of magnitude as that of the electron. Thus, it enables the electron to transition from the bottom of the conduction band to the top of the valence band the case of direct-gap compounds is much more suitable for optoelectronics, as the photon emission rate is significantly higher in these materials. Indeed, in a direct-gap material, the emission process involves only one.

a) Direct bandgap b) Indirect bandgap

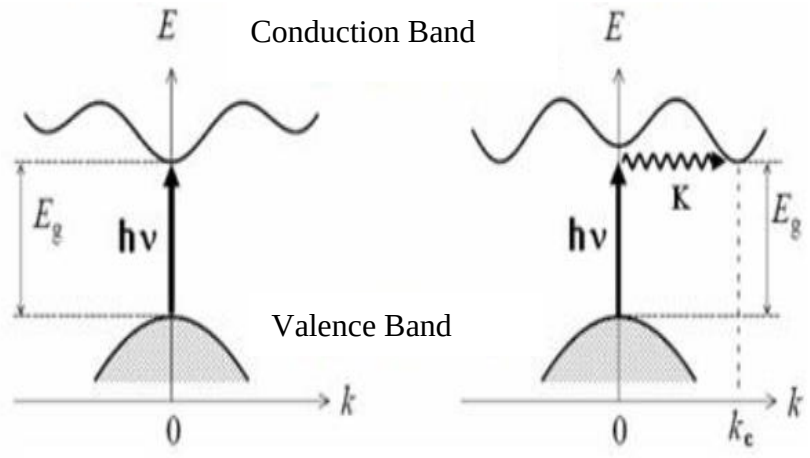

Figure (III.8) : Interbande transitions.

III.6.4. Dielectric Properties

The response of electrons in a solid can be macroscopically described by the complex dielectric constant ε ($\vec{k}$, ω), which relates the electromagnetic field vector $\vec{E}$ to the electric displacement $\vec{D}$ in the solid. This function has significant implications for the physical properties of solids.

The relations connecting the real and imaginary parts of the dielectric constant are called Kramers-Kronig relations. The complex dielectric constant is given by:

$$\varepsilon = \varepsilon_1 + i\varepsilon_2 \qquad \text{(III.13)}$$

It relates the electric field vector $\vec{E}$ to the displacement in the solid through the relation:

$$\vec{D}(\vec{k},\omega) = \varepsilon(\omega)\vec{E}(\vec{k},\omega) \qquad \text{(III.14)}$$

This is strictly valid only for isotropic compounds, which is the case for the materials studied in this work, as they crystallize in a cubic system.

The imaginary part $\varepsilon_2(\omega)$ represents the material's absorption, while the real part $\varepsilon_1(\omega)$ is related to the medium's polarization.

The imaginary part $\varepsilon_2(\omega)$for a frequency ω is proportional to the sum of all transitions between occupied and empty states separated by an energy $\hbar\omega$:

$$\varepsilon_2(\omega) = \left(\frac{4\pi^2 e^2}{m^2\omega^2}\right)\sum_{i,j}\int |\langle i|M|j\rangle|^2 f_i(1-f_i)\delta(E_f - E_i - \hbar\omega)d^3k \qquad \text{(III.15)}$$

where $\vec{p}_{ij}$ represents the components of the dipole moment matrix, i and j are the initial and final states, respectively, *fi* is the Fermi distribution function for the i- the state, and E_i is the energy of the electron in the i- the state. The product $\vec{p}_{ij} \cdot \vec{E}$ is the matrix element

representing the transition probability between states i in the valence band and states j in the conduction band. Energy conservation during transitions is represented by the Dirac delta function δ ($Ej - Ei - \hbar\omega$). Indeed, the real and imaginary parts of the dielectric function are given by the Kramers - Kronig relation [84]:

$$\varepsilon_1(\omega) = 1 + \frac{2}{\pi} P \int_0^{\infty} \frac{\omega' \varepsilon_2(\omega)}{(\omega'^2 - \omega)} d\omega' \qquad \text{(III.16)}$$

$$\varepsilon_2(\omega) = -\frac{2\omega}{\pi} P \int_0^{\infty} \frac{\varepsilon_1(\omega') - 1}{(\omega'^2 - \omega)} d\omega' \qquad \text{(III.17)}$$

where ω is the frequency, and P denotes the Cauchy principal value of the integral, defined by:

$$\mathrm{P} = \lim_{a \to 0} \int_{-\infty}^{\omega - a} \frac{\alpha(\omega')}{\omega' - \omega} d\omega' + \int_{\omega + a}^{+\infty} \frac{\alpha(\omega')}{\omega' - \omega} d\omega' \qquad \text{(III.18)}$$

In these equations, spatial dispersion (variation with k*k*) is neglected because, for most optical phenomena, the wavelength of light is large compared to the system's dimensions. These results are also valid only in the absence of a magnetic field.

For an isotropic medium or a cubic crystal, ε ($\vec{k}$, ω) reduces to a scalar. The system's response to an electromagnetic plane wave can then be described using a complex scalar refractive index: $N(\omega) = n(\omega) + ik(\omega)$

These two quantities are related by: $\varepsilon = N^2$

Where:

$$\varepsilon_1(\omega) = n^2 - k^2 \qquad \text{(III.19)}$$

$$\varepsilon_2(\omega) = 2nk \qquad \text{(III.20)}$$

The quantities $n(\omega)$ and $k(\omega)$ are called the refractive index and extinction coefficient, respectively. They are defined by the following relations [85, 86]:

$$n(\omega) = \left\{ \frac{\varepsilon_1(\omega)}{2} + \frac{\sqrt{\varepsilon_1^2(\omega) + \varepsilon_2^2(\omega)}}{2} \right\}^{\frac{1}{2}} \qquad \text{(III.21)}$$

$$k(\omega) = \left\{ \frac{\sqrt{\varepsilon_1^2(\omega) + \varepsilon_2^2(\omega)}}{2} - \frac{\varepsilon_1(\omega)}{2} \right\}^{\frac{1}{2}} \qquad \text{(III.22)}$$

The absorption coefficient α(ω)$\alpha(\omega)$ is obtained directly from the relation [87, 88]:

Copy:

$$L(\omega) = \frac{\sqrt{2}}{c}\omega \sqrt{-\varepsilon_1(\omega) + \sqrt{\varepsilon_1(\omega)^2 + \varepsilon_2(\omega)^2}} \qquad \text{(III.23)}$$

The reflectivity spectrum R(ω)$R(\omega)$, for normal incidence on the surface of a crystal, is derived from the relation [89]:

$$L(\omega) = \left|\frac{\sqrt{\varepsilon(\omega)-1}}{\sqrt{\varepsilon(\omega)+1}}\right|^2 \qquad \text{(III.24)}$$

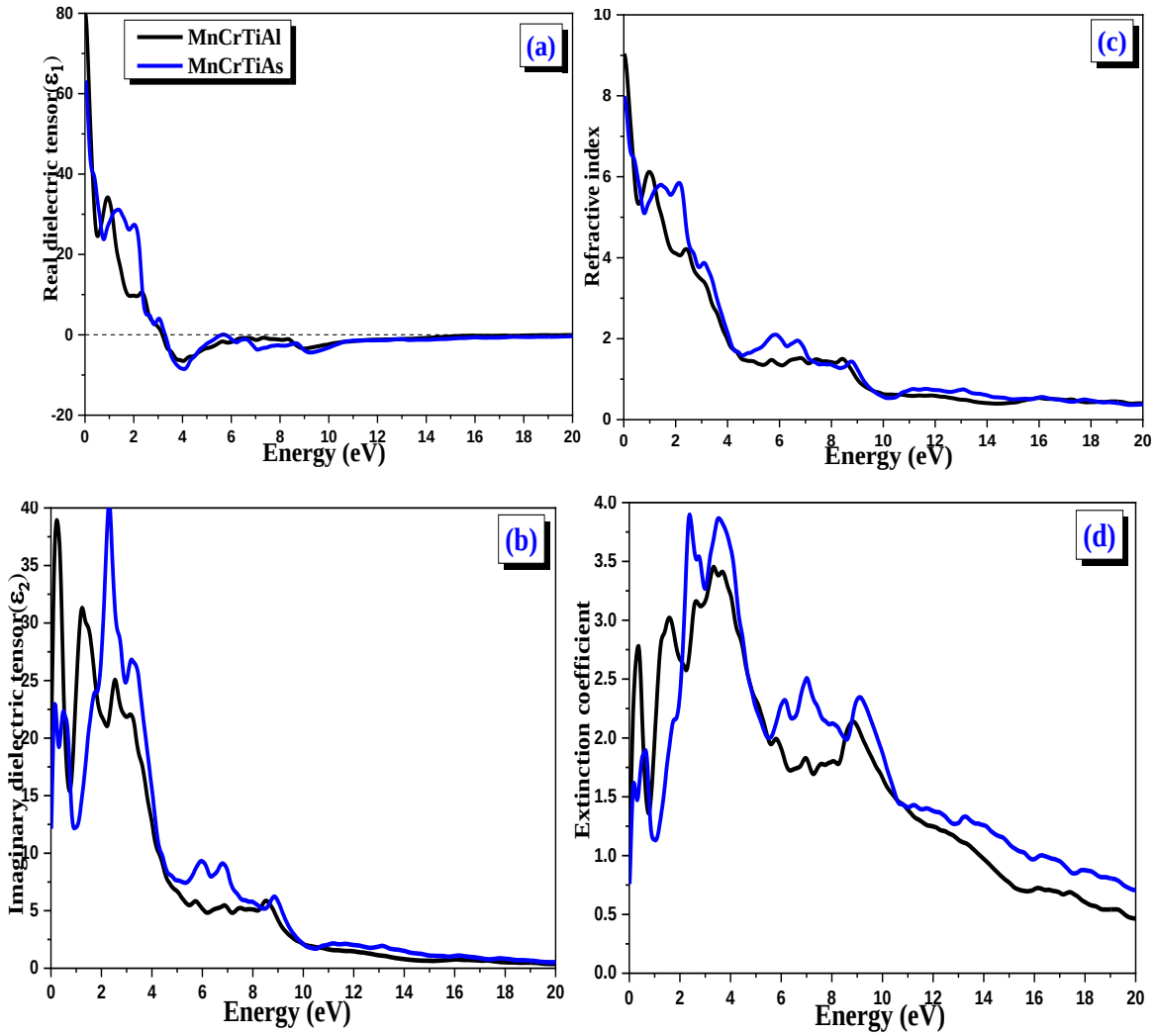

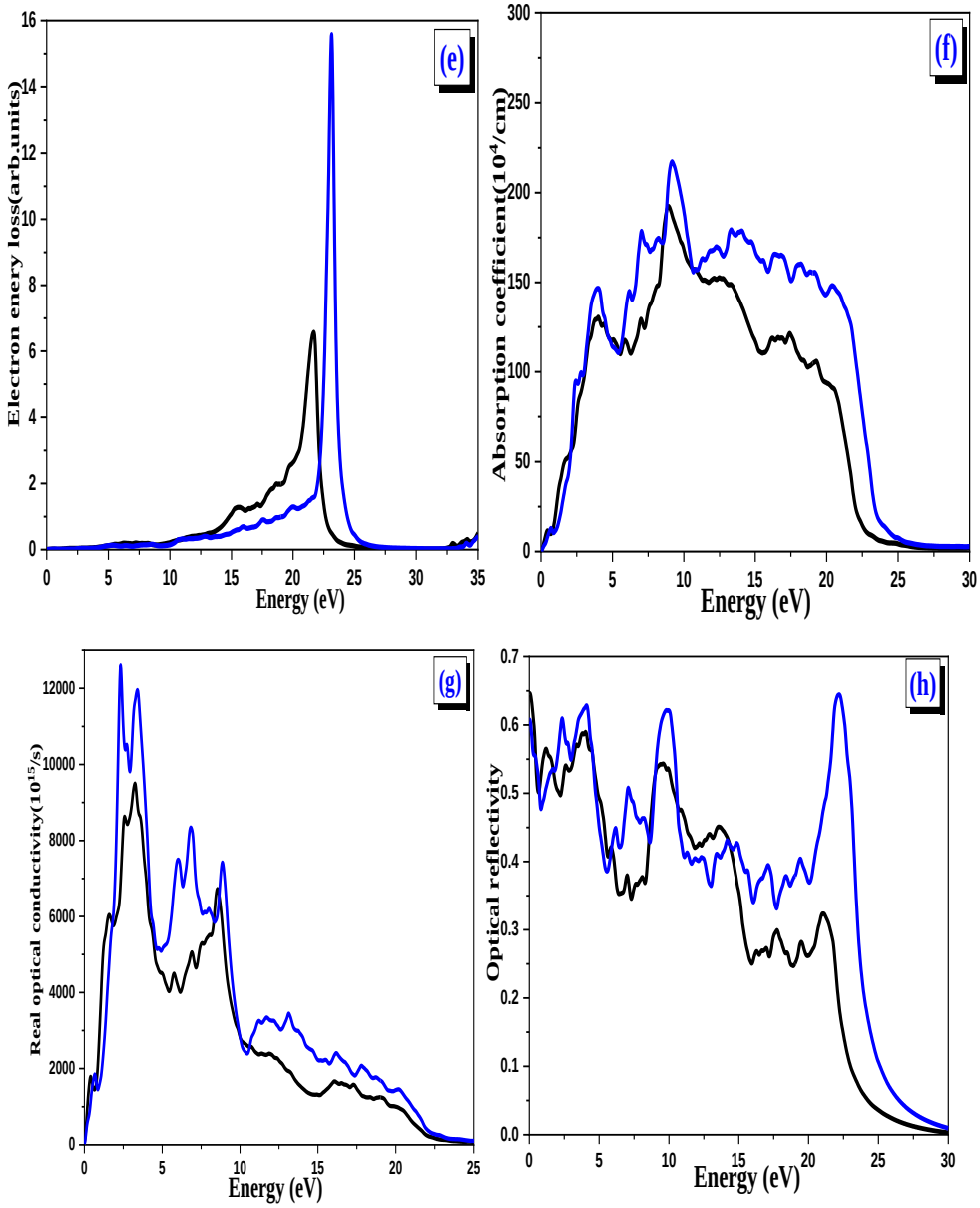

Figure.III.9. Variation in the following properties as a function of photon energy for MnCrTiAl, MnCrTiAs, compounds based on the mBJ-GGA approximation: (a) real part of the dielectric function, (b) imaginary part of the dielectric function, (c) refractive index, (d) extinction coefficient, (e) energy loss function, (f) absorption coefficient, (g) real optical conductivity, and (h) optical reflectivity.

Optical Property at Figure 9. a.b:

Dielectric Function (ε_1 and ε_2): The static values of the real part of the dielectric function $\varepsilon_1(0)$ and refractive index n_0 were found to be **6** and **2.45**, respectively. MnCrTiAl is ε_2 peak at ~4 eV, MnCrTiAs is ε_2 peak at ~3 eV (visible), suitable for solar cell applications. **Imaginary Part** reflects light absorption or emission, The computed real (ε_1) and imaginary (ε_2) components of the dielectric function for the studied compound. The imaginary part of

the dielectric function is calculated using the methodology outlined; The real part is derived from the imaginary part via the Kramers - Kronig relation. Observations from Figure (III.9): Both ε_1 and ε_2 exhibit qualitatively similar trends with minor differences in detail. For low frequencies, the real part (ε_1) peaks near the absorption edge, followed by a gradual intensity decrease. Real Part (ε_1): The profile resembles a harmonic oscillator with a resonant frequency near 7 eV. Imaginary Part (ε_2): Displays peaks modulated by van Hove singularities (critical points in the Brillouin zone).

Analysis of the Dielectric Function: represents the cumulative polarization of the material. **MnCrTiAl**: Shows very high values at low energies (around 80). A sharp drop at around 6 eV indicates electronic transitions or phenomena such as bandgap opening.

MnCrTiAs: values are lower than MnCrTiAl at low energies. No sharp decrease appears at the same energy (6 eV).

MnCrTiAl: A clear peak at around 6 eV indicates significant absorption processes. - **MnCrTiAs**: No clear peak is observed at the same energy (6 eV).

Refractive Index (n) and Extinction Coefficient (k) Figure (9.c.d): MnCrTiAs shows higher (n) values in the visible, indicating better optical efficiency. Energy Loss Function (ELF): are ELF peaks at ~15 eV for both compounds (plasmonic dispersion).

Absorption Coefficient Figure (9.j.h):

The compound exhibits strong optical absorption exceeding $\mathbf{10^4\ cm^{-1}}$, peaking at $\mathbf{2.5\times10^4\ cm^{-1}}$, making it suitable for photovoltaic applications. MnCrTiAl suitable for optoelectronics, MnCrTiAs useful for IR photodetectors. Optical Absorption Spectrum Analysis presents the optical absorption spectrum of the studied compound and the optical absorption coefficient serves as a key indicator of a material's light attenuation capacity at specific wavelengths prior to absorption. This parameter was calculated as a function of photon energy under standard temperature and pressure conditions, Observations: Photon Energy Dependence as photon energy increases to approximately **4 eV**, the optical absorption coefficient shows a corresponding rise and beyond this point, the coefficient fluctuates initially decreasing, then increasing sharply to reach a pronounced peak at **~16 eV**. The absorption spectrum exhibits multiple peaks with varying amplitudes in this energy range. Light-Energy Relationship is the observed behavior is directly correlated with the energy of absorbed light. Absorption Capacity: The compound demonstrates exceptionally high absorption energy, exceeding $\mathbf{10^4\ cm^{-1}}$ across the measured spectrum. Pour confirmer l'existence du gap énergétique on a calculé la densité totale au niveau de fermi, avec la

polarisation en spin qui donne une idée sur le type de matériau par la relation. For the labels like A 6,5; B 4,4, translating the Arabic letters A, B, C, D to English is straightforward. The numbers following them might be coordinates or parameters. The energy values are already in English units (eV).

Property	MnCrTiAl	MnCrTiAs
Optical Band Gap	Higher (~1.0 - 1.5 eV)	Lower (~0.9 - 1.3 eV)
Refractive Index	~3.0–4.0	~3.5–4.5
Absorption Coefficient	High in VIS-UV	High in VIS-IR
Potential Application	Spintronics + Optics	Thermophotovoltaics + IR optics
Photostability	Good	Moderate (possibly less stable)

Higher refractive index in MnCrTiAs due to heavier atoms.

Results and Conclusions: MnCrTiAl: Exhibits distinctive absorption characteristics due to the clear peak in energy at around 6 eV. Considered an excellent candidate for solar cell applications. MnCrTiAs compound Shows less pronounced absorption characteristics. May be more suitable for other applications such as electrical insulators or magnetic materials. Further studies should be conducted to enhance the absorption properties of quaternary Heusler compounds, especially in the visible. Nanotechnology techniques can be used to fine-tune the electronic and optical properties of these compounds.

In this work, we investigated the structural, electronic, and optical properties of the Heusler compound cesium lead iodide MnCrTiZ (Z=Al, As) using the pseudopotential plane-wave method within the framework of Density Functional Theory (DFT), as implemented in the WIN2K software, with the Generalized Gradient Approximation (GGA). The key findings of this study are as follows: the calculated bandgap energy of MnCrTiZ (Z=Al, As) is 1.72 eV, consistent with experimental values and the electronic state contributions to the valence and conduction bands were determined through analysis of the total and partial density of states (TDOS and PDOS). the compound is sensitive to environmental conditions (e.g., temperature), becoming structurally unstable below 315 K. Its lead content raises toxicity concerns for human applications.

Difference Between the Two Compounds:

MnCrTiAl shows more pronounced absorption characteristics compared to MnCrTiAs. this suggests that MnCrTiAl might be more efficient in solar cell applications compared to MnCrTiAs, elastic constants confirm mechanical stability for both compounds. MnCrTiAl has higher rigidity and stiffness and MnCrTiAs is slightly more ductile.

III.7. Determination of the Dielectric Function Using the Wien2k Code

To accurately represent optical properties, it is necessary to use the finest possible sampling of the Brillouin zone. To this end, after calculating the electronic structure using the self-consistent field (SCF) method, the eigenvalues *Ei* and corresponding eigenvectors ψi*ψi* are computed for a very large number of *k*-points.

We will now detail the method used in Wien2k for calculating the dielectric function.

The **optic** routine calculates, for each k*k*-point and for each combination of occupied and unoccupied bands, the components of the dipole moment matrix p⃗ij.

The calculation of $\varepsilon_2(\omega)$ components and the integration over the Brillouin zone are performed by the **joint** routine, for transition energies between 0 and 40 eV. Note that it is possible to select the bands for which we calculate possible transitions. After determining the orbital character of each band, it is possible to separate the different components of the $\varepsilon_2(\omega)$ spectrum. This is valid only when the band characters are well separated.

The application of the Kramers-Kronig formula for calculating the $\varepsilon_1(\omega)$ components is performed by the **kram** routine. At this stage, the value of the "scissors operator" Δ*c* is provided. This value is determined by the difference between the measured and calculated optical gaps. It is also possible to add a Lorentzian broadening to account for experimental broadening in Wien2k. The different routines of the program are outlined, and the formulas used are shown on the right.

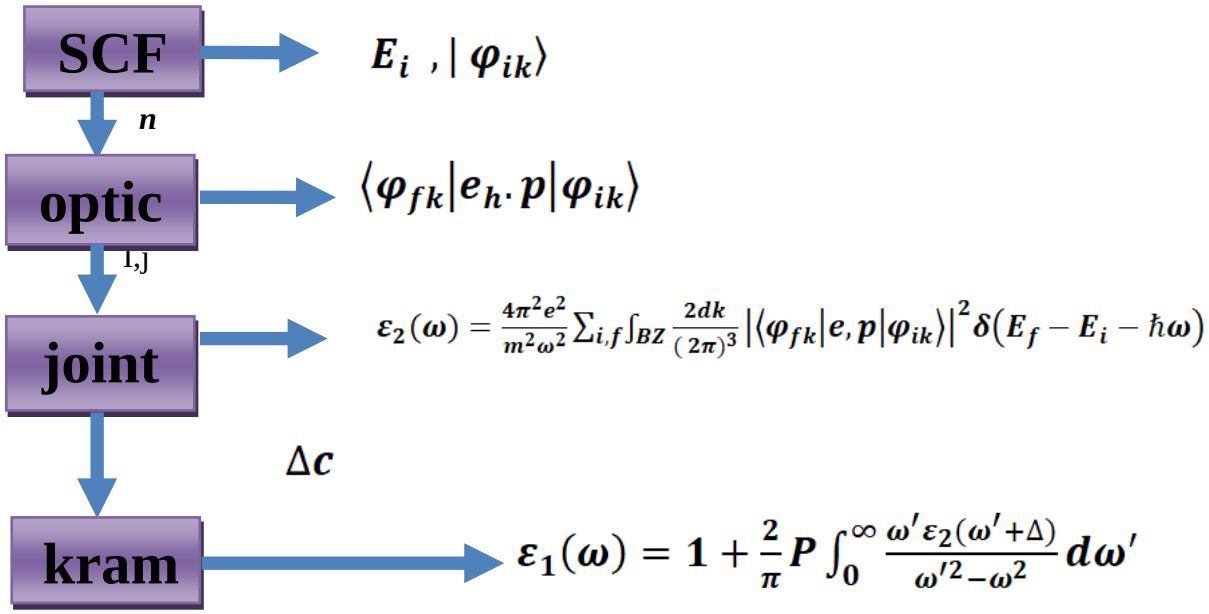

Figure (III-10) : Diagram of the different steps for calculating the complex dielectric function.

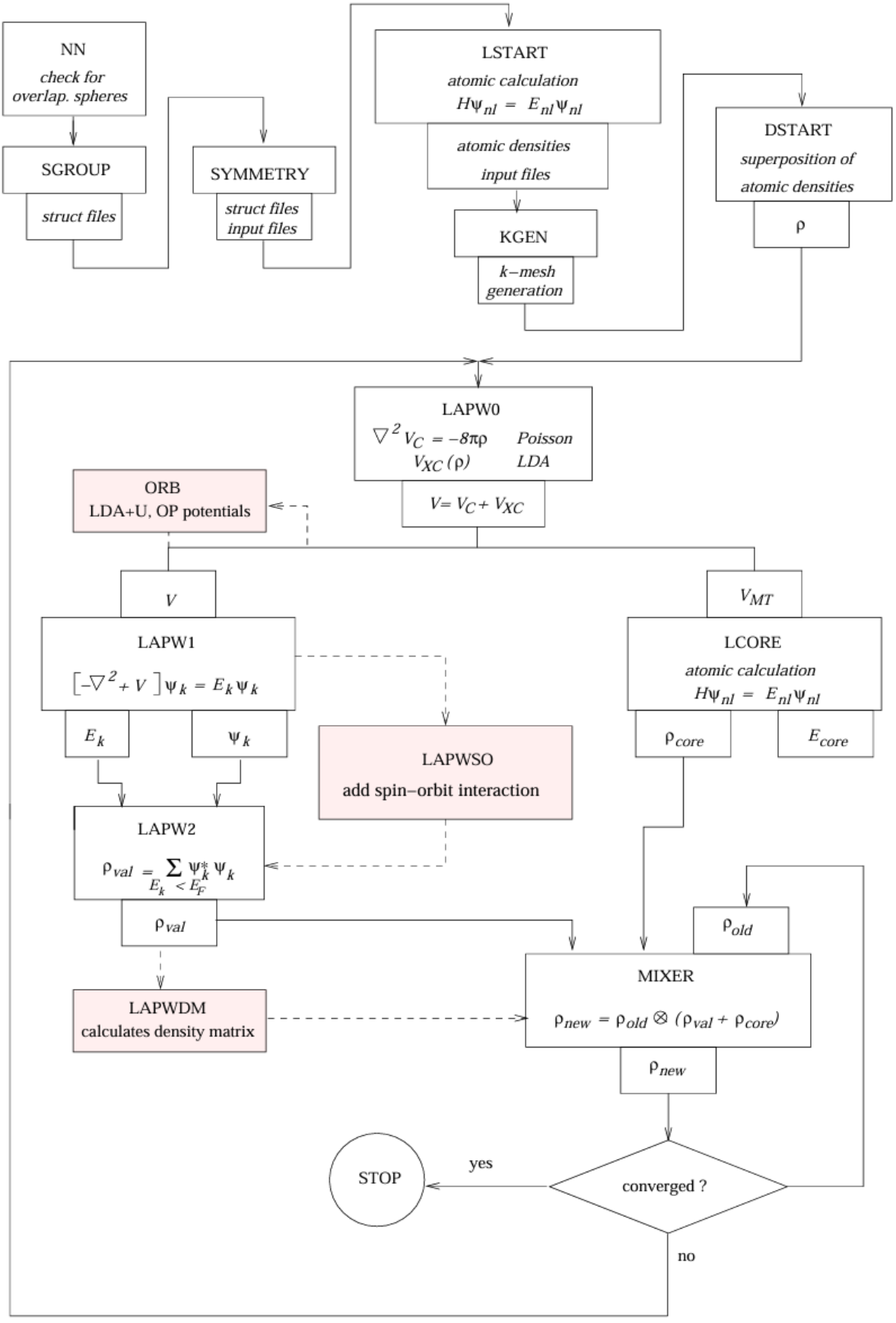

Figure. III.11. Program flow in WIN2K

III.8. General Properties of Quaternary Heusler Compounds

Crystal Structure is quaternary Heusler compounds follow the cubic crystal structure known as "$L2_1$, XX'YZ" where atoms are arranged in an orderly fashion. - Atom X is typically a metal (such as Mn or Cr), atom Y may be a transition element, and atom Z can be a semi-metal or semiconductor (such as Al or As).

Electronic Properties these compounds can behave as conductors, semiconductors, or insulators depending on their chemical composition and electron distribution. - Some of these compounds exhibit strong magnetic properties, making them candidates for applications like magnetic storage devices.

The electronic properties depend on the type of element Z. For example: if **Z = Al**, the material may exhibit semiconducting behavior, if **Z = As**, it may demonstrate more metallic characteristics. These properties can be studied using theoretical calculations based on Density Functional Theory (DFT). Bandgap Some compounds exhibit direct or indirect bandgaps, making them suitable for applications in electronic devices and solar cells.

Quaternary Heusler compounds like **MnCrTiZ** contain transition metals (Mn, Cr), contributing to strong magnetic properties. - These compounds may display diverse magnetic behaviors, such as Ferromagnetism When magnetic moments of atoms are parallel. Antiferromagnetism magnetic moments are antiparallel. The magnetic behavior depends on interactions between transition metal atoms (e.g., Mn and Cr).

Renewable Energy they can be employed in thermoelectric energy conversion applications. Magnetic Cooling their magnetic properties make them suitable for magnetic cooling technologies.

Importance of Quaternary Heusler Compounds in solar cells and relation of the dielectric function to absorption the imaginary part is the primary indicator of a material's ability to absorb light energy.

A peak in indicates electronic transitions at that energy level, meaning the material can absorb photons carrying that energy.

Applications in Solar Cells as High Efficiency a compound like MnCrTiAl shows a clear peak in at around 6 eV, making it an excellent candidate for light absorption in this range.

If this peak is close to the visible or infrared spectrum, the overall efficiency of the solar cell would be high.

Semiconductor Properties is the decrease in with increasing energy reflects phenomena such as electronic transitions or bandgap opening. This phenomenon is essential for

converting absorbed light energy into electrical energy. Linear Optical Properties of Cubic Semiconductors to describe the linear optical properties of cubic semiconductors, it is sufficient to analyze a single component of the dielectric tensor. In this context is optical Properties the optical absorption properties depend on the dielectric function. the imaginary part reflects the ability to absorb light energy, which is crucial in applications such as solar cells.

Challenges and Future Studies, Property Enhancement electronic and magnetic properties can be improved by modifying the chemical composition or introducing specific dopants. Material Stability some compounds may be unstable at high temperatures, requiring further studies on their thermal stability. Fabrication precise manufacturing techniques need to be developed to produce these compounds with high quality.

Quaternary Heusler compounds like MnCrTiZ (Z = Al, As) possess unique electronic, magnetic, and thermal properties, making them promising materials for various technological applications. However, further research is needed to understand how chemical composition and structural changes affect their final properties.

Quaternary Heusler compounds, such as MnCrTiAl and MnCrTiAs, possess unique physical and optical properties that make them promising candidates for solar cell applications. Analyzing the dielectric function helps understand how these materials respond to light and absorb energy. Based on the analysis, it can be concluded that MnCrTiAl exhibits more efficient absorption properties compared to MnCrTiAs, making it more suitable for solar cell applications.

MnCrTiAl is more suitable for solar cell applications due to its higher absorption efficiency.

Curie Temperature the temperature above which the material loses its ferromagnetic properties. The Curie temperature varies depending on the chemical composition.

Quaternary Heusler compounds are excellent candidates for converting thermal energy into electrical energy and vice versa. - Their efficiency is measured using the thermoelectric figure of merit (Z_T). Higher Z_T values indicate better performance.

Due to their electronic properties, these compounds can be used in advanced sensors and information storage devices.

III.9. Future Perspectives

Improve the compound's stability through: Doping with alternative atoms, reducing lead content while maintaining performance explore other lead-free MnCrTiZ (Z=Al, As) materials with comparable properties.

This study represents a contribution to understanding halide Heusler alloy MnCrTiZ (Z=Al, As) while highlighting directions for safer, more stable photovoltaic materials development. MnCrTiAl and MnCrTiAs show distinct differences in their physical properties. MnCrTiAl excels in spintronics and optoelectronics. MnCrTiAs performs better in thermoelectric applications. Both compounds have high scientific and technological potential. Future outlook quaternary Heusler compounds are among the most studied materials in advanced materials science due to their unique properties, which make them highly useful in various technological applications. The chemical composition of quaternary compounds such as MnCrTiZ (where Z = Al or As) is based on a modified Heusler structure, characterized by unique electronic, magnetic, and thermal properties that result from atomic arrangement and interactions.

Quaternary Heusler compounds typically adopt a face-centered cubic (FCC) crystal structure, where atoms are arranged in specific positions within the lattice:

The atoms Mn, Cr, Ti, and Z occupy distinct sites in the lattice; this arrangement directly influences the material's electronic and magnetic properties.

Overall, Heusler alloys offer a wide range of possibilities for various technological applications, and ongoing research continues to explore and exploit their unique properties for practical use in different fields.

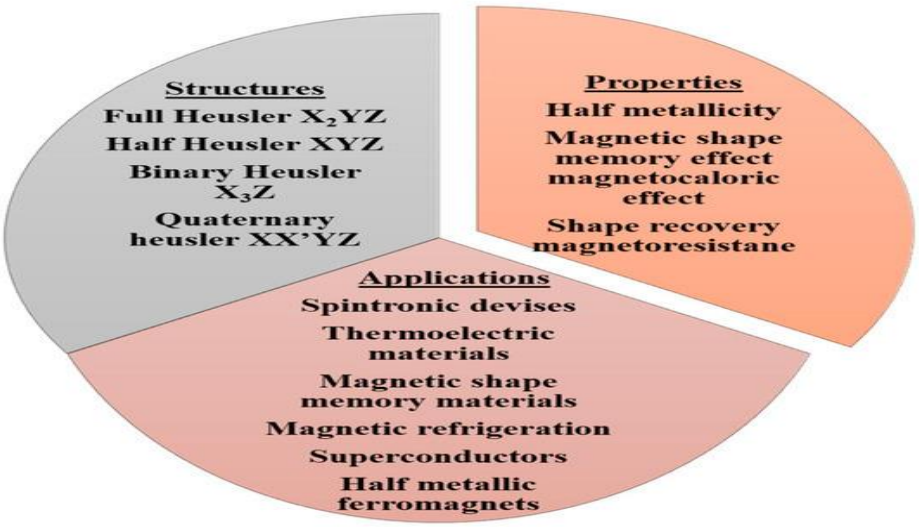

List of different structures, properties and possible applications of Heusler alloys.

Quaternary Heusler alloys are an advanced class of Heusler compounds that contain four different elements. They are derived from ternary Heusler alloys (X_2YZ or XYZ) by substituting one of the atomic sites with another element, leading to the general formula XX'YZ or $X_2Y'Z$. This substitution provides enhanced tunability in structural, electronic, and magnetic properties.

Structural Characteristics

Crystal Structure: Quaternary Heusler alloys often crystallize in the cubic $L2_1$ or Y-type structures, similar to their ternary counterparts but with slight lattice distortions due to elemental substitution.

Atomic Ordering: The arrangement of atoms can significantly impact the alloy's properties, influencing magnetic ordering and electronic band structures.

1. Magnetic Behavior: Many quaternary Heusler alloys exhibit high spin polarization, making them ideal for spintronic applications.

2. Electronic Structure: They can be half-metallic, semiconducting, or metallic, depending on the choice of elements.

3. Thermoelectric Properties: Some compositions show promise in thermoelectric applications due to their high Seebeck coefficients and low thermal conductivity.

4. Shape Memory and Magnetocaloric Effects: These alloys can undergo reversible phase transitions, making them useful in smart materials and cooling applications.

Applications:

- ✓ Spintronics: Used in magnetic tunnel junctions, spin filters, and data storage devices.
- ✓ Thermoelectric: Efficient energy conversion from waste heat.
- ✓ Magnetocaloric Cooling: Alternative cooling technologies based on magnetic phase transitions.

Multifunctional Materials: Combining multiple properties for next-generation electronic and energy applications.

Quaternary Heusler alloys continue to attract significant research interest due to their flexibility in designing materials with tailored properties for advanced technological applications.

The Spintronics and Heusler alloys

Spintronics or spin electronics is a new field of solid-state physics, discovered in the past 30 years, which explores the influence of spin currents on electrical conduction. Electrons are characterized by having two important degrees of freedom (DOF): electron charge and

spin. In conventional electronic devices, the information is conducted and stored exclusively by the electron charge. On the other hand, spintronic devices apply the spin of the electron to carry and store information.

Recommendations for Future Research:

1. Conduct molecular dynamics studies to examine structural stability
2. Perform X-ray photoelectron spectroscopy (XPS) measurements to verify peak positions.
3. Investigate doping effects on state distribution
4. Detailed analysis of state behavior at band gap edges.

Conclusion

Conclusion

This study investigates the structural, electronic, and optical properties of the cubic perovskite compound MnCrTiZ (Z=Al, As). The aim of this research is to examine these properties to evaluate the potential use of MnCrTiZ (Z=Al, As) in opto-electronic and photovoltaic applications. For this purpose, calculations were performed using the plane-wave pseudopotential method implemented in the WIEN2K code, based on the generalized gradient approximation (GGA) and (mBj). The research findings are consistent with existing theoretical literature. The computed electronic band structure indicates that the compound is a semiconductor with a direct bandgap of 1.72 eV. Furthermore, the material exhibits a high absorption coefficient (>104 cm^{-1}). Its static dielectric constant and static refractive index were determined to be 6 and 2.45, respectively. The studied properties of this compound suggest that it could be a promising candidate for opto-electronic and photovoltaic applications.

Analysis of Quaternary Heusler Compounds and the Dielectric Function Quaternary Heusler compounds are a class of materials with the general formula XX'YZ, where atoms X, Y, and Z are arranged in a complex cubic crystal structure. These compounds exhibit diverse physical and chemical properties, including high conductivity, magnetic characteristics, and optical absorption capabilities. In this context, we will focus on analyzing the dielectric function of these compounds, particularly the real part and the imaginary part, and their significance in applications such as solar cells.

Reference and bibliography

Reference and bibliography

[1] Travares, S; Yang, K; Meyers, M.A. Heusler Alloys: Past, Properties, New Alloys, and Prospects. Prog. Mater. Sci. 2023, 132, 101017.

[2] F. Heusler, Verh DPG 5(1903) 219-220.

[3] C. Felser, G.H. Fecher, B. Balke, Angew Chem Int Ed 46 (2007) 668. Sakurada, N.

[4] Wei, Z. Y.; Liu, E. K.; Li, Y.; Han, X. L.; Du, Z. W.; Luo, H. Z.; Liu, G. D.; Xu, X. K.; Zhang, H. W.; Wang, W. H.; et al. Magneto structural Martensitic Transformations with Large Volume Changes and Magneto Strains in All-d-Metal Heusler Alloys. Appl. Phys. Lett. 2016, 109, 71904.

[5] S. Anand, M. Wood, Y. Xia, C. Wolverton, G.J. Snyder, Double Half-Heusler, Joule 3 (5) (2019) 1226–1238.

[6] Hebri S; Abdelli, A.B.; Belfedal, N; Bensaid, D. Investigating the Structural, Electronic, and Elastic properties of Li-Based Quaternary Heusler Alloys Semiconductors Using Hybrid Functional-HSE06 Band gap Recalculations. Inorg. Chem. Commun. 2023, 150, 110479.

[7] Galanakis, I.H.; Dederichs, P. Half-Metallicity and Slater-Pauling Behavior in the Ferromagnetic Heusler Alloys. In Half-Metallic Alloys; Springer: Berlin/Heidelberg, Germany, 2006; pp. 1–39.

[8] Salahedeen, M.; Wederni, A.; Ipatov, M.; Zhukova, V.; Anton, R.L.; Zhukov, A. Enhancing the Squareness and Bi-Phase Magnetic Switching of Co_2FeSi Microwires for Sensing Application. Sensors 2023, 23, 5109.

[9] Elphick, K.; Frost, W.; Samei Pour, M.; Kubota, T.; Takahashi, K.; Sukegawa, H.; Miura, S.; Hirohata, A.Heusler Alloys for Spintronic Devices: Review on Recent Development and Future Perspectives.

[10] Ozduran, M.; Candan, A.; Akbudak, S.; Kushwaha, A.K.; İyigör, A. Structural, Elastic, Electronic, and Magnetic Properties of Si-Doped Co_2MnGe Full-Heusler Type Compounds. J. Alloys Compd. 2020, 845, 155499.

[11] Jodin, L.; Tobola, J.; Pecheur, P.; Scherrer, H.; Kaprzyk, S. Effect of Substitutions and Defects in Half-Heusler FeVSb Studied by Electron Transport Measurements and KKR-CPA Electronic Structure Calculations. Phys. Rev.. B 2004, 70, 184207.

[12] Wederni, A.; Salaheldeen, M.; Ipatov, M.; Zhukova, V.; Zhukov, A. Influence of the Geometrical Aspect Ratio on the Magneto-Structural Properties of Co2MnSi Microwires. Metals 2023, 13, 1692.

[13] Salaheldeen, M.; Wederni, A.; Ipatov, M.; Zhukova, V.; Zhukov, A. Preparation and Magneto-Structural Investigation of High-Ordered ($L2_1$ Structure) Co2MnGe Microwires. Processes 2023, 11, 1138.

[14] Wederni, A.; Salaheldeen, M.; Ipatov, M.; Zhukova, V.; Zhukov, A. Influence of the Geometrical Aspect Ratio on the Magneto-Structural Properties of Co_2MnSi Microwires. Metals 2023, 13, 1692.

[15] Wederni, A.; Salaheldeen, M.; Ipatov, M.; Zhukova, V.; Zhukov, A. Influence of the Geometrical Aspect Ratio on the Magneto-Structural Properties of Co2MnSi Microwires. Metals 2023, 13, 1692.

[16] Graf, T.; Casper, F.; Winterlik, J.; Balke, B.; Fecher, G.H.; Felser, C. Crystal Structure of New Heusler Compounds. Z. Anorg. Allg. Chem. 2009, 635, 976–981.

[17] Elphick, K.; Frost, W.; Samiepour, M.; Kubota, T.; Takanashi, K.; Sukegawa, H.; Mitani, S.; Hirohata, A. Heusler Alloys for Spintronic Devices: Review on Recent Development and Future Perspectives. Sci. Technol. Adv. Mater. 2021, 22, 235–271.

[18] Khandy, S.A.; Islam, I.; Wani, A.F.; Ali, A.M.; Sayed, M.A.; Srinavasan, M.; Kaur, K. Strain Dependent Electronic Structure, Phonon and Thermoelectric Properties of CuLiX (X=S, Te) Half Heusler Compounds. Phys. B Condens. Matter 2024, 677, 415698.

[19] Graf, T.; Felser, C.; Parkin, S.S.P. Simple Rules for Understanding Heusler Compounds. Prog. Solid. State Chem. 2011, 39, 1–50.

[20] Wjin, H.P.J. Alloys and Compounds of d-Elements with Main Group Elements; Part 2; Springer: Berlin/Heidelberg, Germany, 1988.

[21] Resnina, N.; Belyaev, S.; Shelykov, A.; Ubyvovk, E. Violation of the Sequence of Martensite Crystals Formation on cooling and Their Shrinking on Heating during B2-B19 Martensite Transformation in Ti40,7Hf9,5 Ni44.8Cu5 Shape- Memory Alloys. Phase Transit. 2017, 90, 289-298.

[22] Bachagha, T.; Suñol, J.J. All-d-Metal Heusler Alloys: A Review. Metals 2023, 13, 111.

[23] Chen, C.; Yu, L; Zhu, J.; Tan; C/ The Mechanical Properties of Ni-Mn-Sn Alloys Thin Films with Fe Doping. Integr. Ferroelectrics 2020, 207, 156-165.

[24] H.U. Schuster, H.W. Hinterkeuser, W. Schäfer, G. Will, *Z Naturforsch B* **31** (1976) 1540.

[25] P.J. Sebastian, H. Eckert, S. Rayaprol, R.D. Hoffmann, R. Pöttgen, *Solid State Sci* **8** (2006) 560.

[26] Hehn M, Montaigne F, and Schuhl A, Magnétorésistance géante et électronique de Spin , Techniques de l'Ingénieur l'expertise technique et scientifique de référence, 10(11) (2002)

[27] P.J. Webster, K.R.A. Ziebeck, *Landolt-Börnstein - Group III Condensed Matter*, vol. 19C. Berlin: Springer; 1988. pp. 75–184.

[28] P. Villars, L.D Calvert. Pearson's handbook of crystallographic data for intermetallic phases. American Society of Metals; 1991.

[29] P. Villars, L.D. Calvert. *Pearson's Handbook of Crystallographic Data for Intermetallic Phases*. American Society of Metals; 1991. J. Nuss, M. Jansen, *Z Anorg Allg Chem* **628** (2002) 1152.

[30] W.H. Butler, C.K.A. Mewes, C. Liu, T. Xu, arXiv:1103.3855v1

[31] M. Puselj, Z. Ban, Croat Chem Acta 41 (1969) 79.

[32] H.C. Kandpal, V. Ksenofontov, M. Wojcik, R. Seshadri, C. Felser, J Phys D Appl Phys 40 (2007) 1587.

[33] R. Juza, F. Hund, *Z Anorg Chem* **257** (1948) 257.

[34] A.E. Carlsson, A. Zunger, D.M. Wood, *Phys Rev B* **32** (1985) 1386.

[35] H. Nowotny, F. Holub, Monatsh Chem 91 (1960) 877.

[36] F. Casper, C. Felser, Z Allgem Anorg Chem 634 (2008) 2418.

[37] C.M. Fang, G.A. de Wjis, R.A. de Groot, J Appl Phys 91 (2002) 8340.

[38] S. Ogitt, K.M. Rabe, Phys Rev B 51 (1995) 10443.

[39] J. Kübler, A.R. Williams, C.B. Sommers, Phys Rev B 28 (1983) 1745.

[40] R. Weht, W.E. Pickett, Phys Rev B 60 (1999) 13006.

[41] T. Graf, G.H. Fecher, J. Barth, J. Winterlik, C. Felser, J Phys D Appl Phys 42 (2009) 084003.

[42] J. Barth, B. Balke, G.H. Fecher, H. Stryhanyuk, A. Gloskovskii, S. Naghavi, J Phys D Appl Phys 42 (2009) 185401.

[43] F. Casper, C. Felser, Z Allgem Anorg Chem 634 (2008) 2418.

[44]G. Z. Xu. E. K Lui Y. Du. G. J. Li. Gd.L;U W.H.Wang, and G.H W Euro Phys lett 102. 17007(2013). Slater. Pauling in LiMgPdSn . type multifunctional quaternary Heusler. Page 7.

Chapter II :

[45] J. F. Hamilton, Adv. Phys. 37,(1988). 359.

[46] B. E. Mellander, Phys. Rev. B26, (1982) 5886

[47] D. R. Hartree, *Proc. Cambridge Phil. Soc.* **1928**, *24*, 89.

[48] W. Pauli Jr., *Z. Physik*, **1925,** *31*, 765

[49] V.Z. Fock, *Z. Phys.* **1930**, *61*, 126.

[50] J.C. Slater, *Phys. Rev.*, **1929**, *34***,** 1293.

[51]. Richard M. Martin, *electronic structure Basic Theory and practical methods*, Cambridge University Press (2004).

[52] V. Fock. Naherungsmethode zur losaung des quanten-machanischen Mehrkorperprob-lerne. Z. phys.. 61 :126-148, 1930.

[53] L. Thomas, "The calculation of atomic fields," Proc. Cambridge Phil. Roy. Soc., vol. 23, p. 542, 1927.

[54]. P. Hohenberg, W. Kohn, Phys. Rev. 136 (1964) 864.

[55] R. M. Dreizler, E. K. U. Gross, Density Functional Theory : An Approach to the QuantumMany-Body Problem, Springer-Verlag, Berlin, 1990.

[56] R. G. Parr, W. Yang, Density-Functional Theory of Atoms and Molecules, Oxford University Press, Oxford, 1989.

[57] W. Kohn, Rev. Mod. Phys. 71 (1999) 12531266

Chapter III :

[58] P. Hohenberg et W. Kohn, *Phys. Rev*. *B*136 (1964) 864-871.

[59] W. Kohn et L. J. Sham, *Phys. Rev*. 140 (1965) 1133-1138.

[60] P. Blaha, K. Schwarz, G. K. H. Madsen, D. Kvasnicka, et J. Luitz, *WIEN2K*, edité par K. Schwarz, *Vienna University of Technology, Austria*, (2001).

[61] J.P. Perdew, K. Burke, M. Ernzerhof, *Phys. Rev. Lett*. 77 (1996) 3865-3868.

[62] J.P. Perdew, Y. Wang, *Phys. Rev. B* 45 (1992) 13244-13249.

[63] F. D. Murnaghan, *Proc. Nat. Acad. Sci.USA* 30 (1944) 244.

[64] Florian J. Pucher, Franziska Hummel, et Wolfgang Schnick, *Eur. J. Inorg. Chem*.

[65] W. Schnick et J. Lücke, Z. Anorg. *Allgem. Chem.*, 19 (1990) 588.

[66] W. Schnick et J. Lücke, *Solid State Ionics* 38 (1990) 271.

[67] C. S. Wang, W. E. Pickett, *Phys. Rev. Lett*. 51 (1983) 597-600

[68] R. O. Jones et O. Gunnarsson, *Rev. Mod. Phys*. 61, (1989) 689-746.

[69] J. E. Jaffe et A. Zunger *Phys. Rev. B* 29 (1984) 1882.

[70] K. Landskron, S. Schmid, et W. Schnick, Z. Anorg. *Allgem. Chem*. 627 (2001) 2469-2472.

[71] Alijani V, Ouardi S, Fecher G H, Winterlik J, Naghavi S S, Kozina X, Stryganyuk G, Felser C, Ikenaga E, Yamashita Y, Ueda S and Kobayashi K 2011 Electronic, structural, and magnetic properties of the half-metallic ferromagnetic quaternary Heusler compounds CoFeMn Z (Z = Al , Ga, Si, Ge) *Phys. Rev. B* **84** 224416

[72] A. V. Kosobutsky, *J. Phys. Condens. Matter* 21(2009) 405404.

[73] M. O'Keeffe, B. G. Hyde, *Acta Crystallogr., Sect. B32* (1976) 2923-2936.

[74] Özdoğan K, Şaşıoğlu E and Galanakis I 2013 Slater-Pauling behavior in LiMgPdSn-type multifunctional quaternary Heusler materials: Half-metallicity, spin-gapless and magnetic semiconductors *J. Appl. Phys.* **113**

[75] R. D. Shannon, *Acta Cryst A 32*, (1976) 751-767.

[76] N. A. Goryunova et Yu. A. Valov (eds.), *Sovetskoe Radio, Moscow* (1974).

[77] S. Adachi, *J. Appl. Phys.* 61 (1987) 4869.

[78] H. Mathieu, *4 Ed. Masson* 21-30 (1998) 419-420.

[79] N.V. Smith, *Phys. Rev. B3* (1971) 1862.

[80] F. Bassani, G. Pastroi, Parravicini, *Pergamon Press, Oxford*, (1973).

[81] C. Ambrosch-Draxl, R. Abt, The Calculation of Optical Properties Within WIEN97, ICTP Lecture Notes 1998, unpublished; S. Sharma, C. Ambrosch-Draxl, M.A. Khan, P. Blaha, S. Auluck, *Phys. Rev. B* 60 (1999) 8610.

[82] C. A. Draxl, R. Abt, ICTP *lecture notes, unpublished*, (1998).

[83] P. Y. Yu, M. Cardona, *Berlin: Springer-Verlag*, (1999) 233.

[84] A. Delin, A. O. Eriksson, R. Ahuja, B. Johansson, M. S. Brooks, T. Gasche, et al. *Phys. Rev. B* 54 (1996) 1673.

[85] M. Dressel, G. Gruner, *Cambridge University Press.* (2002).

[86] G. Murtaza, B. Amin, S. Arif, M. Maqbool, I. Ahmad, A. Afaq, S. Nazir, M. Imran, et M. Haneef, *Computational Materials Science*. 58 (2012) 71.

[87] J. L. Erskine et E. A. Stern, *Phys. Rev. B* 12 (1975) 5016.

[88] D.R. Hartree. *Proc.Camb. Philos. Soc*. 24 (1928) 89.

[89] W. Shan, W. Walukiewicz, J.W. Ager III, E.E. Haller, J. F. Geisz, D. J. Friedman, J. M.

Abstract

The results obtained by the authors align with existing data in the current literature. The computed electronic band structure reveals that the material is a semiconductor with a direct band gap of 1.72 eV. Additionally, the material exhibits a high absorption coefficient (>104 cm^{-1}). The static dielectric constant and static refractive index were determined to be 6 and 2.45, respectively. The investigated properties of MnCrTiZ (Z=Al, As) suggest that it could be a promising candidate for optoelectronic and photovoltaic applications These optical properties enhance its potential for solar energy conversion.

This study indicated that MnCrTiZ (Z=Al, As) compounds are stable in the B_1 (NaCl-type) phase under hydrostatic pressure. These compounds undergo a phase transition to the CsCl (B_2) phase and a further transition from the B_1 (NaCl) phase to the L10 (tetragonal) phase. The electronic properties show that these materials are half-metals in the B_1 (NaCl) phase. The magnetic moment is equal to $2\mu_B$.

Résumé

Cette étude vise à analyser les propriétés structurales, électroniques et optiques des composés de Heusler cubiques MnCrTiZ (Z=Al, As), afin d'évaluer leur potentiel pour des applications photovoltaïques. Pour ce faire, nous avons utilisé la méthode des ondes planes (FP-LAPW) dans le cadre de la théorie de la fonctionnelle de la densité (DFT), avec l'approximation du gradient généralisé (GGA) et le potentiel modifié de Becke-Johnson (mBJ) pour décrire les effets d'échange-corrélation (XC).

Les propriétés structurales calculées sont en accord avec les données théoriques et expérimentales disponibles, ce qui suggère que ces composés pourraient constituer une alternative prometteuse aux matériaux photovoltaïques actuels.

Les résultats révèlent que MnCrTiZ est un semi-conducteur à gap direct de 1,72 eV, une caractéristique idéale pour les applications optoélectroniques. De plus, le composé présente:

- Un coefficient d'absorption élevé.
- Une constante diélectrique statique de 6. Un indice de réfraction de 2,45.

Ces propriétés optiques renforcent son potentiel pour la conversion de l'énergie solaire.

الملخص:

تهدف هذه الدراسة إلى تحليل الخصائص البنيوية والإلكترونية والبصرية لمركب هسلر المكعبي MnCrTiZ(Z=Al,As) ، وذلك لتقييم إمكانية استخدامه في التطبيقات الكهروضوئية . ولتحقيق هذا الغرض، استخدمنا طريقة الموجات المستوية وشبه الكمون ضمن تقريب التدرج المعمم (GGA) وتقريب المعد المعدّل (mBJ) لحساب التبادل – الارتباط (XC) في إطار هذه الدراسة في الحسابات، التي تعتمد على نظرية دالة الكثافة (DFT) . قمنا بحساب الخواص البنائية والنظرية المتوفرة وذلك لتقييم إمكانية استخدامه في التطبيقات الكهروضوئية مما يجعلها بديلاً جيداً للخيارات الحالية في هذا المجال..

أظهرت نتائج الدراسة توافقاً مع النتائج النظرية السابقة، حيث كشفت حسابات بنية النطاق الإلكتروني أن المركب المدروس عبارة عن شبه موصل بفجوة نطاق مباشرة تبلغ قيمتها 1.72 إلكترون فولت. بالإضافة إلى ذلك، وجد أن للمركب معامل امتصاص مرتفع، حيث بلغت قيم السكون لدالة العزل الكهربائي ومعامل الانكسار 6 و2.45 على التوالي.

النتائج:

- تبين أن المركب MnCrTiZ(Z=Al,As) مستقر في الطور (B_1 (NaCl-type تحت تأثير الضغط.
- يحدث تحول من البنية NaCl إلى البنية (B_2) CsCl والبنية L10 (tetragonal) تحت تأثير الضغط.
- أظهرت النتائج أن جميع المركبات MnCrTiZ(Z=Al,As) (لديها خاصية "نصف المعدنية.(demi-métallicité) "
  - المركبان MnCrTiAs هو معدن في تقريبGGA ، لكنه يصبح نصف معدني في تقريب.mBJ
  - المركب MnCrTiAl هو نصف معدن في كلا التقريبين GGA و.mBJ

الخصائص الإلكترونية: تم حساب كثافة الحالات الكلية (DOS) وكثافة الحالات الجزئية (PDOS) لوحظ أن منحنيات كثافة الحالات لكل من المركبات MnCrTiZ(Z=Al,As) شبه متطابقة.

- تبين أن مساهمة الذرة Mn-p هي الغالبة.

العزم المغناطيسي: تم استخدام تقريب GGA وتقريب mBJ لحساب العزم المغناطيسي. وقد تبين أن العزم المغناطيسي لهذه المركبات يبلغ حوالي μ_B 2، مما يشير إلى أن الذرة Z لا تؤثر على العزم المغناطيسي.

الاستخدامات:

أكثر شيوعًا من MnCrTiAs في التطبيقات الصناعية.

- إلكترونيات الدوران (Spintronics) بسبب خاصية نصف الفلزّية.
- أقطاب مغناطيسية في أجهزة MRAM أو مجسات مغناطيسية.
- تطبيقات حرارية كهروضوئية. (Thermophotovoltaics)
- أقطاب في أجهزة. IR detectors
- Spin Photovoltaics إذا تم تعديل التركيب.

أقل شيوعًا من MnCrTiAl في التطبيقات الصناعية.

- قد يستخدم في تطبيقات حرارية كهربائية (Thermoelectric) بسبب زيادة الكتل الذرية.
- ممكن استخدامها في Spintronicsإذا تم تعديل تركيبتها.
- أقطاب شفافة مغناطيسية. (Transparent Magnetic Electrodes)
- مواد لـ. Spin Optoelectronics
- حساسات ضوئية مغناطيسية.

الكلمات المفتاحية: دالة الكثافة، التحول الطوري، سبينترونيك. براسيوديميوم شالكوجينيد.